REVIEW

EnergyChem

www.journals.elsevier.com/energychem

Non-noble metal-based molecular complexes for CO_2 reduction: From the ligand design perspective

Dong-Cheng Liu,[a,b] Di-Chang Zhong,[*,a] and Tong-Bu Lu[a]

[a] MOE International Joint Laboratory of Materials Microstructure, Institute for New Energy Materials and Low Carbon Technologies, Tianjin University of Technology, Tianjin 300384, China

[b] School of Chemistry and Pharmaceutical Sciences, Guangxi Normal University, Guilin 541004, China

[*] Correspondence: zhong_dichang@hotmail.com (D.-C. Z.)

ABSTRACT: Molecular catalysts for electrochemical and photochemical CO_2 reduction have developed rapidly during the past two decades. Using non-noble metal (Ni, Co, Mn, Fe, and Cu) complexes as molecular catalyst, numerous catalytic systems have shown good catalytic performance for CO_2 reduction. It is useful to draw conclusions from the results of reported works and identify concepts that may provide future frameworks in catalyst design for CO_2 reduction. It is well-known that the ligand in molecular complexes is one of the key factors affecting catalytic performance. Modification of the ligand structure has become an important strategy to improve the catalytic performance. This review, beginning with a brief general introduction to molecular catalysis of CO_2 reduction, intends to reveal ligand effects of non-noble metal complexes on the catalytic performance for CO_2 reduction. The latest progress on both electrocatalytic and photocatalytic CO_2 reduction by non-noble metal complexes has been summarized, wherein, emphasis has been placed on the effect of ligands on catalyst efficiency, selectivity and stability. New developments involving immobilization of non-noble metal complexes on solid supports or electrodes have also been discussed. Finally, several constructive suggestions in designing efficient molecular catalysts for CO_2 reduction have been put forward.

Keywords: *Non-noble metal, Molecular complex, CO_2 reduction, Photocatalysis, Electrocatalysis*

INTRODUCTION

The conversion of CO_2 into fuels or chemicals through electrocatalytic or photocatalytic process is a green and economical strategy to achieve a sustainable energy supply technology.[1–3] Due to its inertness, direct reduction of CO_2 by one electron to $CO_2^{\cdot-}$ is highly unfavorable, which requires a formal reduction potential as high as −1.90 V vs NHE in neutral aqueous solution.[4–6] An alternative and more favorable pathway is to reduce CO_2 through proton-assisted multiple-electron transfer.[7,8] In this case, CO_2 can be reduced to diverse products (HCOOH, CO, HCHO, CH_3OH, C_2H_4, CH_4, etc.) with more positive redox potentials (Eqs. (1)–(7), the standard redox potentials E^0 correspond to aqueous solutions at pH = 0).[5,9] Increase of electrons and protons involved in CO_2 reduction reaction shifts the standard reduction potential anodically, favoring CO_2 reduction thermodynamically. However, because the kinetic barrier generally increases with the increase of electrons and protons, deep reduction of CO_2 to $HCHO/CH_3OH/C_2H_4/CH_4$ is still more difficult than to HCOOH/CO.[10] Besides, the reduction of proton is a strong competition reaction with CO_2 reduction, as the reduction potential is −0.41 V vs NHE, more positive than that of some CO_2 reduction reactions.[11–15] Therefore, the development of proper catalysts to enhance the efficiency and selectivity of CO_2 reduction reaction is indispensable.

$$CO_2 + e^- + H^+ \rightarrow (1/2)H_2C_2O_4,\ E^0 = -0.50\ \text{V vs SHE} \quad (1)$$

$$CO_2 + 2e^- + 2H^+ \rightarrow HCOOH,\ E^0 = -0.25\ \text{V vs SHE} \quad (2)$$

$$CO_2 + 2e^- + 2H^+ \rightarrow CO + H_2O,\ E^0 = -0.11\ \text{V vs SHE} \quad (3)$$

$$CO_2 + 4e^- + 4H^+ \rightarrow HCHO + H_2O,\ E^0 = -0.07\ \text{V vs SHE} \quad (4)$$

$$CO_2 + 6e^- + 6H^+ \rightarrow CH_3OH + H_2O,\ E^0 = +0.02\ \text{V vs SHE} \quad (5)$$

$$CO_2 + 6e^- + 6H^+ \rightarrow (1/2)C_2H_4 + 4H_2O,\ E^0 = +0.06\ \text{V vs SHE} \quad (6)$$

$$CO_2 + 8e^- + 8H^+ \rightarrow CH_4 + 2H_2O,\ E^0 = +0.17\ \text{V vs SHE} \quad (7)$$

Homogeneous molecular catalysts have attracted wide interest in CO_2 reduction, because their definite spatial structures facilitate structural design/modification, performance-structure analysis and mechanistic study. Transition metal complexes are prime candidates for CO_2 reduction as molecular catalysts, because metal centers usually exhibit diverse oxidation states and ligands can tune the electron distribution around metal centers to regulate the reactivity.[16] The accessible modification to the structures of metal complexes provides the opportunity to promote the catalytic efficiency in CO_2 reduction. Furthermore, the formal reduction potentials can be systematically tuned through ligand modification to well match the potential required for CO_2 reduction.[7]

Several parameters are commonly used to evaluate the performance of molecular catalysts in CO_2 reduction (Eqs. (8)–(14)).[7,17] Product selectivity is the first important parameter,

Received: January 7, 2020
Revised: April 24, 2020
Accepted: April 26, 2020
Published: 20 May 2020

DOI: 10.1016/j.enchem.2020.100034
EnergyChem **2**, 100034 (2020)

which can be calculated through division of the amount of target CO_2 reduction product by the total amount of reduced products including the byproduct H_2 (Eq. (8)).

$$\text{Selectivity}\,(100\%) = 100 \times [\text{target product (mol)}]/[\text{all reduced products (mol)}] \quad (8)$$

Turnover number (TON) and Turnover frequency (TOF) are another two important parameters for molecular catalysis of CO_2 reducton. TON is the amount of a specific product that per catalyst amount over its lifetime, which indicates the stability of the catalyst (Eq. (9)). TOF is defined as the TON per unit time, which indicates the speed of the catalytic cycle (Eq. (10)). TON and TOF are also calculated in some electrocatalytic CO_2 reduction by employing Eqs. (11) and (12),[18,19] where E is the applied potential, E_{cat} is the standard potential for a catalyst, k_{cat} is the intrinsic catalytic rate constant, T is the reaction temperature, and F is the Faraday constant. By this way, large TON and TOF values are usually obtained. However, these values may not reflect the real reactivity of the catalysts, as using TOF value obtained in short time CV experiment to extrapolate TON number in electrolysis (TON = TOF (CV) × t) often overestimates the real TON. Therefore, the calculation approach to reliable TON and TOF values is to do an extended electrolysis and then to divide the mol number of product by the total mol number of catalyst in the solution (Eqs. (9) and (10)).

$$\text{TON} = [\text{product(mol)}]/[\text{catalyst(mol)}] \quad (9)$$

$$\text{TOF} = \text{TON}/[\text{reaction time}] \quad (10)$$

$$\text{TON} = \frac{k_{cat}}{1+\exp\left[\frac{F}{RT}(E-E_{cat})\right]} \times t \quad (11)$$

$$\text{TOF} = \frac{k_{cat}}{1+\exp\left[\frac{F}{RT}(E-E_{cat})\right]} \quad (12)$$

$$\eta = E^0 - E \quad (13)$$

Besides TON and TOF, overpotential (η) and Faradaic efficiency (FE) are also important parameters to describe the electrocatalyst performance. η is defined as the difference between the real potential E at which the electrolysis is operated and the standard potential E^0 for a specific CO_2 reduction reaction (Eq. (13)). FE represents the conversion efficiency from electricity to chemical energy. An excellent molecular electrocatalyst is expected with high TON, TOF and FE values with a low η.

In photocatalytic process, the quantum yield (Φ) is meaningful to describe the catalyst performance, which indicates the conversion efficiency from light energy to chemical energy. It can be calculated through Eq. (14). Most sacrificial electron donors (e.g., triethylamine (TEA), triethanolamine (TEOA), 1-benzyl-1,4-dihydronicotinamide (BNAH), and ascorbic acid ($AscH_2$)) function as a one-electron donor during the photocatalytic reaction. The maximum Φ for a single-electron reduction is 1, while for n electron reductions, it is $1/n$. It should be noted that 3-dimethyl-2-phenyl-2,3-dihydro-1H-benzo[d]-imidazole (BIH) can act as a two-electron donor with one-photon excitation of a photosensitizer, which result in maximum Φ higher than 1.[20,21]

$$\Phi(100\%) = 100 \times [CO_2\ \text{reduction products}]/[\text{incident photons}] \quad (14)$$

Among molecular metal complexes, non-noble metal complexes are more desirable for CO_2 reduction than noble ones for practical application. Non-noble metal complexes for electrochemical and photochemical CO_2 reduction had aroused the first wave of interest in 1980s and 1990s,[22–25] and have received renewed attention recently for modern energy and environmental challenges (Scheme 1).[18,26–32]

In electrocatalytic CO_2 reduction, Tinnemans and co-workers initially designed several tetraaza-macrocyclic Co(II) and Ni(II) complexes in 1984, which were found electrochemically active for CO_2 reduction.[24] After that, many non-noble metal (Ni, Co, Mn, Fe, and Cu) complexes with macrocycle, porphyrin or phosphine ligands were designed and used as CO_2 reduction electrocatalysts.[33] A significant progress has been made in 2010. The Bouwman group achieved the electrocatalytic reduction of CO_2 to oxalate by using a binuclear copper complex bearing a tetrapodal disulfide ligand.[34] Later, two polypyridine Mn complexes were employed as efficient electrocatalysts for CO_2 reduction by Deronzier and collaborators.[35] These designed electrocatalysts show an excellent efficiency, selectivity and stability for the CO_2-to-CO conversion at a moderate overpotential. In 2012, Costentin, Savéant and co-workers systematically studied the effect of the substituents of porphyrin complexes on the electrocatalytic efficiency for CO_2 reduction.[36] They demonstrated that an Fe porphyrin with phenolic groups at the ortho positions shows extremely enhanced electrocatalytic efficiency for CO_2 reduction to CO. Subsequently, various non-noble metal complexes were covalently or noncovalently attached to solid supports or electrodes for the development of efficient heterogeneous electrocatalytic systems for CO_2 reduction.[37,38] In 2016, Robert and co-workers immobilized a pyrene-derivatized Fe triphenylporphyrin on multiwalled carbon nanotubes via noncovalent interactions. The resulting modified carbon material can serve as an efficient, selective, and stable electrocatalyst for CO_2-to-CO conversion at low overpotential (480 mV) in neutral aqueous solution.[37] In 2018, Chang and co-workers developed an efficient supramolecular electrocatalyst by embedding Fe-TPP (iron tetraphenylporphyrin) into a supramolecular porous organic cage.[39] This new strategy results in a larger amount of exposed electroactive Fe centers, which significantly improves the catalytic activity and durability for CO_2-to-CO conversion in pH 7.3 aqueous condition.

In photocatalytic CO_2 reduction, the first homogeneous photocatalytic system based on non-noble metal catalyst was reported by Lehn's group in 1982, in which $CoCl_2$ was used as molecular catalyst.[25] Then, a large number of non-noble metal (Ni, Co, Mn, Fe, and Cu) complexes with various kinds of ligands (macrocycle, polypyridyl, porphyrin, and phosphine ligands etc.) were prepared for photochemical CO_2 reduction. In 1992, Kimura and co-workers developed a bimetallic photocatalyst composed of a macrocyclic complex $Ni(cyclam)^{2+}$ as a catalytic site and a $Ru(phen)_3^{2+}$ (phen = 1,10-phenanthroline) subunit as a photosensitizer, which exhibits a higher CO selectivity than the mixed system comprising $Ni(cyclam)^{2+}$ and $Ru(phen)_3^{2+}$.[40] Due to the high density of catalytically active sites, excellent CO_2 adsorption capacities, and tailorable light-absorption abilities,[41–44], metal-organic frameworks (MOFs) have also been explored for photocatalytic CO_2 reduction.[45] In 2014, Wang and co-workers found that a Co-based zeolitic imidazolate framework can catalyze the photoreduction of CO_2 to CO under mild reaction conditions, giving a TON_{CO} of 450 within 2.5 h.[29] In 2016, two highly efficient and selective Fe and Co quaterpyridine complexes were employed as catalysts for photocatalytic CO_2 reduction.

DOI: 10.1016/j.enchem.2020.100034
EnergyChem 2, 100034 (2020)

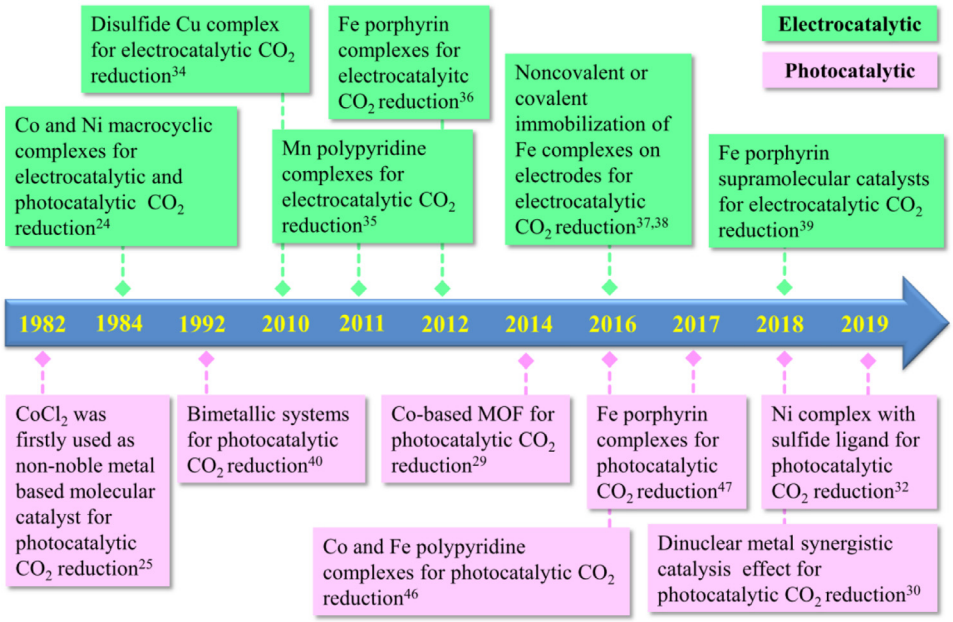

Scheme 1. The timeline of non-noble metal-based molecular complexes for CO_2 reduction.

Significantly, these complexes are also efficient and selective catalysts when using organic dye purpurin as the photosensitizer.[46] Later, Robert et al. demonstrated an Fe tetraphenylporphyrin complex functionalized with trimethylammonio groups can serve as a robust and efficient catalyst not only for reduction of CO_2 to CO, but also for reduction of CO_2 to CH_4 upon visible light irradiation.[47] In 2018, our group designed and synthesized a dinuclear heterometallic complex which displays extremely high activity and selectivity for photocatalytic CO_2 reduction in a water-containing solution, with CO selectivity and TON value as high as 98% and 65,000,[30] respectively. Experiments and theory calculations revealed that dinuclear metal synergistic catalysis (DMSC) effect dramatically boosts the photocatalytic CO_2-to-CO conversion. Very recently, a novel Ni complex supported by a S_2N_2-tetradentate ligand with two noncoordinating pyridine pendants was developed by Kojima and co-workers. They found that the addition of Lewis-acidic Mg^{2+} ions in the catalystic system greatly boosted photocatalytic CO_2-to-CO conversion, as compared to the other Ni complex without the Lewis-acid capturing sites.[32]

It can be seen that great progresses have been achieved in molecular catalysis for CO_2 reduction by non-noble metal complexes during the past several decades, which have been summarized in many recent reviews. Some of them are broad full reviews,[5,9,48] and more of them discussed the effect of metal centers on the catalyst performance for CO_2 reduction, including transition metal complexes,[2,20] earth abundant metal complexes,[11] one or two special metal (e.g., Ni,[49–50] Mn,[16] Co,[4] Co and Fe,[51] or Ir and Ru[52]) complexes, or special metal and/or ligand based complexes (e.g., iron porphyrin complexes[26] and polypyridine-based metal complexes[53]) and so on. Besides, some reviews focus on molecular photocatalysts[17,54] and mechanisms/methods[5,10] for CO_2 reduction. In fact, the environments around metal centers (i.e., the ligand or the coordination atoms) also play significant roles in affecting the catalytic performance. Therefore, a review from the perspective of ligand design is necessary to give possible guidance for researchers a new direction for the invention of excellent molecular catalysts.

This review is intended, from the perspective of ligand design, to introduce the significant progress on CO_2 reduction by molecular non-noble metal complexes. Efforts have been made on summarizing the reported ligand design and modification of catalysts for improving the catalytic performance for CO_2 reduction. Emphasis has been placed on concluding the effect of ligand optimization on the catalyst efficiency, selectivity and stability, as well as providing constructive suggestions for researchers on designing CO_2 reduction catalysts with improved catalytic performance. Up to now, the exellent works on ligand modification used to develop highly efficient molecular catalyst for CO_2 reduction, are mainly for Ni, Co, Mn, Fe, or Cu-based complexes. Therefore, other non-noble metal (Cr, Mo, W, etc.) based complexes are not described in detail in this review.[55,56] To well summarize the research progresses on CO_2 reduction by molecular non-noble metal (Ni, Co, Mn, Fe, and Cu) complexes, this review has been divided between electrocatalytic and photocatalytic CO_2 reduction structurally. This division is to compare the activity of catalysts with similar structures under similar catalytic system, based on which reliable activity-structure relationship could be revealed. Within these sections, reports have been further divided by ligand type. In detail, in the first section, the researches on electrochemical CO_2 reduction were summarized, and in the second, the researches on photochemical CO_2 reduction were reviewed. To well demonstrate the ligand design concept, we divide the non-noble metal molecular catalysts into six major categories according to ligand types: (1) metal complexes with macrocyclic ligands, (2) metal complexes with polypyridine ligands, (3) metal complexes with porphyrin and porphyrin-like ligands, (4) metal complexes with nonplanar N_4 ligands, (5) metal complexes with N-heterocyclic carbene ligands, and (6) metal complexes with phosphine/sulfur/bridging ligands. After the summarization and discussion of significant progress of CO_2 reduction driven by non-noble metal complexes, a perspective on development of non-noble metal complexes with excellent catalytic performance for CO_2 reduction has been given.

DOI: 10.1016/j.enchem.2020.100034
EnergyChem **2**, 100034 (2020)

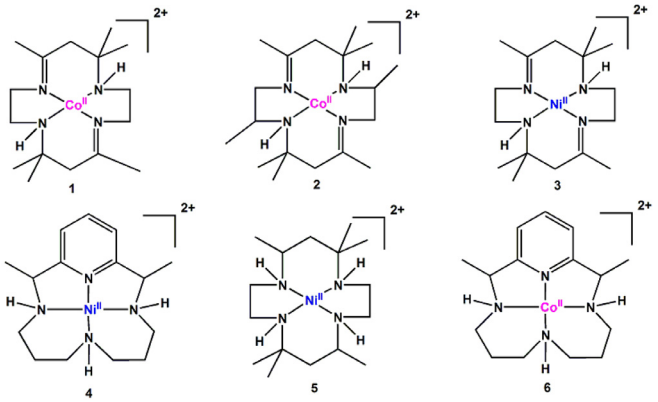

Fig. 1. Ni/Co complexes based on tetraazamacrocycles as molecular electrocatalysts for CO_2 reduction.

ELECTROCATALYTIC CO_2 REDUCTION

Electrochemical CO_2 reduction, using renewable electricity energy to convert CO_2 to useful fuels or feedstocks, is a desirable way to simultaneously solve the coming energy and climate problems. An electrocatalyst for CO_2 reduction participates in an electron transfer reaction and accelerates the whole chemical reaction. Electrocatalysts should offer critical solutions to lower the overpotentials, improve selectivity, and increase the reaction kinetics of CO_2 reduction. These aspects can be optimized by chemical tuning of the metal centers via appropriate ligand design and systematic ligand modification in homogeneous systems.[7] The data discussed below for electrochemical CO_2 reduction were summarized in Table 1.

Metal complexes with macrocyclic ligands

Among a variety of ligands in construction of metal complex electrocatalysts for CO_2 reduction, a macrocyclic ligand is known to be capable of stabilizing the reduced species formed in the catalytic cycle.[57] The development of complexes using macrocyclic ligands for electrocatalytic CO_2 reduction was pioneered by Eisenberg et al. in the 1980s.[22,23] They found that Co and Ni tetraazomacrocyclic complexes (**1**–**5**; Fig. 1) were able to reduce CO_2 to CO with high current efficiency but low TOFs (Table 1, entries 1–5).[22,58] Then, a representative example of Co tetraazomacrocyclic complex (**6**; Fig. 1) was designed and synthesized.[24,59] It was found that at 940 mV overpotential, the electrolysis in acetonitrile (CH_3CN) at a carbon electrode produced CO in 20–30% FE without byproduct H_2 (Table 1, entry 6).[59]

$Ni(cyclam)^{2+}$ (**7**) (cyclam = 1,4,8,11-tetraazacyclotetradecane; Fig. 2) is a remarkable macrocyclic complex reported by Sauvage et al.,[60–64] with which the electrochemical CO_2-to-CO conversion occurs efficiently and selectively in water (pH 4 to 5) at a mercury electrode. In a CO_2 saturated water solution without any added buffer (pH 4.1), electrolysis by **7** for 4 h at −1.45 V vs Fc^+/Fc, corresponding to an overpotential of 640 mV, led to the formation of CO with FE of 96% (Table 1, entry 7).[60,65] It was interesting that when using an aprotic solvent of dimethyl formamide (DMF) instead of water solution as a solvent, after electrolysis for 5 h, HCOOH was found the major product, with a FE of 75% (FE of 24% for CO) (Table 1, entry 8).[11,61] The catalyst was operated at a mercury electrode which has specific interactions with the catalytic species, making it uncertain to determine the active catalytic species.[66–68] Then the ligand cyclam of **7** was structurally modified to improve the electrocatalytic performance for CO_2 reduction (Fig. 2.[49,69–74] Methyl substitution of the amines on the cyclam ring one by one was explored, obtaining Ni(II) complexes (**7**–**11**; Fig. 2).[72] The result showed that with the increase of the N-methyl substitution in **7**, the electronic and steric properties around the catalytic center Ni(II) were modified. It was found that the adsorption of the Ni(II) complexes (**7**–**11**; Fig. 2) on the mercury electrode increased but the stability of the reduced Ni(I) form lowered at the same time. CO_2 binding requires the catalyst to be in the stable, adsorbed and reduced *trans* I (or RSRS) Ni(I) form. Without stable Ni(I) catalytic form, the tetramethyl substituted derivative tetramethylated $Ni^{II}(TMC)^{2+}$ cyclam (**11**) (TMC = 1,4,8,11-tetramethyl-1,4,8,11-tetraazacyclotetradecane) exhibits inertness in CO_2 reduction. Therefore, the highest catalytic activity for electrocatalytic CO_2 reduction is still the unsubstituted Ni(II) cyclam complex **7**. However, due to the high affinity to CO, the concentration of active **7** gradually decreases in the catalytic system. An elegant way to resume this deactivation is using a CO scavenger, and the tetramethylated cyclam complex **11** was subsequently designed.[75] The one-electron reduced species $Ni^{I}(TMC)^{+}$ of **11** has both a very large binding constant for CO ($K = 1.2 \times 10^5$ M^{-1}) and a lower reactivity toward CO_2 than the unsubstituted cyclam complex **7**. When **7** and **11** with a molar ratio of 1:20 in H_2O/CH_3CN (v:v = 1:4) solution were simultaneously used to catalyze CO_2 reduction, the catalytic current was significantly increased, indicating a larger number of catalytic turnovers. These studies also demonstrated a degradation pathway due to Ni(0) species formed from reduction of the $Ni^{I}(cyclam)(CO)^{+}$ species. Although the N-methylation of the cyclam in **7** could not enhance the electrochemical activity for CO_2 reduction, the Ni(II) complex of hydroxyethyl azacyclam appeared effective. The resulting **12** (Fig. 2) showed more active than the unsubstituted cyclam complex **7** for electrochemical CO_2 reduction in an acetate electrolyte.[76]

Besides, Fujita and co-workers systematically investigated the electrocatalytic activity of Ni complexes with cyclam derivatives for CO_2 reduction. They found that stronger CO_2 binding ability of the complex endows the corresponding complex higher catalytic performance.[69] The CO_2 binding constants of $[Ni(HTIM)]^{2+}$ (**13**; HTIM = C-RRSS-2,3,9,10-tetramethyl-1,4,8,11-tetraazacyclotetradecane; Fig. 2) and $[Ni(MTC)]^{2+}$ (**14**; MTC = 2,3-trans-cyclohexano-1,4,8,11-tetraazacyclotetradecane Fig. 2) with high catalytic activity are

DOI: 10.1016/j.enchem.2020.100034
EnergyChem **2**, 100034 (2020)

Table 1. Non-noble metal (Ni, Co, Mn, Fe and Cu) complexes as molecular catalysts for electrochemical CO_2 reduction.

Entry	CAT	Conditions (Solvent, Electrode, Time)	TOF[a] (Product)	Potential (V)	FE% (Product)	Ref
1	**1** (1.2 mM)	H_2O/CH_3CN ($v/v = 2:1$), 0.1 M KNO_3 or H_2O only, Hg pool, 1.1 h	7.8 h^{-1} ($CO + H_2$) in 1.1 h	−1.6 V vs SCE/[−1.76 V][f]	93% ($CO + H_2$)	22
2	**2** (1.2 mM)	H_2O/CH_3CN ($v/v = 2:1$), 0.1 M KNO_3 or H_2O only, Hg pool, 1.1 h	9 h^{-1} ($CO + H_2$) in 1.1 h	−1.5 V vs SCE/[−1.66][f]	90% ($CO + H_2$)	22
3	**3** (1.2 mM)	a number of solvent systems, Hg pool, 1.1 h	nr	−1.5 V vs SCE/[−1.66][f]	nr	22
4	**4** (2.5 mM)	H_2O/CH_3CN ($v/v = 2:1$), 0.1 M KNO_3, Hg pool, 1.1 h	2.1 h^{-1} (CO) in 1.1 h	−1.3 V vs SCE/[−1.46][f]	44% (CO)	22
5	**5** (1.2 mM)	H_2O/CH_3CN ($v/v = 2:1$), 0.1 M $LiClO_4$, Hg pool, 1.1 h	6 h^{-1} ($CO + H_2$) in 1.1 h	−1.6 V vs SCE /[−1.76 V][f]	98% ($CO + H_2$)	22
6	**6** (1 mM)	CH_3CN, pyrolytic graphite, 0.5 h	nr	−1.54 V vs SCE/[−1.92 V][f]	20–30% (CO)	59
7	**7** (0.17 mM)	H_2O (pH 4.1), Hg pool, 4 h	32 h^{-1} (CO) in 4 h	−1.05 V vs NHE/[−1.45 V][f]	96% (CO)	60,65
8	**7** (0.2 mM)	DMF, Hg pool, 5 h	[0.64 h^{-1} ($HCOO^-$), 0.2 h^{-1} (CO)][b] in 5 h	−1.4 V vs SCE/[−1.87 V][f]	75% ($HCOO^-$) 24% (CO)	61
9	**7** (50 μM)	H_2O (pH 5), Hg pool, 1 h	nr	−0.96 V vs NHE/[−1.36 V][f]	84% (CO)	69
10	**13** (50 μM)	H_2O (pH 5), Hg pool, 1 h	nr	−0.96 V vs NHE/[−1.36 V][f]	88% (CO)	69
11	**14** (50 μM)	H_2O (pH 5), Hg pool, 1 h	nr	−0.96 V vs NHE/[−1.36 V][f]	88% (CO)	69
12	**17** (1.5 mM)	CH_3CN, Hg pool, 43 h	nr	nr	90% ($C_2O_4^{2-}$)	78
13	**20** (3 μM)	H_2O (pH 2.0), Hg pool, 1 h	nr	−0.99 V vs NHE/[−1.39 V][f]	66% (CO) 15% (H_2)	70
14	**21** (1.0 mM)	CH_3CN (+20% H_2O), glassy carbon, 0.5 h	[1.28 h^{-1} (CO), 6.6 h^{-1} (H_2)][b] in 0.5 h	−1.7 V[e]	10.3% (CO) 53.4% (H_2)	81
15	**22** (1.0 mM)	CH_3CN (+20% H_2O), glassy carbon, 0.5 h	[9 h^{-1} (CO), 8 h^{-1} (H_2)][b] in 0.5 h	−1.7 V[e]	80.0% (CO) 7.3% (H_2)	81
16	**23** (1.0 mM)	CH_3CN (+20% H_2O), glassy carbon, 0.5 h	[0.5 h^{-1} (CO), 0.74 h^{-1} (H_2)][b] in 0.5 h	−1.7 V[e]	29.1% (CO) 44.1% (H_2)	81
17	**24** (1.0 mM)	CH_3CN (+20% H_2O), glassy carbon, 0.5 h	nd	−1.7 V[e]	nd	81
18	**25** (0.2 mM)	DMF, Hg pool, 5 h	[0.152 h^{-1} (CO), 0.64 h^{-1} ($HCOO^-$)][b] in 5 h	−1.4 V vs SCE/[−1.87 V][f]	16% (CO) 68% ($HCOO^-$)	61
19	**26** (0.5 mM)	CH_3CN/H_2O ($v/v = 4:1$), glassy carbon, 6 h	190.0 s^{-1} (CO)/[1.54 h^{-1} CO)][c] in 6 h	−1.16 V vs NHE/[−1.85 V][f]	95% (CO)	18
20	**27** (0.5 mM)	CH_3CN/H_2O ($v/v = 4:1$), glassy carbon, 6 h	4.2 s^{-1} (CO)/[0.27 h^{-1} (CO)][c] in 6 h	−1.16 V vs NHE/[−1.85 V][f]	25% (CO)	18
21	**28** (1.0 mM)	CH_3CN/H_2O ($v/v = 4:1$), glassy carbon, 6 h	5.0 s^{-1} (CO)/[0.35 h^{-1} (CO)][c] in 6 h	−1.16 V vs NHE/[−1.85 V][f]	62% (CO)	18
22	**29** (1.0 mM)	DMF, glassy carbon, 1 h	nr	−1.5 V vs SCE/[−1.97 V][f]	82% (CO)	12
23	**30** (1.0 mM)	DMF, glassy carbon, 3 h	[420 h^{-1}][b] in 3 h	−1.25 V vs SCE/−1.72 V][f]	75%−80% ($HCOO^-$)	12
24	**31** (0.5 mM)	DMF (+ 1.2 M TFE), glassy carbon, 2 h	170 s^{-1} (CO)/[3.1 h^{-1} (CO)][c] in 2 h	−2.8 V[e]	98% (CO)	85
25	**32** (0.5 mM	DMF (+ 1.2 M TFE), glassy carbon, 2 h	0.5 s^{-1} (CO)/[0.15 h^{-1} (CO)][c] in 3 h	−2.35 V vs SCE/[−2.82 V][f]	23% (CO)	85
26	**33** (0.5 mM)	DMF (+ 1.2 M TFE), glassy carbon, 2 h	<0.0016 s^{-1} (CO)/[nc][d] in 2 h	−2.35 V vs SCE/[−2.82 V][f]	<1% (CO)	85
27	**34** (1 mM)	CH_3CN (+ 5% H_2O), glassy carbon, 22 h	nr	−1.40 V vs SCE/[−1.78 V][f]	85% (CO) 15% (H_2)	35,90

(*continued on next page*)

DOI: 10.1016/j.enchem.2020.100034
EnergyChem **2**, 100034 (2020)

Table 1 (*continued*)

28	**35** (1 mM)	CH_3CN, glassy carbon, 18 h	[1.89 h^{-1} (CO)][b] in 18 h	−1.40 V vs SCE/[−1.78 V][f]	100% (CO)	35
29	**36** (1 mM)	CH_3CN (+ 1.4 M TFE), glassy carbon, more than 3 h	340 s^{-1} (CO)/[nc][d] in 3 h	−2.2 V vs SCE/[−2.58 V][f]	100% (CO)	94
30	**37** (1 mM)	CH_3CN (+ 0.3 M TFE), glassy carbon, 7 h	5×10^3 s^{-1} (CO)/[nc][d] in 7 h	−1.8 V vs SCE/[−2.58 V][f]	98% (CO)	95
31	**39** (1 mM)	CH_3CN (+ 2.0 M TFE), glassy carbon, 1 h	5×10^3 s^{-1} (HCOOH)/[nc][d] in 1 h	−2.03 V[e]	71% (HCOOH)	108
32	**40** (1 mM)	CH_3CN (+ 2.0 M TFE), glassy carbon, 1 h	5.5×10^3 s^{-1} (HCOOH)/[nc][d] in 1 h	−2.03 V[e]	> 60% (HCOOH)	108
33	**41** (1 mM)	CH_3CN (+ 1.0 M TFE), glassy carbon, 1 h	860 s^{-1} (CO)/[nc][d] in 1 h	−1.99 V[e]	nr	108
34	**42** (1 mM)	CH_3CN (+ 1.0 M TFE), glassy carbon, 1 h	840 s^{-1} (CO)/[nc][d] in 1 h	−1.97 V[e]	nr	108
35	**43** (1 mM)	CH_3CN (+ 2.0 M TFE), glassy carbon, 1 h	700 s^{-1} (CO)/[nc][d] in 1 h	−2.01 V[e]	nr	108
36	**44** (1 mM)	CH_3CN (+ 2.0 M TFE), glassy carbon, 1 h	860 s^{-1} (CO)/[nc][d] in 1 h	−2.02 V[e]	nr	108
37	**45** (1 mM)	CH_3CN (+ 2.0 M TFE), glassy carbon, 1 h	5.2×10^3 s^{-1} (HCOOH/[nc][d] in 1 h	−2.00 V[e]	63% (HCOOH)	108
38	**46** (1 mM)	CH_3CN (+ 2.0 M TFE), glassy carbon, 1 h	4.0×10^3 s^{-1} (HCOOH)/[nc][d] in 1 h	−2.07 V[e]	> 60% (HCOOH)	108
39	**47** (1 mM)	CH_3CN (+ 2.0 M TFE), glassy carbon, 1 h	7.5×10^3 s^{-1} (HCOOH)/[nc][d] in 1 h	−2.01 V[e]	nr	108
40	**48** (1 mM)	CH_3CN, glassy carbon, 4 h	1.4 s^{-1} (CO)/[nc][d] in 4 h	−1.8 V vs SCE/[−2.18 V][f]	70% (CO) 22% ($HCOO^-$)	110
41	**50** (1 mM)	CH_3CN (+ 5% H_2O), glassy carbon, 4 h	[0.68 h^{-1} (CO)][b] in 4 h	−1.5 V vs SCE/[−1.88 V][f]	76% (CO)	111
42	**51** (1 mM)	CH_3CN (+ 5% H_2O), glassy carbon, 4 h	[0.23 h^{-1} (CO)][b] in 4 h	−1.5 V vs SCE/[−1.88 V][f]	67% (CO)	111
43	**52** (0.93 mM)	CH_3CN (+0.5 M PhOH), graphite rod, nr	nr	−2.2 V[e]	93% (CO) 6% (CO)	112
44	**53** (1 mM)	CH_3CN (+0.5 M PhOH), graphite rod, nr	nr	−2.2 V[e]	129% (CO) 1% (H_2)	112
45	**56** (1 mM)	CH_3CN (+ 5% H_2O), glassy carbon, 4 h	nr	−1.90 V[e]	73% (CO)	115
46	**57** (1 mM)	CH_3CN (+ 5% H_2O), glassy carbon, 4 h	nr	−2.59 V[e]	40% (CO)	115
47	**61**(0.2–0.4 mM)	CH_3CN, glassy carbon, 1 h	nr	−1.7 V vs SCE/[−2.08 V][f]	Trace (CO)	117
48	**62**(0.2–0.4 mM)	CH_3CN, glassy carbon, 1 h	[20 h^{-1} (CO)][b] in 1 h	−1.7 V vs SCE/[−2.08 V][f]	80% (CO)	117
49	**62** (0.5 mM)	CH_3CN (+ 2% H_2O), 3 M PhOH, glassy carbon, 3 h	533 s^{-1} (CO)/[5.67 h^{-1} (CO)][c] in 3 h	−1.1 V vs SCE/−1.48 V][f]	94% (CO)	118
50	**63**(0.2 mM)	CH_3CN (+ 2% H_2O, TFE), glassy carbon, nr	nr	−1.2 V vs SCE/[−1.58 V][f]	48% (CO)	118
51	**64** (8.5 nmol cm^{-1})	H_2O (0.5 M $NaHCO_3$, pH 7.3), multi-walled carbon nanotube, 4.5 h	5.45 s^{-1} (CO)/[nc][d] in 4.5 h	−0.48 V vs. RHE/[−1.31 V][f]	100% (CO)	122
52	**65** (2 mM)	DMF/H_2O (v/v = 19:1), Hg pool, 3 h	nr	−1.72 V[e]	20% (CO)	123
53	**65** (0.25 mM)	CH_3CN/H_2O (v/v = 3:1), glassy carbon, 1 h	[2.4 h^{-1} (CO)][b] in 1 h	−1.83 V[e]	33.7% (CO)	125
54	**66** (0.25 mM)	CH_3CN/H_2O (v/v = 3:1), glassy carbon, > 1 h	[1.9 h^{-1} (CO)][b] over 1 h	−1.83 V[e]	25.8% (CO)	125
55	**67** (0.25 mM)	CH_3CN/H_2O (v/v = 3:1), glassy carbon, > 1 h	[2.2 h^{-1} (CO)][b] over 1 h	−1.83 V[e]	28.4% (CO)	125
56	**68** (0.25 mM)	CH_3CN/H_2O (v/v = 3:1), glassy carbon, 1 h	[1.7 h^{-1} (CO)][b] in 1 h	−1.83 V[e]	45.2% (CO)	125
57	**69** (1 mM)	DMF/H_2O (v/v = 95:5), glassy carbon, 4 h	nr	nr	31% (CO) 2% (H_2)	127
58	**70** (1 mM)	DMF/H_2O (v/v = 95:5), glassy carbon, 4 h	nr	nr	12% (CO) 5% (H_2)	127

(*continued on next page*)

DOI: 10.1016/j.enchem.2020.100034
EnergyChem **2**, 100034 (2020)

Table 1 (*continued*)

59	**71** (1 mM)	DMF/H_2O (v/v = 95:5), glassy carbon, 4 h	nr	nr	11% (CO) 18% (H_2)	[127]
60	**72** (1 mM)	DMF/H_2O (v/v = 95:5), glassy carbon, 4 h	nr	nr	4% (CO) 23% (H_2)	[127]
61	**73** (1 mM)	DMF/H_2O (v/v = 95:5), glassy carbon, 4 h	nr	nr	37% (CO) 4% (H_2)	[127]
62	**78** (1 mM)	DMF (+ 0.1 M PhOH), Hg pool, nr	nr	−1.46 V vs NHE/[−2.18 V][f]	100% (CO)	[147]
63	**79** (1 mM)	DMF (+ 2 M H_2O), carbon crucible, 2 h	[32.5 h^{-1}][b] in 2 h	−1.16 V vs NHE/[−1.88 V][f]	94% (CO)	[36]
64	**79** (1 mM)	DMF (+ 2 M H_2O), glassy carbon, nr	maximum $10^{4.2}$ s^{-1} (CO)/[nc][d], no time information	−1.33 V vs NHE/[−2.05 V][f]	nr	[36]
65	**80** (1 mM)	DMF (+ 2 M H_2O), glassy carbon, nr	maximum $10^{2.5}$ s^{-1} (CO)/[nc][d], no time information	−1.69 V vs NHE/[−2.41 V][f]	nr	[36]
66	**79** (1 mM)	DMF (+ 2 M PhOH), glassy carbon, nr	maximum $10^{3.8}$ s^{-1} (CO)/[nc][d], no time information	−1.35 V vs NHE/[−2.07 V][f]	nr	[150]
67	**81** (1 mM)	DMF (+ 2 M PhOH), glassy carbon, nr	maximum $10^{4.0}$ s^{-1} (CO)/[nc][d], no time information	−1.28 V vs NHE/[−2 V][f]	nr	[150]
68	**82** (0.5 mM)	H_2O (pH 6.7), glassy carbon, 72 h	nr	−1.263 V vs SHE/[−1.663 V][f]	93% (CO)	[27]
69	**83** (0.5 mM)	DMF (+ 0.1 M H_2O, 3 M PhOH), 84 h	maximum 10^{6} s^{-1} (CO)/[nc][d] in 84 h	−0.944 V vs SHE/[−1.664][f]	100% (CO)	[27]
70	**84** (0.5 mM)	DMF (+10% H_2O), glassy carbon, nr	maximum $10^{4.2}$ s^{-1} (CO)/[nc][d], no time information	−1.25 V vs NHE/[−1.97 V][f]	nr	[151]
71	**85** (0.5 mM)	DMF (+10% H_2O), glassy carbon, nr	maximum $10^{4.5}$ s^{-1} (CO)/[nc][d], no time information	−1.34 V vs NHE/[−2.06 V][f]	nr	[151]
72	**86** (0.5 mM)	DMF (+10% H_2O), glassy carbon, nr	maximum $10^{3.6}$ s^{-1} (CO)/[nc][d], no time information	−1.35 V vs NHE/[−2.07 V][f]	nr	[151]
73	**87** (0.5 mM)	DMF (+10% H_2O), glassy carbon, nr	maximum $10^{4.3}$ s^{-1} (CO)/[nc][d], no time information	−1.40 V vs NHE/[−2.12 V][f]	nr	[151]
74	**88** (0.5 mM)	DMF (+10% H_2O), glassy carbon, nr	maximum $10^{5.8}$ s^{-1} (CO)/[nc][d], no time information	−1.60 V vs NHE/[−2.32 V][f]	nr	[151]
75	**89** (0.5 mM)	DMF (+10% H_2O), glassy carbon, nr	maximum $10^{4.7}$ s^{-1} (CO)/[nc][d], no time information	−1.35 V vs NHE/[−2.07 V][f]	nr	[151]
76	**91** (2.5 wt%)	H_2O (0.1 M $KHCO_3$, pH 6.8), carbon nanotube, 10 h	2.7 s^{-1} (CO)/[nc][d] in 10 h	−0.63 V vs. RHE/[−1.43 V][f]	92% (CO)	[154]
77	**92** (3.5 wt%)	H_2O (0.1 M $KHCO_3$, pH 6.8), carbon nanotube, 10 h	4.1 s^{-1} (CO)/[nc][d] in 10 h	−0.63 V vs. RHE/[−1.43 V][f]	96% (CO)	[154]
78	**92**	H_2O (pH ca.14, M KOH), **92**/carbon nanotube cathode catalyst, 10 h	nr	2.0 V vs RHE/[0.77 V][f]	94% (CO)	[155]
79	**92**	H_2O (pH ca.14,1 M KOH), SnO_2/carbon nanotube cathode catalyst, 35 h	nr	2.3 V s RHE/[1.07 V][f]	82% ($HCOO^-$)	[155]
80	**93**	H_2O (pH 14, 1 M KOH), carbon powder, 0.3 h	3.9 s^{-1} in 0.3 h	−0.92 V vs RHE/[−2.15 V][f]	94% (CO)	[156]
81	**94**	H_2O (pH 7.3, bicarbonate buffer), carbon fabric, 24 h	360 h^{-1} (CO)/[33.1 (CO)][c] in 24 h	−0.67 V vs RHE/[−1.50 V][f]	nr	[159]
82	**95**	H_2O (pH 7.3, bicarbonate buffer), carbon fabric, 24 h	2500 h^{-1} (CO)/[56.3 (CO)][c] in 24 h	−0.67 V vs RHE/[−1.50 V][f]	90% (CO)	[159]
83	**96**	H_2O (pH 7.3, bicarbonate buffer), carbon fabric, 24 h	[162.5 (CO)][b] in 24 h	−0.67 V vs RHE/[−1.50 V][f]	91% (CO)	[159]
84	**97**	H_2O (pH 7.3, 0.5 M $KHCO_3$), glassy carbon, 24 h	0.64 s^{-1} (CO)/[nc][d] in 24 h	−0.63 V vs RHE/[−1.46 V][f]	100% (CO) 2% (H_2)	[39]

(*continued on next page*)

DOI: 10.1016/j.enchem.2020.100034
EnergyChem **2**, 100034 (2020)

Table 1 (*continued*)

85	**78**	H_2O (pH 7.3, 0.5 M $KHCO_3$), glassy carbon, 24 h	0.38 s^{-1} (CO)/[nc][d] in 24 h	−0.63 V vs RHE/[−1.46 V][f]	96% (CO) 6% (H_2)	39
86	**98**	H_2O (+ 0.5 M $KHCO_3$), carbon (gas diffusion electrode, 20 atm CO_2), nr	nr	−1.2 V vs Ag/AgCl/[−1.40 V][f]	97% (CO)	161
87	**99**	H_2O (pH 4.6, 5.0 mM Na_2SO_4), glassy carbon, supported on multiwalled carbon nanotubes, 28 h	140 h^{-1} (CO)/[39.3 h^{-1} (CO)][c] in 28 h	−1.1 V vs NHE/[−1.50 V][f]	80% (CO)	170
88	**100**	H_2O (pH 3.0, 10 atm CO_2), pyrolytic graphite, 1.5 h	nr	−0.8 V vs RHE/[−1.38 V][f]	50% (CO)	162
89	**100**	H_2O (pH 1.0), pyrolytic graphite, 10 atm CO_2, 1.5 h	nr	−0.8 V vs RHE/[−1.26 V][f]	2.3% (CH_4) 6.7% (CO)	162
90	**101**	H_2O (pH 7.3), carbon plate, Nafion membrane, 3 h	144 h^{-1} (CO)/[nc][d] in 3 h	−1.03 V vs NHE/[−1.72 V][f]	93% (CO) 4% (H_2)	37
91	**102** (1 mM)	CH_3CN/H_2O (v:v = 4:1), glassy carbon plates, 5 h	[1.96 h^{-1} (CO)][b] in 5 h	−1.03 V vs NHE/[−1.72 V][f]	72% (CO)	175
92	**103** (1 mM)	CH_3CN/H_2O (v:v = 4:1), glassy carbon plate, 5 h	[1.6 h^{-1} (CO)][b] in 5 h	−0.96 V vs NHE/[−1.65 V][f]	74% (CO)	175
93	**104** (1 mM)	CH_3CN/H_2O (v:v = 4:1), glassy carbon plate, 5 h	[0.24 h^{-1} (CO)][b] in 5 h	−0.91 V vs NHE/[−1.60 V][f]	84% (CO)	175
94	**105** (1 mM)	CH_3CN/H_2O (v:v = 4:1), glassy carbon plate, 5 h	[1.2 (CO)][b] in 5 h	−0.85 V vs NHE/[−1.54 V][f]	41% (CO)	175
95	**106** (1 mM)	DMF (+ 5 M H_2O), glassy carbon plate, 24 h	22.1 s^{-1} (CO)/[0.43 h^{-1}][c] in 24 h	−1.24 V vs NHE/[−1.96 V][f]	91% (CO)	177
96	**107**	Wet CH_3CN, glassy carbon, 2 h	3.9 h^{-1} (CO) in 2 h	−1.5 V vs SCE/[−1.88 V][f]	nr	178
97	**108**	Wet CH_3CN, glassy carbon, 2 h	4.2 h^{-1} (CO) in 2 h	−1.5 V vs SCE/[−1.88 V][f]	nr	178
98	**109**	Wet CH_3CN, glassy carbon, 2 h	5.9 h^{-1} (CO) in 2 h	−1.5 V vs SCE/[−1.88 V][f]	nr	178
99	**110** (0.02 mM)	CH_3CN, glassy carbon, 8 h	[4.38 h^{-1} (CO)][b] in 8 h	−1.8 V vs SCE/[−2.18 V][f]	90% (CO) in 0.5 h;22% (CO) in 8 h	28
100	**115** (0.2 mM)	CH_3CN (+ 2% H_2O), glassy carbon rod, 1 h	nr	−2.25 V[e]	5% (CO) 93% (H_2)	179
101	**116** (0.2 mM)	CH_3CN (+ 2% H_2O), glassy carbon rod, 1 h	21.7 s^{-1} (CO)/[nc][d] in 1 h	−2.42 V[e]	56% (CO) 43% (H_2)	179
102	**117** (0.2 mM)	CH_3CN (+ 2% H_2O), glassy carbon rod, 1 h	47.5 s^{-1} (CO)/[nc][d] in 1 h	−2.44 V[e]	87% (CO) 11% (H_2)	179
103	**118**	CH_3CN, glassy carbon rod, nr	10 s^{-1} (CO)/[nc][d], no time information	−2.30 V[e]	nr	182
104	**119**	CH_3CN, glassy carbon rod, nr	3 s^{-1} (CO)/[nc][d], no time information	−2.50 V[e]	nr	182
105	**120**	CH_3CN, glassy carbon rod, nr	1 s^{-1} (CO)/[nc][d], no time information	−1.7 V[e]	nr	182
106	**121** (2 mM)	DMF (+ 10 mM TEA), glassy carbon, 1 h	nr	−1.09 V[e]	1% (CO) 51% (H_2)	184
107	**121** (2 mM)	DMF (+ 10 mM TEA), glassy carbon, 1 h	nr	−2.25 V[e]	2% (CO) 55% (H_2)	184
108	**122** (2 mM)	DMF (+ 10 mM TEA), glassy carbon, 1 h	nr	−2.00 V[e]	4% (CO) 91% (H_2)	184
109	**122** (2 mM)	DMF (+ 10 mM TEA), glassy carbon, 1 h	nr	−2.35 V[e]	2% (CO) 96% (H_2)	184
110	**123** (1 mM)	CH_3CN (+ 5% H_2O, $HClO_4$, pH 3.7), glassy carbon rod, 4 h	nr	−1.46 V vs SCE/[−1.84 V][f]	35% (CO)	185
111	**124** (1 mM)	CH_3CN (+ 5% H_2O, pH 3.7, $HClO_4$), glassy carbon rod, nr	0.08 s^{-1} (CO)/[nc][d], no time information	nr	nr	185
112	**125**	CH_3CN (+ 5% H_2O, pH = 3.7, $HClO_4$), glassy carbon rod, 4 h	nr	−1.93 V[e]	48% (CO)	186
113	**126** (1 mM)	CH_3CN (+ 5% H_2O, pH = 3.7, $HClO_4$), glassy carbon rod, 4 h	nr	−1.77 V[e]	72% (CO)	186

(*continued on next page*)

DOI: 10.1016/j.enchem.2020.100034
EnergyChem **2**, 100034 (2020)

Table 1 (*continued*)

114	**127** (1 mM)	CH_3CN, glassy carbon rod, 4 h	2100 s^{-1} (CO)/[14 h^{-1} (CO)][c] in 4 h	−2.32 V[e]	92% (CO)	187
115	**127** (1 mM)	CH_3CN (+ 0.56 M H_2O), glassy carbon rod, 6 h	320,000 s^{-1} (CO)/[2.5 h^{-1} (CO)][c] in 6 h	−2.32 V[e]	98% (CO)	187
116	**128**	CH_3CN, glassy carbon, nr	nr	−0.63 V NHE/[−1.32 V][f]	nr (CO)	189
117	**131**	CH_3CN, Pt, nr	1.0 s^{-1} (CO), no time information	−1.3 V[e]	nr (CO)	188
118	**133** (1 mM)	CH_3CN, glassy carbon, over 5 h	nr	−2.30 V[e]	100% (CO)	195
119	**133** (1 mM)	CH_3CN (+ 5% H_2O), glassy carbon, 1.7 h	nr	−2.30 V[e]	nr (CO) 41% (H_2)	195
120	**134** (0.3 mM)	CH_3CN, Pt gauze, 24 h	> 2.0 h^{-1} (CO)/[nc][d] in 24 h	−1.7 V vs Ag/AgCl/[−2.22 V][f]	50% (CO)	197
121	**135** (0.5 mM)	DMF (+ 1.1 M H_2O), glassy carbon, 1 h	650 s^{-1} ($HCOO^-$)/[23 h^{-1} ($HCOO^-$)][c] in 1 h	−2.25 [e]	98% ($HCOO^-$) 5% (H_2)	200
122	**135** (0.5 mM)	DMF (+ 0.56 M H_2O), glassy carbon, 1 h	[15 h^{-1} ($HCOO^-$)][b] in 1 h	−2.25 V[e]	92% ($HCOO^-$) 10% (H_2)	200
123	**136** (0.5 mM)	DMF (+ 1.1 M H_2O), glassy carbon, 1 h	180 s^{-1} ($HCOO^-$)/[9 h^{-1} ($HCOO^-$)][c] in 1 h	−2.15 V[e]	99% ($HCOO^-$) 3% (H_2)	200
124	**137** (0.5 mM)	DMF (+ 1.1 M H_2O), glassy carbon, 1 h	40 s^{-1} ($HCOO^-$)/[4 h^{-1} ($HCOO^-$)][c] in 1 h	−2.05 V[e]	86% ($HCOO^-$) 6% (H_2)	200
125	**138** (0.5 mM)	DMF (+ 5.6 M H_2O), glassy carbon, 1 h	[1.5 h^{-1} ($HCOO^-$)][b] in 1 h	−2.10 V[e]	38% ($HCOO^-$) 67% (H_2)	200
126	**139** (0.5 mM)	CH_3CN (+ 2 M TFE), Hg pool, 4 h	89 s^{-1} ($HCOO^-$)/[2.25 h^{-1} ($HCOO^-$), 0.75 h^{-1} (CO), 0.38 h^{-1} (H_2)][c] in 4 h	− 1.9 V vs Ag/AgCl/[−2.40 V][f]	60% ($HCOO^-$) 19% (CO) 9% (H_2)	205
127	**140** (0.5 mM)	CH_3CN (+ $LiClO_4$), glassy carbon, 7 h	[0.88 h^{-1} ($C_2O_4^{2-}$)][b] in 7 h	−0.03 V vs NHE/[−0.72 V][f]	96% ($C_2O_4^{2-}$)	34

[a] TOFs calculated by Eq. (10).
[b] TOFs recalculated by Eq (10) using the reported catalytic data.
[c] TOFs calculated by Eq. (12), as well as Eq. (10) using the reported catalytic data.
[d] nc = TOFs can not be recalculated by Eq. (10) because of no reported catalytic data.
[e] Potentials in V vs Fc^+/Fc.
[f] Potentials recalculated with respect to the Fc^+/Fc potential in a given solvent according to references [53,213,214]. The complexes without activity or without enough electrochemical data of CO_2 reduction were not listed in the table, despite discussed in the text. nr = not reported. nd = not detected.

8.3 and 13 M^{-1}, respectively, whereas other Ni macrocycles (e.g. **15** and **16**; Fig. 2) with poor catalytic activity show negligible CO_2 binding.[69,71,77] Furthermore, they found that **13** and **14** show notably higher current densities than the parent **7** at pH 5 (Table 1, entries 9–11). The higher activities may originate from their configurations which are more suitable for adsorption onto the mercury electrode surface and the electronic effects from the increased alkyl groups, a favorable environment for accommodating and reducing CO_2 at the metal center.[9]

In 2000, a series of Ni amide-functionalized macrocyclic complexes (**17**–**19**; Fig. 2) were found capable of electrocatalytic reduction of CO_2 to oxalate.[78] The complexes with $-COOC_2H_5$ or $-COCH_3$ groups at the R_2 position are much more stable during electrocatalysis than those without $-COOC_2H_5$ or $-COCH_3$ groups. The catalytic CO_2 reduction with these electrocatalysts possibly undergoes a dimerization of two $CO_2^{\cdot-}$ radical anions to generate oxalate. Complex **17** shows the best activity and stability in anhydrous CH_3CN solution at a mercury electrode, with a FE ($C_2O_4^{2-}$) over 90% (Table 1, entry 12). More recently, a carboxylate-functionalized cyclam ligand was further employed to prepare a Ni complex **20** (Fig. 2) as an electrocatalyst for CO_2-to-CO conversion.[70,79–80] Impressively, complex **20** exhibits higher electrocatalytic activity for CO_2 reduction than the parent **7** at pH 2 aqueous conditions (Table 1, entry 13). The improved performance is tentatively attributed to the pendant carboxylic groups which can serve as a good proton relay.

Ren and co-workers presented four derivatives (**21**–**24**; Fig. 2) of **7** in 2017.[81] The pendant aryl groups on the macrocycle allow facile tuning of the steric and electronic effects of the catalytic center by changing the substituents on the aryl groups (Table 1, entries 14–17).[81] Similar to **7**,[82] complexes **21**–**23** do not require a Hg electrode and allow the use of environmentally

DOI: 10.1016/j.enchem.2020.100034
EnergyChem **2**, 100034 (2020)

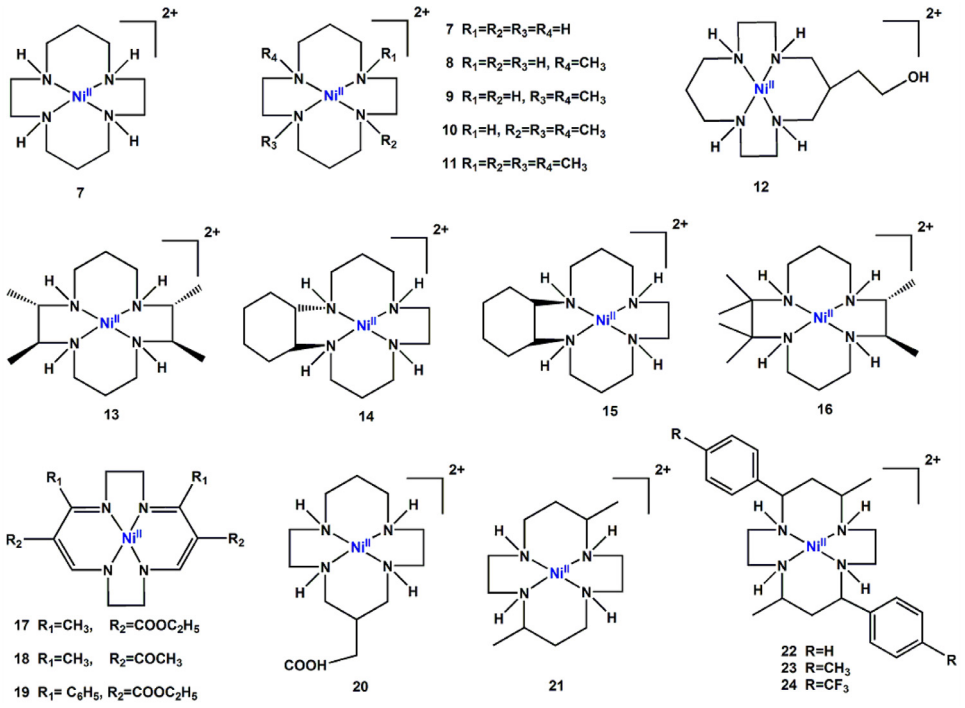

Fig. 2. Ni complexes based on tetraazamacrocycles as molecular electrocatalysts for CO_2 reduction.

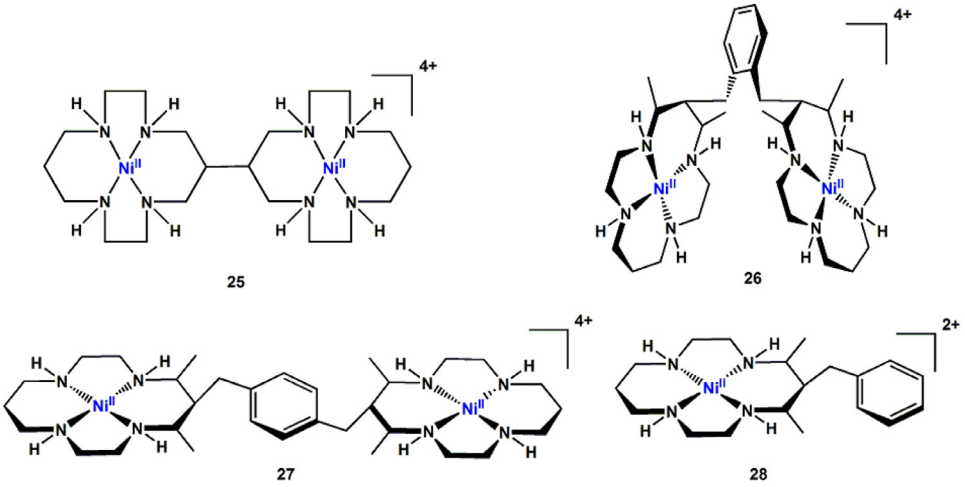

Fig. 3. Dinuclear and mononuclear Ni complexes of tetraazamacrocycles as molecular electrocatalysts for CO_2 reduction.

benign carbon working electrodes. Electrochemical investigation of these complexes demonstrated that the electron-withdrawing substituents on the aryl group deactivate the Ni center during the reduction of CO_2 and H^+, whereas the phenyl, *p*-tolyl, and aryl-free derivatives display surprisingly disparate levels of catalytic activity, with the phenyl derivative **22** demonstrating the highest activity for CO_2 reduction (Table 1, entry 15).[81]

Besides mononuclear metal cyclam complexes, dinuclear metal cyclam complexes have also been designed for electrocatalytic CO_2 reduction. In 1987, a dinuclear Ni cyclam complex $Ni_2(biscyclam)^{4+}$ (**25**; Fig. 3) was found to have similar catalytic activity to its parent **7**. In **25**, two Ni atoms are indirectly linked via a bridge ligand. C2 products were expected to be obtained via a potential synergistic effect within the dinuclear Ni cyclam complex.[61,83,84] However, no C2 product was generated in the reaction system. Instead, a significant amount of H_2 was formed, and liquid product of $HCOO^-$ with a maximum FE of 68% was detected (Table 1, entry 18).[61] Very recently, we designed and synthesized two dinuclear Ni macrocycle complexes (**26** and **27**; Fig. 3) and a mononuclear Ni macrocycle complex **28** supported by three modified macrocyclic ligands.[18,50] Electrochemical experiments and density functional theory (DFT) calculations revealed that complex **26** showed the best performance for electrochemical CO_2-to-CO conversion, with a FE (CO) of 95%, and TOF values of 1.54 h^{-1}, respectively (Table 1, entry 19). Under the same conditions, the FE (CO) is 62% for the mononuclear complex **28** (Table 1, entry 21), and 25% and 1.62 for the other dinuclear complex **27** (Table 1, entry 20).[18] The

DOI: 10.1016/j.enchem.2020.100034
EnergyChem **2**, 100034 (2020)

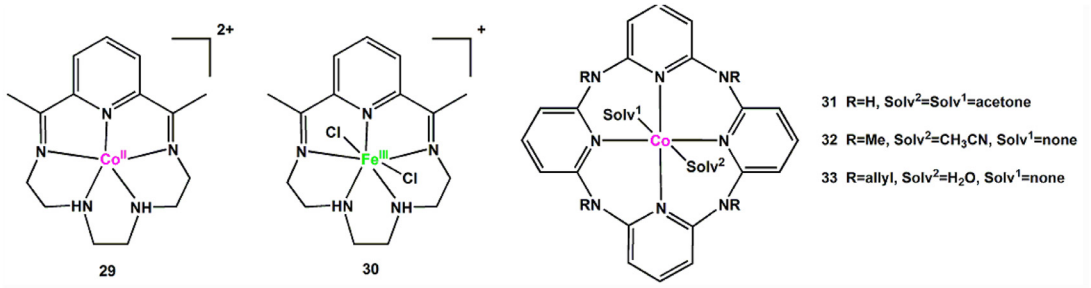

Fig. 4. Metal complexes with pentadentate N_5 macrocycles and aminopyridine macrocycles as molecular electrocatalysts for CO_2 reduction.

much enhanced catalytic activity of **26** can be ascribed to the suitable distance between two Ni(II) catalytic centers, which boosts the electrochemical CO_2-to-CO conversion by synergistic catalysis.

The pentadentate N_5 macrocyclic ligands have also been used to synthesize metal complexes for electrochemical CO_2 reduction (see Fig. 4). Robert group recently discovered that both Co^{II} (**29**) and Fe^{III} complex (**30**) of N_5 macrocycle were active towards CO_2 reduction at a carbon electrode, with catalytic-center-dependent reduction products.[12] For complex **29**, a controlled potential electrolysis (CPE) at −1.97 V vs Fc^+/Fc for 1 h led the formation of CO exclusively, with an 82% faradaic yield, a current density of 0.4 mA cm^{-2} and an overpotential of 566 mV (Table 1, entry 22). During long term electrolysis, deactivation of **29** was observed. In contrast, for Fe^{III} complex **30**, a CPE at −1.72 V vs Fc^+/Fc for 3 h resulted exclusively in HCOOH with FE of 75%−80% and a current density of 0.09 mA cm^{-2} (Table 1, entry 23). A relatively low overpotential of 310 mV and a catalytic rate $k_{cat} = 0.3\ s^{-1}$ was estimated for the average current electrolysis. Remarkably, changing the metal catalytic centers can completely change the CO_2 reduced products.[51] Besides, Co complexes based on aminopyridine macrocycles (**31**–**33**; Fig. 4) were also found active for CO_2 electroreduction.[85] In the presence of weak Brønsted acids, large catalytic currents were observed for **31** in catalyzing the reduction of CO_2 to CO in DMF solution, with an excellent FE of 98% at an applied potential of −2.8 V vs Fc^+/Fc (Table 1, entry 24).[85] In comparison, when the pendant N–H group was replaced by a N−Me group (**32**) or a N−allyl group (**33**) (Table 1, entries 25–26), TONs steeply decreased 300 times lower than that of complex **31**. These results indicate that the presence of the linking NH moiety in complex **31** is crucial to its electrocatalytic activity.[85,86] The presence of NH groups also leads to a positive shift in the reduction potential of the $Co^{I/0}$ couple, resulting in a decreased overpotential for CO_2 reduction. The mechanism for CO_2-to-CO conversion by complex **31** was finally proposed. Firstly, the Co^{II} in complex **31** is reduced by one electron to generate the Co^{I} complex, which is further reduced to Co^0. Then, CO_2 binds to the Co^0 complex to produce the CO_2 adduct ($[Co(CO_2)]^0$), which is stabilized by intramolecular H-bonds of the pendant secondary amines.[27] The successive protonation of the CO_2 complex produces CO and H_2O and complex **31** regenerates simultaneously.[85,86]

Metal complexes with polypyridine ligands

Polypyridine ligands have been used extensively in catalysis for the activation of small molecules.[87] In CO_2 reduction, polypyridine ligands are also appropriate to construct catalysts, as they can not only stabilize the reduced metal centers but also mediate the multi-electron/multi-proton transformations through the ligand π system.[53,88] Early developments of CO_2 reduction molecular catalysts have indeed involved polypyridine ligands in 1983, by using a Re complex for photocatalytic CO_2-to-CO conversion.[89] Recently, the field was revitalized with a particular focus on non-noble metal complexes. In 2011, Chardon-Noblat and Deronzier et al. firstly reported Mn complexes based on bipyridine ligand for electrocatalytic CO_2 reduction. Both complexes **34** bearing a 2,2′-bipyridine and **35** bearing a 4,4′-dimethyl-2,2′-bipyridine can catalyze electrochemical CO_2 reduction to CO efficiently (Fig. 5).[35,90–92] After 22 h electrolysis with **34**, CO was produced with 85% FE (Table 1, entry 27) and the current reaches a perfectly stable value (0.06 mA cm^{-2}). **35** showed better catalytic activity in terms of selectivity and durability. Even at CPE of −1.78 V vs Fc^+/Fc for 18 h electrolysis, CO was the sole product and no deactivation was observed (Table 1, entry 28). Further pulsed-EPR studies complemented by DFT calculation have shown that the catalytic mechanism involves the formation of a Mn^0-Mn^0 dimer after one electron reduction of the Mn^I starting complex. Oxidative addition of CO_2 and H^+ then leads to a Mn^{II}-carboxylic acid intermediate which finally gets reduced with a second electron and protonates to evolve a CO and a H_2O molecule. Very recently, Hartl and co-workers explored the catalytic performance of **34** for CO_2 reduction combined electrochemical and photochemical, which significantly reduce overpotential for electrocatalytic CO_2 reduction.[93] A ca. 500 mV of onset potential positively shifted by electricity and light compared with that driven by exclusively electricity.

Since then, the modification of the polypyridine ligands was extensively used to improve the catalytic performances for CO_2 reduction to CO.[94–97] Complex **36** (Fig. 5) supported on 4,4′-ditertbutyl-2,2′-bipyridine gave a current density as high as 30 mA/cm^2 and the faradaic efficiency as high as 100% during CPE at −2.58 V vs Fc^+/Fc in the presence of 1.4 M trifluoroethanol (TFE) (Table 1, entry 29).[94] To minimize dimer Mn species formation, increasing the steric hindrance around the metal center was an effective strategy.[95,98,99] Based on 6,6′-dimesityl-2,2′-bipyridine, complex **37** (Fig. 5) affords a high FE for CO evolution after 7 h of electrolysis (Table 1, entry 30).[95] The resulting activity improvement was attributed to the inhibition of inactive Mn-dimer formation during the catalysis.[95,100] Two other strategies to minimize dimerization were also investigated. One is immobilization of these molecular complexes on the electrode surface or within substrates such as metal organic frameworks and carbon nanotubes;[101,102–105] the other is replacement of the halide counter anions with a cyano group, which can stabilize the reduced Mn^0.[106]

DOI: 10.1016/j.enchem.2020.100034
EnergyChem **2**, 100034 (2020)

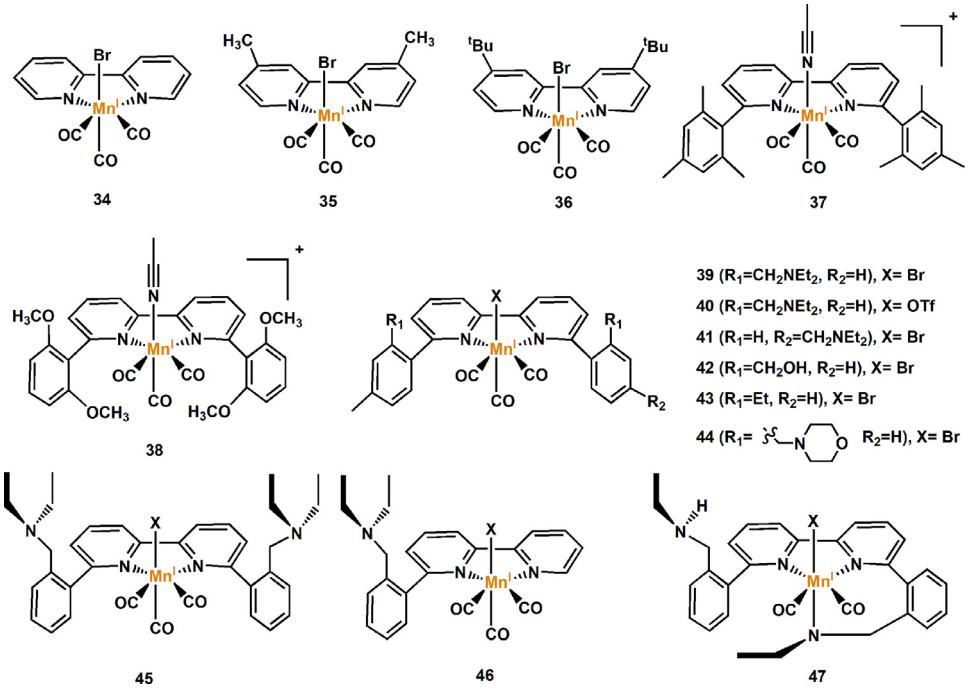

Fig. 5. Mn complexes based on polypyridines as molecular electrocatalysts for CO_2 reduction.

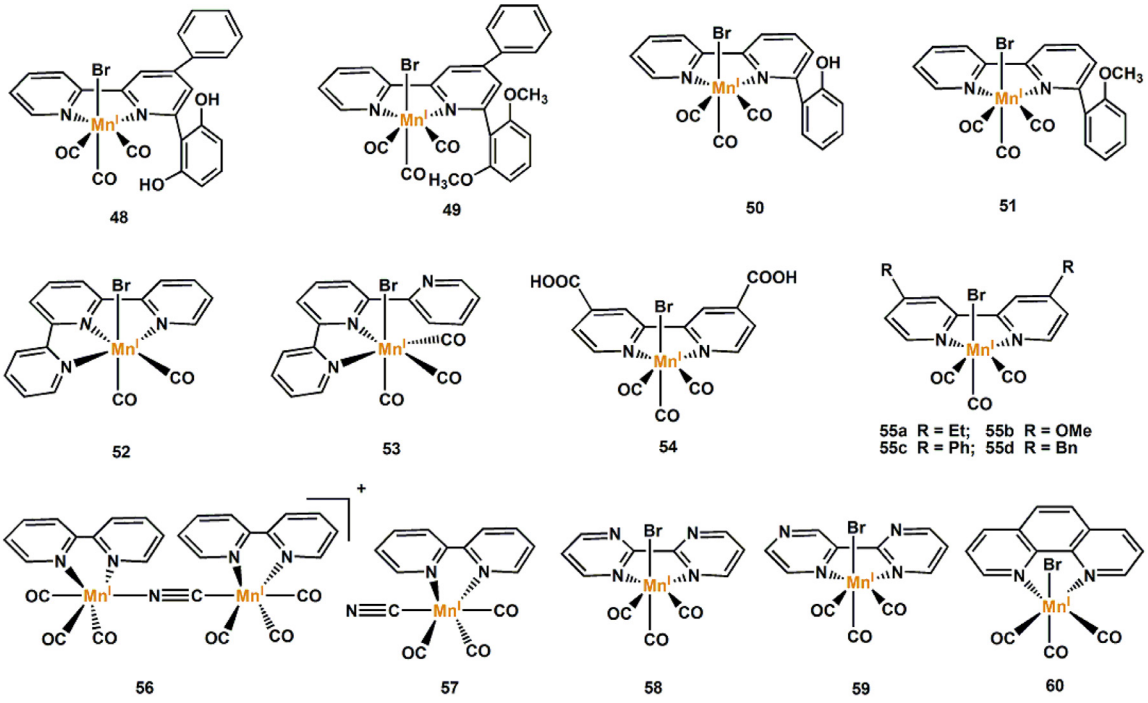

Fig. 6. Mn complexes based on polypyridines as molecular electrocatalysts for CO_2 reduction.

In addition to mesityl group, the 6,6′-positions can also be modified with methoxy–phenyl. The resulting complex **38** (*fac*-$Mn^I([(MeO)_2Ph]_2bpy\text{-}CO)_3(CH_3CN))^+$ (Fig. 5; $[(MeO)_2Ph]_2bpy$ = 6,6′-bis(2,6-dimethoxy-phenyl)−2,2′-bipyridine) possesses higher catalytic activity than **37** when proton source of either PhOH, TFE, H_2O, or MeOH is used.[107] Because the $[(MeO)_2Ph]_2bpy$ ligand in **38** introduces an additional electronic influence and noncovalent hydrogen-bonding interactions between C−OH and the pendant methoxy group that significantly lowers the activation barrier for C−OH bond cleavage from the metallocarboxylic acid intermediate. This provides an access to the protonation-first pathway, minimizing the overpotential required for electrocatalytic CO_2-to-CO conversion. It is well known that controlling the selectivity for different CO_2 reduction products is a significant scientific challenge. Very recently, Daasbjerg and co-workers

DOI: 10.1016/j.enchem.2020.100034
EnergyChem **2**, 100034 (2020)

explored a series of Mn complexes (**39–47**, Fig. 5) with modified bipyridine and phenanthroline ligands which can act as selective electrocatalysts for CO_2 reduction.[108] In this work, they found that the designed Mn complexes can reduce CO_2 to either HCOOH when the ligand contains tertiary amines in the ortho positions (**39, 40, 45, 46**, and **47**), or CO when the amine groups are absent in the modified ligand (**42, 43**, and **44**) or placed far from the metal center (**41**). Besides, the amine modified Mn complexes **39, 40, 45**, and **46** were able to reduce CO_2 to HCOOH at low overpotentials exceeding current state-of-the-art molecular catalysts (Table 1, entries 31–39).[108] Experimental and computational mechanistic investigations showed that the role of the amines is to act as proton shuttles leading to the formation of a key intermediate Mn-hydride species that enerates formic acid after CO_2 insertion and an additional protonation.

Introduction of local proton sources to molecular catalysts can effectively enhance the selectivity and activity for electrochemical CO_2 reduction. 4-phenyl-6-(1,3-dihydroxybenzen-2yl)−2,2′-bipyridine (dhbpy) ligand with a local proton source, and 4-phenyl-6-(1,3-dimethoxybenzen-2yl)−2,2′-bipyridine (dmobpy) without local proton source were introduced into Mn complexes respectively.[109,110] The complex $Mn(dhbpy)(CO)_3Br$ (**48**) (Fig. 6; Table 1, entriy 40), containing two −OH groups in proximity to the Mn center, was reported to electrochemically catalyze the reduction of CO_2 to CO, with a TOF similar to that of complex **34** even in the absence of an external proton source.[109,110] In contrast, the complex $Mn(dmobpy)(CO)_3Br$ (**49**; Fig. 6) containing methoxy groups showed no activity under the same conditions. These results demonstrate that local proton source is significant to enhance the activity of CO_2 reduction. Besides, Bocarsly and co-workers prepared MnBr(6-(2–hydroxyphenol)−2,2′-bipyridine)$(CO)_3$ (**50**) containing *a* −OH group and the counterpart (**51**) containing a methoxy group (Fig. 6).[111] They found that **50** shows to produce CO efficiently in good yield (76% in 4 h electrolysis) at 540 mV overpotential in CH_3CN/H_2O (95:5) mixture (Table 1, entry 41). In the presence of 5% water as the proton source, they observed that the hydroxyphenol derivative **50** shows increased current density and product yields when compared to the methoxy derivative **51** (Table 1, entry 42), further confirming the effect of local proton source on CO_2 electrochemical reduction. The Kubiak group later succeeded in attaching the κ^3-tpy and κ^2-tpy ligand with Mn^I to form complex **52** and **53** (Fig. 6), respectively.[112] Both **52** and **53** exhibited moderate activity for CO evolution and selective CO production (Table 1, entries 43–44). The κ^2-tpy of complex **53** evolved to bond with CO ligand (perhaps forming the κ^3-complex in situ), resulting in an abnormal FE(CO) value of 129%. These two complexes exhibit good activity for the electrocatalytic CO_2 reduction, whereas the competing degradation pathways limit their overall efficiency. This anomaly reminds researchers of paying attention to the catalyst stability.

Very recently, a water-soluble Mn polypyridyl complex $[Mn^I(bpy(COOH)_2)(CO)_3Br]$ (**54**; $(bpy(COOH)_2)$ = 4,4′-dicarboxy-2,2′-bipyridine; Fig. 6) was reported as an efficient electrocatalyst for CO_2 reduction.[113] Although the introduction of electron-withdrawing carboxylic groups did shift the reduction potentials of complex **54** in CH_3CN positively when compared with the unmodified bpy complex **34, 54** exhibited similar catalytic efficiency in CH_3CN/H_2O (95:5) electrolyte to the parent **34**.[113] Bocarsly and co-workers systematically studied the effect of the substituent in the 4,4′-postions of bpy on the catalytic CO_2 reduction. They synthesized several complexes of bpy with different substituents in the 4,4′-postions (**35, 36, 54**, and **55a-55d**; Figs. 5 and 6).[114] They found that these complexes with different aliphatic substituent has similar catalytic performance for CO_2 electroreduction, and increasing the steric bulk at the 4,4′-positions is an effective way to inhibit the formation of deactivated dimer, which improved the electrocatalytic CO_2 reduction efficiency.[95,114] They further designed a cyanide-bridged dinuclear Mn complex $([Mn(bpy)(CO)_3]_2(\mu\text{-}CN))^+$ (**56**) which is both electrocatalytic and photochemically active for CO_2 reduction to CO. Compared to the mononuclear complex $[Mn(bpy)(CO)_3CN]$ (**57**) (Table 1, entry 46), **56** is more efficient for CO_2 electroreduction using H_2O as a proton source (Table 1, entry 45).[115,116] In addition, Bocarsly and co-workers also studied 1,10-phenanthroline- or bipyrazine-based complexes *fac*-$[MnX\text{-}(N\text{–}N)(CO)_3]$ (**58–60**; Fig. 6) for CO_2 reduction. However, these complexes are nearly completely ineffective for catalytic CO_2 reduction as they are electronically deficient.[114]

Compared with Mn complexes, other non-noble-metal complexes of polypyridine ligands used for electrocatalytic CO_2 reduction are sporadically reported. In 1995, Che, Wong and co-workers found that quaterpyridine-based complexes $[Ni(qtpy)(CH_3CN)_2](ClO_4)_2$ (**61**) and $[Co(qtpy)(H_2O)_2](ClO_4)_2$ (**62**) (qtpy = 2,2′:6′,2″:6″,2‴-quaterpyridine; Fig. 7) can electronically catalyze CO_2 reduction.[117] **62** displays high activity and selectivity for CO_2-to-CO reduction in CH_3CN at −2.08 V vs Fc^+/Fc, with an FE of 80% (Table 1, entry 48). However, a film was rapidly formed on the glassy carbon surface electrode followed by a large decrease of CO production. In contrast, no film formation on the electrode was observed **61**. Its catalytic activity towards CO_2 reduction is much worse than that of **62**; only trace amount of CO was observed after CPE at −2.08 V vs Fc^+/Fc for one hour (Table 1, entry 47). In 2018, Robert, Lau and co-workers showed that the electrocatalytic reduction of CO_2 into CO by **62** could occur through two different mechanisms, depending on the presence of phenol (PhOH) in the solution.[118–120] Besides, they found that **62** and $[Fe^{II}(qtpy)(H_2O)_2](ClO_4)_2$ (**63**) feature high selectivity and low overpotential in proton-assisted electrochemical CO_2 reduction to CO in acetonitrile solution (Table 1, entries 49 and 50). For **62**, the two-electron reduced species activates CO_2 in the presence of PhOH, whereas for **63**, the one electron-reduced species Fe^Iqtpy can efficiently bind CO_2 to form the Fe^{II}qtpy $CO_2^{\cdot-}$ adduct which then experiences a one-electron reduction followed by C−O bond cleavage in the presence of a weak acid.[118,121] Then, they further reported an efficient hybrid system comprising another Co quaterpyridine complex $[Co(qpy)](Cl)_2$ (**64**) associated to the multi-walled carbon nanotubes.[122] With this hybrid system, the conversion of CO_2 to CO was achieved in water at neutral pH with 100% selectivity and 100% FE at low catalyst loading and with low overpotential (Table 1, entry 51). A current density 9.3 mA cm^{-2} could be sustained for 4.5 h at only 340 mV overpotential.

In 2014, a terpyridine Ni complex **65** developed by Artero and co-workers also shows activity for electrocatalytic CO_2-to-CO conversion in DMF/H_2O medium, in spite of relatively low FE(CO) (Table 1, entry 52).[123,124] Very recently, Reisner and co-workers modified the structures of complex **65** by using different functional groups (**65–68**; Fig. 7; Table 1, entries 53–56).[125,126] It was found that **65** and **68** display high selectivity for CO_2-to-CO conversion in CH_3CN/H_2O (v:v = 3:1), with over 95% selectivity in the first hour electrolysis. Besides, **65–68** were more efficient in CH_3CN/H_2O than in dry DMF.[123] Four terpyridine

DOI: 10.1016/j.enchem.2020.100034
EnergyChem **2**, 100034 (2020)

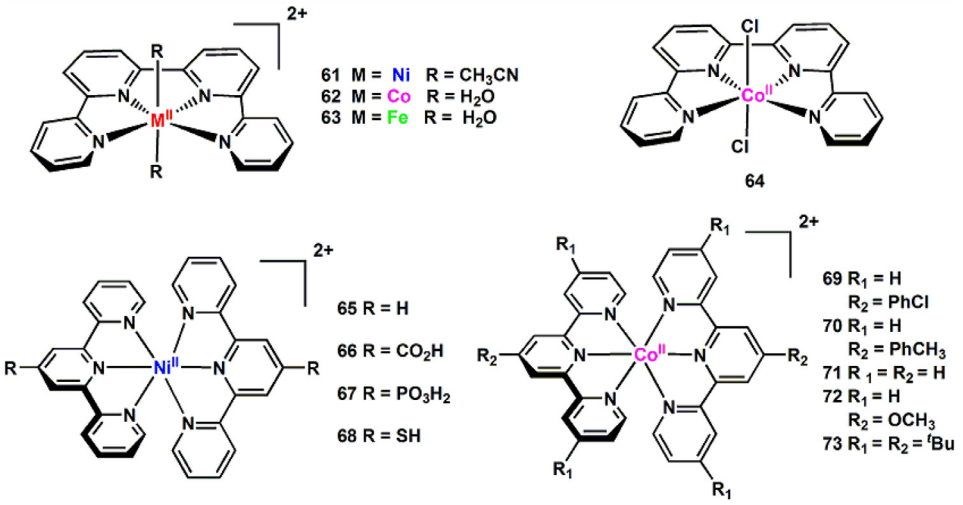

Fig. 7. Fe/Co/Ni complexes based on polypyridines as molecular electrocatalysts for CO_2 reduction.

Co complexes (**69–73**; Fig. 7) have been reported as electrocatalysts for CO_2 reduction to CO while H_2 was simultaneously produced from the requisite proton source.[127,128] Tuning the H_2:CO ratio was available through ligand modification (Table 1, entries 57–61). Different substituents, including withdrawing and donating groups, were attached to *para* positions to the nitrogen that binds with the metal centers. The electrochemical results showed that complexes with more donating groups favor more to proton reduction reaction.[127,129]

There are limited reports on Cu-polypyridyl complexes as electrocatalysts for CO_2 reduction. Durand and co-workers reported that cyclic voltammograms of $[Cu(phen)_3]^{2+}$ (**74**) in DMSO exhibit cathodic current enhancement under CO_2 at −1.96 and −2.12 V vs Fc^+/Fc, respectively.[130] They defined the catalytic mechanism as CO_2 reduction induced by ligand reduction. Based on this work, Costamagna reported a similar behavior of Cu complexes of hexaaza-macrocyclic ligands derived from the condensation of bipyridines $[Cu(hamc\text{-}bpy)]^{2+}$ (**75**) and phenanthrolines $[Cu(hamc\text{-}phen)]^{2+}$ (**76**), but no product was detected.[131–134] Another Cu complex, $[Cu(tpy)_2]^{2+}$ (**77**) for electrocatalytic CO_2 reduction was similarly assessed and electricity current increase was detected under CO_2, along with presence of deposition on carbon electrodes.[123] This observation is similar to electrocatalytic CO_2 reduction to formate by Cu-based electrodeposited materials and Cu electrodes.[135–139] Clearly, a proper ligand that could prevent the corresponding Cu(II) complex from Cu depositing is necessary for developing Cu(II) molecular electrocatalysts.

Besides the above-mentioned metals, other non-noble metals of polypyridyl ligands have also shown activity for electrocatalytic CO_2 reducton,[55,56,140–142] which have been detailedly summarized in some reviews.[5,53]

Metal complexes with porphyrin and porphyrin-like ligands

One of the most thoroughly investigated families of molecular catalysts for CO_2 reduction is iron porphyrins.[26,36,48,143,144] Although a porphyrin ligand is a part of macrocyclic one, we want to give it special attention due to its extensive use in molecular catalyst construction. Substituent effiects on catalyzing the electrochemical CO_2 reduction by Fe tetraphenylporphyrins have been thoroughly investigated. Derived from Fe tetraphenylporphyrin **78** (Fig. 8), complexes **79–83** are a type of very active electrocatalysts for the CO_2-to-CO conversion. Firstly, **78** was reported to catalyze the electrochemical CO_2 reduction at the Fe^I/Fe^0 redox potential (1.17 V vs Fc^+/Fc) in DMF.[145,146] However, the catalytic efficiency was very low and the catalytic activity of **78** was rapidly lost during preparative-scale electrolysis. The presence of weak Brönsted acids or Lewis acids can improve the catalytic efficiency of **78** (Table 1, entry 62).[147] In 2012, Costentin and co-workers introduced phenolic groups on the phenyl groups of Fe tetraphenylporphyrin, the resulting Fe 5,10,15,20-tetrakis(2′,6′-dihydroxyphenyl)porphyrin complex (**79**; Fig. 8) showed extremely enhanced electrocatalytic efficiency for CO_2 reduction to CO, with a CO faradaic yield of 94% after electrolysis at −1.88 V vs Fc^+/Fc for 4 h (Table 1, entry 63).[36] The average current density was 0.31 mA cm^{-2} at an overpotential of 466 mV. When the hydroxy groups in **79** were replaced by methoxy groups, the catalytic activity of obtained complex **80** (Fig. 7) decreased compared with that of **79** (Table 1, entries 64–65).[36] Therefore, the enhanced catalytic activity of **79** can be attributed to the high local concentration of protons supplied by the phenolic hydroxy substituents.[36] The prepositioned –OH groups play roles of H-bonding substituents to stabilize the Fe^0-CO_2 adduct and proton donors (or proton relays) to form protonated intermediate. With enough strong stabilization of the intermediate protonated adduct, the second electron transfer could take place before C−O bond cleavage. It is worthy to point out that the Cu complexes based on the same porphyrin derivatives can not act as molecular electrocatalysts for CO_2 reduction, as they transform into Cu nanoparticles onto the electrode during the electrolysis.[148,149] These examples further demonstrate that preventing Cu(II) complexes from Cu depositing is necessary for developing Cu(II) molecular electrocatalysts. It also reminds researchers of paying more attention to Cu(II)-based molecular electrocatalysts to identify the real active species.

In addition, modification of **79** with the electron-withdrawing substituents on phenyl groups is also an effective way to improve the catalytic efficiency. The strong inductive effect of electron-withdrawing substituents can significantly move the catalytic wave toward positive potentials. For example, introduction of 10 fluorine atoms on 2 phenyl rings of porphyrin complex **81** (Fig. 8) led to higher TOF at even more positive potentials, with

DOI: 10.1016/j.enchem.2020.100034
EnergyChem **2**, 100034 (2020)

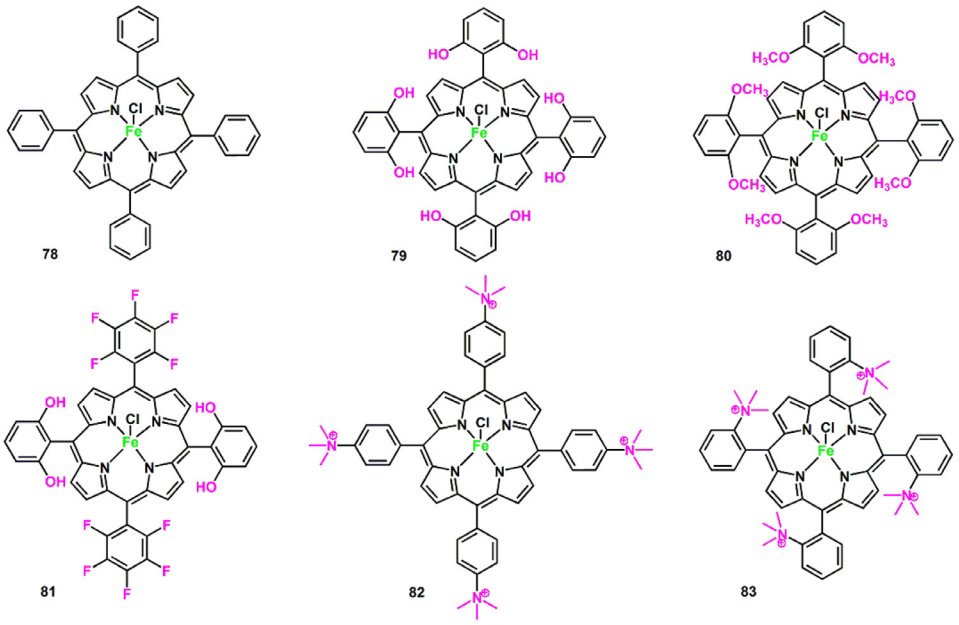

Fig. 8. Fe complexes based on porphyrin ligands as molecular electrocatalysts for CO_2 reduction.

a 70 mV anodic shift of the Fe^I/Fe^0 redox standard potential of **79** (Table 1, entries 66–67).[150] Furthermore, by introducing four charged trimethylanilinium groups in *para*- or *ortho*-position of the phenyls, the obtained **82** and **83** (Fig. 8) exhibited unprecedented catalytic efficiency in the presence of a large concentration of PhOH. The electro-withdrawing inductive effect of the four trimethylanilinium groups at the *para* positions of **82** is responsible for the significant positive shift of E^0 ($E^0 = -1.663$ V vs Fc^+/Fc, 165 mV more positive than **78**) (Table 1, entry 68).[27] This effect is even stronger when the trimethylanilinium groups are placed at the *ortho* positions in complex **83** ($E^0 = -1.344$ V vs Fc^+/Fc, 484 mV more positive than **78**). At −1.664 V vs Fc^+/Fc, **83** exhibits excellent catalytic performance of electrochemical reduction CO_2 to CO, with a FE of 100% (Table 1, entry 69).[27] More importantly, the catalyst is highly stable in catalytic conditions, showing no significant decrease in CO selectivity after electrolysis more than 80 h in DMF with 3 mol/L PhOH.[27] The high stability of **83** probably comes from the stabilization of the initial Fe^0-CO_2 adduct by interactions between the negative charges of oxygen atoms of CO_2 in the adduct and the positive charges of the trimethylanilinium substituents on the porphyrin phenyls.

Besides single Fe porphyrin, Fe porphyrin dimers were also designed and modified (**84–89**; Fig. 9; Table 1, entries 70–75).[151] All of them can efficiently and selectively electrocatalyze CO_2-to-CO conversion with high TOFs. The overpotential and TOF can be improved by the introduction of electronically different substituents to the porphyrin peripheral positions. Introduction of electron-withdrawing perfluorophenyl substituents to the *meso* positions of the dimer **84** reduces overpotential of ca. 300 mV compared with that of **88** with electron-donating mesityl groups. Control experiments demonstrated that the high performance of CO_2-to-CO conversion using these catalysts is due to the presence of dinuclear Fe centers at a suitable Fe-Fe distance. In general, the introduction of electron-withdrawing groups on catalysts promotes the positive shifts of their reduction potentials and consequently decreases the overpotential of the reaction. Therefore, the Fe porphyrin dimers are arranged in the following order with respect to their overpotential for the CO_2 to CO conversion: **84** < **89** < **85** < **86** < **87** < **88**.[151] However, this electron-withdrawing effect also causes the decrease of electron density at the active center, which sacrifices their nucleophilic activities and leads to the decrease of TOF, and vice versa. Thus, **88** with electron-donating mesityl groups on the porphyrin rings shows high TOFs in spite of high η value. Herein, it can be concluded that low overpotential and high TOF by electronic tuning is not compatible.[151] Besides the influence of the electron-withdrawing/donating effect of different substituents on porphyrin ligands, the Fe-Fe separations induced by the steric hindrance of different substituents should also be considered as a possible factor that influences the electracatalytic CO_2 reduction activity.

Other metal complexes with porphyrin-like ligand such as Ni- and Co-phthalocyanine (**90** and **91**; Fig. 9) have also been found electrochemically active to catalyze CO_2 reduction.[152,153] In 2017, Wang and co-workers explored a combination of nanoscale and molecule approach to construct hybrid material **91** as efficient and selective catalysts for electrocatalytic CO_2 reduction to CO.[154] On the nanoscale, **91** are uniformly anchored on carbon nanotubes to afford substantially enhanced catalytic performance, with a FE_{CO} of 92% (Table 1, entry 76). The catalytic performance is further improved by employing the modified Co-phthalocyanine **92** (Fig. 9) with electron-withdrawing cyano groups appended to the phthalocyanine macrocycle. The resulting hybrid catalyst exhibits 96% FE for CO production with a current density of 15.0 mA cm^{-2} at 520 mV in a near-neutral aqueous solution (Table 1, entry 77).[154] Based on this outstanding performance of **92**, Wang and co-workers developed alkaline microflow electrolytic cells with **92**, which can perform selective, durable and efficient CO_2 reduction to CO or $HCOO^-$ at low voltages.[155] **92** and SnO_2 nanoparticles can supported on carbon nanotubes as cathode electrocatalysts for CO_2 reduction to CO and $HCOO^-$, respectively. It was reported that the CO-selective cell starts to operate at an overpotential of 260 mV

DOI: 10.1016/j.enchem.2020.100034
EnergyChem **2**, 100034 (2020)

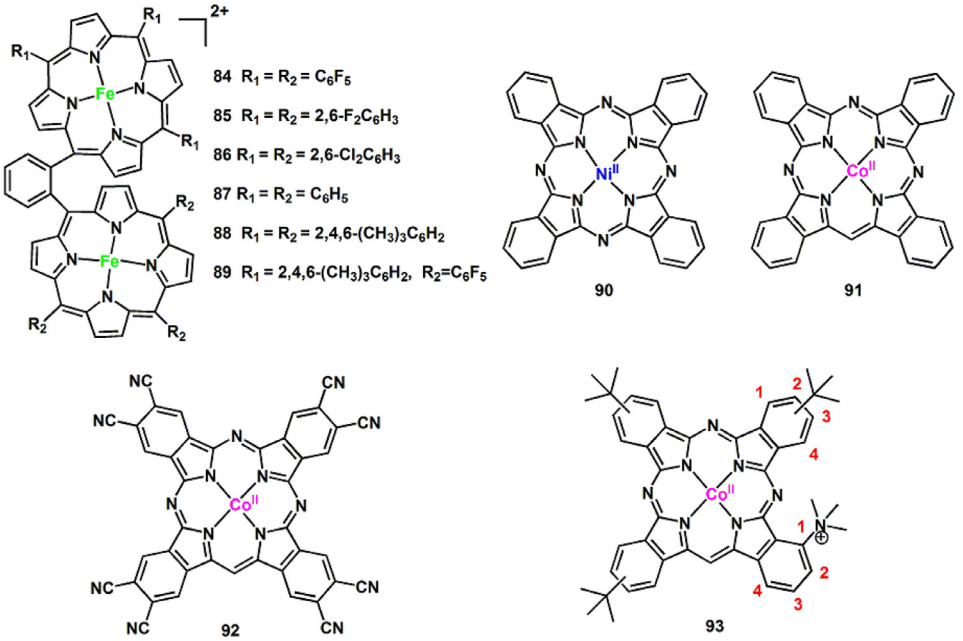

Fig. 9. Fe/Cu/Ni/Co complexes based on porphyrin and porphyrin-like ligands as molecular electrocatalysts for CO_2 reduction.

and reaches a FE of 94% (Table 1, entry 78). With a SnO_2-based cathode, the $HCOO^-$-selective cell starts to operate at an overpotential of 760 mV and reaches a FE of 82% (Table 1, entry 79).[155] In 2019, Robert and co-workers reported a new Co-phthalocyanine **93** (Fig. 9) bearing a trimethyl ammonium moiety and three tert–butylgroups appended to the phthalocyanine macrocycle. They found that the co-immobilization of **93** into porous films of carbon black powder or carbon nanotubes on a carbon paper cathode can efficiently electrocatalyze the CO_2-to-CO conversion in water over a broad pH range of 4–14. In a flow cell configuration operating in basic conditions (pH = 14), CO production occurs with good selectivity (ca. 95%), and good stability, with a maximum partial current density of 165 mA cm^{-2} (at −2.15 V vs Fc^+/Fc) (Table 1, entry 80).[156]

The single metal porphyrin can be connected together to form 3D framework material as heterogeneous electrocatalysts for CO_2 reduction.[39,157–160] In 2015, Zhang, Diercks, and Lin et al. designed a covalent organic framework (COF) by the condensation of Co porphyrin precursor **94** with 1,4-benzenedicarboxaldehyde.[159,160] The obtained catalyst **95** (Fig. 10) displays high activity, selectivity and stability for electrochemical reduction of CO_2 to CO in pH 7.3 water solution, with an initial TOF of 56.3 h^{-1}. The FE(CO) reaches as high as 90% after electrolysis for 24 h (Table 1, entry 82). **95** shows a substantial improvement over the precursor **94** which has an initial TOF of 33.1 h^{-1} under the same conditions (Table 1, entry 81). It is reasoned that a larger pore size would allow higher capacity of CO_2 adsorption inside the framework as well as higher electrochemical and chemical accessibility of the catalytic Co porphyrin active sites. Based on this knowledge, an analog of **96** (Fig. 10) by replacing 1,4-benzenedicarboxaldehyde with biphenyl-4,4′-dicarboxaldehyde was designed. As expected, **96** exhibits improved catalytic efficiency compared with **95**, with FE(CO) of 91% (Table 1, entry 83).[159] These results indicate that lattice expansion allows more efficient exposure of the electroactive sites to the substrate molecules. Besides, X-ray absorption data showed that the COF framework can directly influence the electronic structure of the catalytic Co centers in a manner similar to redox noninnocent ligand behavior observed in molecular systems. This effect greatly contributes to the increase of reaction selectivity and activity and is beyond the steric effects of surface area and site isolation. Recently, Chang et al. designed a porous organic cage (**97**; Fig. 11) for electrochemical CO_2-to-CO conversion, which is composed of six molecular catalysts **78**.[39] The porous architecture of **97** results in a larger amount of exposed electroactive iron centers compared with the monomeric counterpart **78**, which facilitates CO production with superior rate, current density, and stability. It was found that **97** exhibits a TOF of 0.64 s^{-1} after electrolysis for 24 h in 0.5 M $KHCO_3$ water solution (Table 1, entry 84).[39] In contrast, **78** attained a lower TOF of 0.38 s^{-1}after 24 h under the same conditions (Table 1, entry 85).[39]

For metal-porphyrin molecular electrocatalysts with bad solubility, coating them on electrodes or other supports can extend their catalytic functions.[152,155,161–169] The tetraphenyl Co porphyrin (**98**; Fig. 12) was deposited at a carbon black gas diffusion electrode, which produces CO with 97% FE at −1.40 V vs Fc^+/Fc under 20 atm of CO_2 in 0.5 M $KHCO_3$ solution (Table 1, entry 86). More recently, a Co-porphyrin-like complex (**99**; Fig. 12) adsorbed onto carbon nanotubes can also electrochemically reduce CO_2, with the FE(CO) of 80%, and TOF of 39.3 h^{-1} at 700 mV overpotential (Table 1, entry 87).[170] Besides, a Co protoporphyrin (**100**; Fig. 12) adsorbed onto pyrolytic graphite can produce CO even at high acidity of pH 3 under 10 atm of CO_2, with a 50% FE and 500 mV overpotential (Table 1, entry 88). At pH 1, 2.3% FE of CH_4 was also obtained (Table 1, entry 89).[162,171] Very recently, a pyrene-derivatized Fe triphenylporphyrin **101** (Fig. 12) derived from **79** was adsorbed on multiwalled carbon nanotubes via non-covalent interactions. The modified carbon material is able to catalyze CO_2-to-CO conversion at low overpotential in neutral pH unbuffered water solution.[37] After optimization, CO was formed with a high selectivity (CO/H_2 = 92:8) and an excellent total faradaic yield (97%; Table 1, entry 90).

DOI: 10.1016/j.enchem.2020.100034
EnergyChem **2**, 100034 (2020)

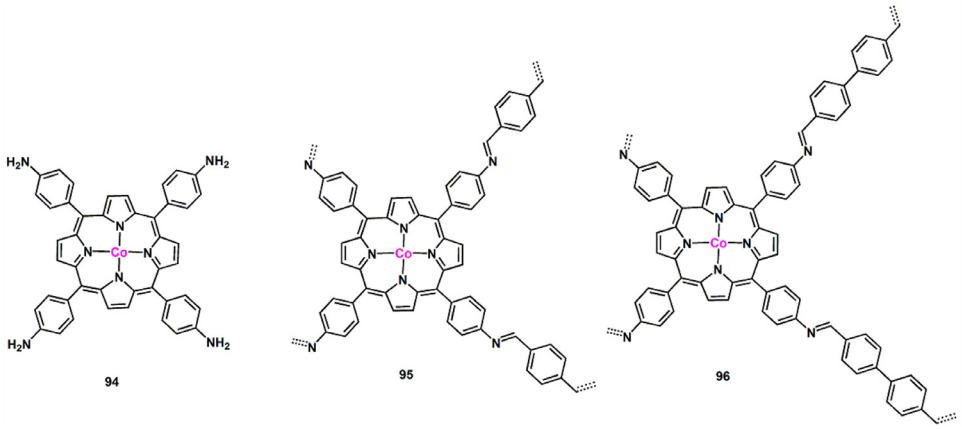

Fig. 10. Co porphyrin and the derived COFs as electrocatalysts for CO_2 reduction.

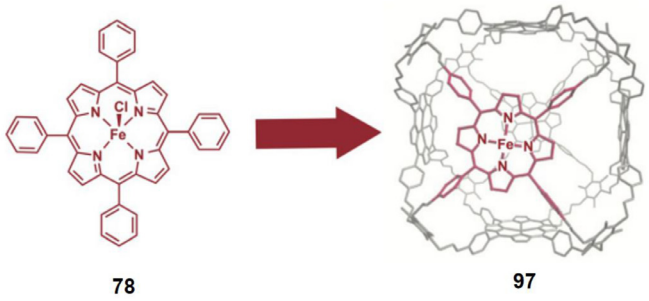

Fig. 11. Fe porphyrin **78** and the derived cage **97** catalyst used for electrochemical CO_2 reduction. Reproduced with permission.[39] Copyright 2018, Wiley-VCH.

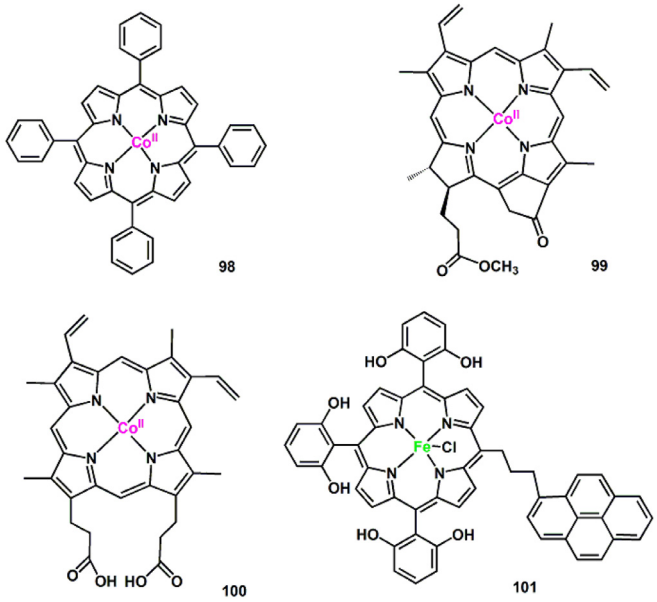

Fig. 12. Metal porphyrins and their derivatives/analogues as CO_2 electrocatalysts.

DOI: 10.1016/j.enchem.2020.100034
EnergyChem **2**, 100034 (2020)

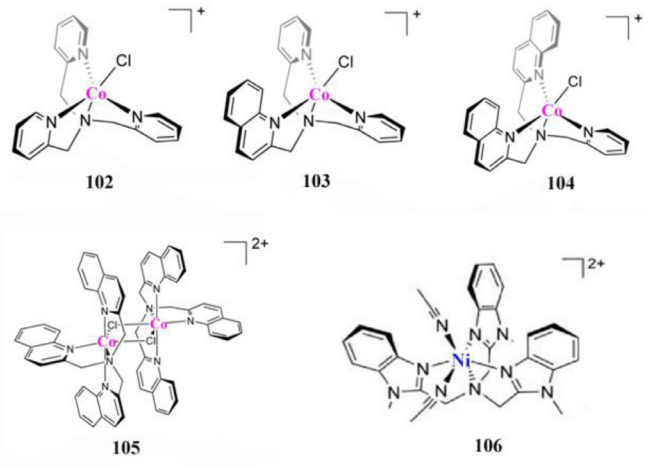

Fig. 13. Co/Ni complexes based on nonplanar N_4 ligands as molecular electrocatalysts for CO_2 reduction.

Metal complexes with nonplanar N_4 ligands

Metal complexes supported by nonplanar N_4 ligands always display trigonal bipyramidal geometry or *cis*-octahedral coordination geometry, in which the axial coordination site always combines with a solvent molecule. The solvent molecule can be easily disociated, generating unsaturated coordination site for CO_2 activation and transformation.[172–174] Thus, metal complexes supported by nonplanar N_4 ligands are potential catalysts for CO_2 reduction. Recently, our group developed four Co complexes with nonplanar tetradentate N_4 tripodal ligands for CO_2-to-CO conversion (**102–105**; Fig. 13).[175] It was found that replacing pyridyl groups in the ligand with quinolyl groups one by one led to positive shifts of the $Co^{II/I}$ reduction waves (from −1.72 to −1.54 V vs Fc^+/Fc), which indicates the increasingly easier $Co^{II/I}$ reduction and better catalytic activity. This positive shift can be attributed to the weaker basicity[27] of quinolyl group than pyridyl group. The Co^{II} center surrounded by quinolyl groups possesses a lower electron density and is easier to undergo $Co^{II/I}$ reduction than the one surrounded by pyridyl groups. **102, 103** and **104** can achieve 72%−84% FE and over 90% selectivity for CO evolution (Table 1, entries 91–93).[175] For **105**, though the CPE showed poor FE (41%) (Table 1, entry 94) for CO formation presumably because the bulky ligand sterically impedes CO_2 binding to Co^I center, **105** is still able to convert CO_2 to CO at a very low reduction potential of −1.54 V vs Fc^+/Fc. The result indicates that the introduction of less basic group into the catalytic center is an effective strategy to enhance the electrocatalytic performance for CO_2 reduction. Furthermore, with the addition of water, the overpotentials of complexes **102** to **105** for electrocatalyzing CO_2 reduction can be further reduced,[175] achieving 260 and 200 mV for **104** and **105,** respectively. These values are lower than those of most reported molecular electrocatalysts.[12,36,96,176] This significant decrease demonstrates the importance of proton source on electrocatalytic performance. Then we further designed and synthesized a tripodal complex $[Ni^{II}(Me_3NTB)(CH_3CN)_2](BF_4)_2$ (**106**; Me_3NTB = tris(N-methylbenzimidazol-2-ylmethyl)amine; Fig. 13). We found that **106** can not only homogeneously electrocatalyze CO_2 reduction, but also electrocatalyze H_2O reduction, to produce syngas with different CO/H_2 ratio (Table 1, entry 95). After compared with the catalytic performance of four other Ni(II) complexes based on nonplanar N_4 ligands structurally similar to NTB, we found that the good catalytic performance of **106**, including the activity and robustness, is closely related with the redox innocence of NTB ligand.[177]

Metal complexes with N-heterocyclic carbene ligands

Based on previous work on Ni macrocyclic complexes that showed high selectivity for activating CO_2 over H_2O under reductive electrocatalytic conditions,[10,58] Chang and co-workers reasoned that planar, electron-rich systems with a d_{z2}-based nucleophile could provide a promising platform for CO_2 reduction. They found that N-heterocyclic carbene ligands can be used to construct metal complexes for electrochemical CO_2 reduction and prepared a series of Ni N-heterocyclic carbene complexes as CO_2 reduction electrocatalysts.[28,178] In 2011, three Ni complexes (**107–109**; Fig. 14) based on tetradentate N-heterocyclic carbene-pyridine ligands were synthesized.[178] Extension of alkyl linkers in the ligand enhances the catalytic performance of corresponding Ni complexes for CO_2 reduction, yielding a more positive catalytic potential and a higher TOF during CPE (TOF of 3.9, 4.2 and 5.9 h^{-1} for **107, 108** and **109**, respectively) (Table 1, entries 96–98). This relationship is attributed to the structural flexibility of the Ni complex provided by the extended linkers, which enable a more distorted tetrahedral geometry in d^9 Ni^I species and thus facilitate reduction events.[178] Then in 2013, Chang and co-workers expanded the π conjugation system of the ligand and discovered that the extended conjugation at appropriate location enhances the catalytic performance of the corresponding Ni complexes (**110–114**; Fig. 14).[28] By systematically tuning the location and type of conjugations in **110–114**, Chang and co-workers found that N-heterocyclic carbene-isoquinoline complex **110**, in which pyridyl groups were replaced with isoquinolyl ones, has the lowest overpotential at E_{onset} = −1.58 V vs Fc^+/Fc for electrochemical CO_2 reduction. **110** also achieves a FE(CO) of 90% in dry CH_3CN electrolyte for 30 min of CPE. However, when CPE duration extended to 8 h, FE(CO) decreased from 90% to 22% (Table 1, entry 99). Less than 1 μmol of CO was yielded after electrolysis in a 0.02 mM of electrocatalyst at a glassy carbon electrode, which was ascribed to re-oxidation of accumulated products at the counter electrode. Low reactivity and stability of these Ni complexes thus triggered needs for improvement by ligand modification.

DOI: 10.1016/j.enchem.2020.100034
EnergyChem **2**, 100034 (2020)

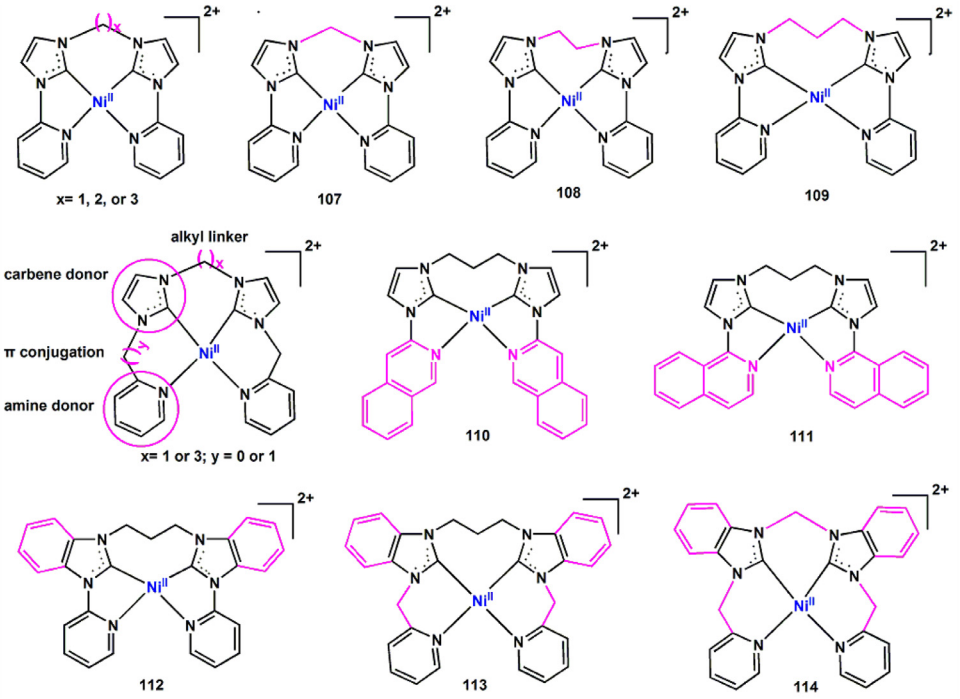

Fig. 14. Ni complexes based on N-heterocyclic carbene ligands as molecular electrocatalysts for CO_2 reduction.

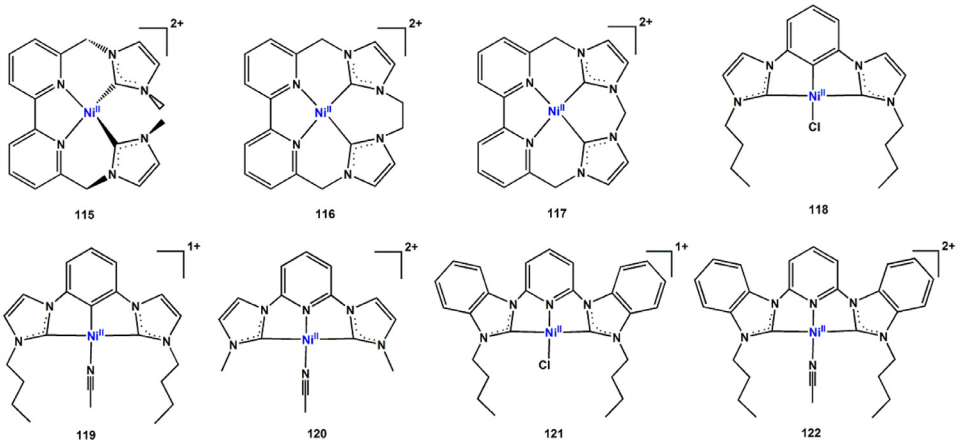

Fig. 15. Ni complexes based on N-heterocyclic carbene ligands as molecular electrocatalysts for CO_2 reduction.

A case of selectivity enhancement by ligand modification was achieved for Ni complexes (**115–117**; Fig. 15).[179–181] CPE of each complex was carried out in CO_2-saturated CH_3CN solutions containing 2% H_2O.[179] **115** supported by a non-macrocyclic ligand gave a FE of 93% for H_2 and only 5% for CO (Table 1, entry 100), whereas the less rigid 16-membered macrocyclic complex **116** exhibits moderate selectivity for both CO (56%) and H_2 (43%) (Table 1, entry 101).[179] On the other hand, the 15-membered macrocyclic complex **117** gives high selectivity for CO_2 reduction to CO with a FE of 87% at an applied potential of 2.44 V vs Fc^+/Fc (Table 1, entry 102).

Hollis et al. reported that a CCC–NHC pincer Ni complex (**118**; Fig. 15) could electrochemically catalyze CO_2 reduction to CO efficiently.[182] A TOF of 10 s^{-1} in the absence of water was estimated from cyclicvoltammetry measurements (Table 1, entry 103). To probe the influence of Cl^- in **118**, the Cl^- was replaced with acetonitrile. The resulting complex (**119**; Fig. 15) are also active for electrochemical CO_2 reduction, yielding a TOF of 3 s^{-1} (Table 1, entry 104). However, complex **119** could not be served as a suitable counterpart, as **118** is neutral while **119** is cationic.[182] It deserves to be mentioned that the catalytic rate of **119** is 2 times higher than that of the CNC–Ni complex **120**[183] (Table 1, entry 105) supported by a carbene-pyridine-carbene ligand, also vividly demonstrating the significance of the ligand modification. Recently, another two charged bis(N-heterocyclic carbene) pincer Ni complexes **121** and the corresponding dicationic acetonitrilo species **122** (Fig. 15) were designed and used for electrochemical CO_2 reduction.[184] For **121**, electrolysis was performed at −1.90 and −2.25 V vs Fc^+/Fc, yielding little CO in the headspace gas (2%

DOI: 10.1016/j.enchem.2020.100034
EnergyChem **2**, 100034 (2020)

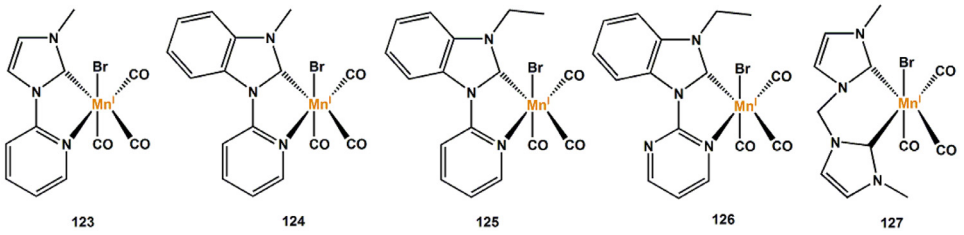

Fig. 16. Mn complexes based on N-heterocyclic carbene ligands as molecular electrocatalysts for CO_2 reduction.

and 4%, respectively) and a FE of 60% for H_2 and CO combined (Table 1, entries 106–107). In the case of **122**, the overall FE for gas production increased to nearly unity, but also yielded low ratios of CO in the produced gas, with 4% and 2% at −2.00 and −2.35 V vs Fc^+/Fc, respectively (Table 1, entries 108–109).[184]

Asymmetric ligands deviated from the traditional 2,2-bipyridyl ligand scaffold were also utilized for designing CO_2 reduction electrocatalysts. The N-methyl-N'-2-pyridyli midazol-2-ylidine (Me-impy) and N-methyl-N'-2-pyridylbenzi midazol-2-ylidine (Me-bimpy) ligands were two typical ones firstly reported by Agarwal and co-workers.[185] Their Mn complexes (**123** and **124**; Fig. 16) exhibit selective CO formation in CH_3CN electrolyte containing 5% H_2O albeit with poor FE(CO) (< 35%) (Table 1, entries 110–111). To counter the strong electron donation influence of NHC ligand, Agarwal and co-workers later replaced pyridine with the more π-acidic pyrimidine ring to get complex **126** (Fig. 16). This leads to a 160 mV positive shift in catalyst activation relative to **125** (Table 1, entry 112), which results in an improvement in CO production (FE(CO) = 72%) (Table 1, entry 113).[186] In 2018, using methylene bis(N-methylimidazolium), Royo, Lloret-Fillol, and co-workers developed a bis-NHC Mn(I)-based electrocatalyst (**127**; Fig. 16).[187] The strong electron donating character of two NHC coordination sites enables the concerted 2-electron reduction potential shift more negative to −2.30 V vs Fc^+/Fc, a shift of approx −0.3 V vs Fc^+/Fc relative to **123**. Although **127** has a higher overpotential for electrochemical CO_2 reduction, its greater nucleophilicity eliminates the need for an added Brønsted acid, resulting in a peak catalytic current in anhydrous CH_3CN with an impressive TOF_{max} of 14 h^{-1}.[187] CPE conducted at −2.32 V vs Fc^+/Fc gave rise to a current density of 2.5 mA cm^{-2} with FE(CO) of 92% after 4 h (Table 1, entry 114). In-situ IR-SEC electrocatalysis studies confirmed the formation of HCO_3^-/CO_3^{2-} and identified the tetracarbonyl $[Mn(bis\text{-}^{Me}NHC)(CO)_4]^+$ intermediate. Addition of H_2O to the electrolyte resulted in a linear increase in the catalytic current response from 0.09 to 0.56 M H_2O, with an exceptional TOF of 2.5 h^{-1} for **127** in CH_3CN in the presence of 0.56 M H_2O. Highly-selective CO formation (FE(CO) = 98%; Table 1, entry 115) was achieved by CPE conducted at −2.32 V vs Fc^+/Fc in the presence of 0.22 M H_2O for more than 6 h.[187] It is also noteworthy that the catalytic current dropped dramatically with higher concentrations of H_2O over 0.56 M.

Metal complexes with phosphine/sulfur/bridging ligands

Apart from the aforementioned ligand modification, phosphine, sulfur, and bridging ligands were also employed to construct molecular catalysts for CO_2 reduction. In the early stage of electrocatalysis of CO_2 reduction using molecular catalysts, Kubiak and co-workers reported a series of Ni complexes with phosphine ligands for electrocatalytic CO_2 reduction in the 1980s and 1990s.[188–190] They found that a cradle-like dinuclear Ni complex $[Ni_2(\mu\text{-}CNCH_3)(CNCH_3)_2(\mu_2\text{-}dppm)_2]$ (**128**; dppm = bis(diphenylphosphino)methane; Fig. 17) could catalyze the electroreduction of liquid CO_2 to CO at approximately −1.32 V vs Fc^+/Fc (Table 1, entry 116).[189] ^{13}C isotope labeling experiments confirmed the CO_2-to-CO conversion. However, further catalytic reaction was hindered because the dinuclear Ni complex captured the evolved CO to yield a $Ni_2(\mu\text{-}CO)(CO)_2(\mu_2\text{-}dppm)_2$ species. Then, an iodine-capped trinuclear Ni complex, $[Ni_3(\mu_3\text{-}I)(\mu_3\text{-}CNCH_3)(\mu_2\text{-}dppm)_3]PF_6$ (**129**; Fig. 17), was synthesized and used for electrochemical CO_2 reduction.[190–192] The electrocatalytic results show that the transformation of CO_2 in anhydrous DMF proceeds via a reductive disproportionation process, yielding CO and CO_3^{2-} as the predominant products. With addition of proton reagent to the system, the dominant product changes to $HCOO^-$. More recently, another series of dinuclear Ni complexes, $[Ni_2(\mu\text{-}CNR)(CNR)_2(\mu_2\text{-}dppa)_2]$ (R = methyl (**130**), n–butyl (**131**), and 2, 6-$(CH_3)_2C_6H_3$ (**132**); dppa = bis(diphenylphosphine)amine; Fig. 17) were designed and synthesized for electrocatalytic CO_2 reduction.[188,193,194] In these complexes, **131** is an efficient electrocatalyst for CO_2 reduction to CO, achieving a TOF of 0.1 s^{-1} (Table 1, entry 117).

Besides Ni complexes, Mn, Cu and Co complexes of phosphine ligands were also developed as CO_2 reduction electrocatalysts.[195–204] Mn^I complex with a planar coordinating tridentate PNP ligand (**133**; Fig. 17) was recently synthesized and studied. It shows excellent selectivity for CO production (close to 100%) in dry CH_3CN during electrolysis of more than 5 h at 960 mV overpotential (Table 1, entry 118).[195,196] The presence of carbonate indicates the reductive disproportionation of CO_2. Unexpectedly, the catalytic activity dropped when 5% water was added to the solvent with concurrent H_2 evolution (41% FE upon 1.7 h electrolysis), suggesting a competitive pathway to CO_2 reduction (Table 1, entry 119). Kubiak and Haines also studied metal complex based on phosphine ligand for CO_2 reduction. They reported a dinuclear copper complex $[Cu_2(mPPh_2bpy)_2(CH_3CN)_2]^{2+}$ (**134**; PPh_2bpy = 6-diphenylphosphino-2,2′–bipyridine; Fig. 17), which can catalyze reduction of CO_2 to produce CO and CO_3^{2-} selectively (Table 1, entry 120).[197–199] In addition, Artero, Derat and co-workers developed a series of Co complexes $([CpCo(P^R_2N_2^{R'})I]^+$ **135–138**; Fig. 17) based on diphosphine ligands ($P^R_2N_2^{R'}$). The two pendant amine residues in the ligands can act as proton relays during CO_2 reduction processes. These Co complexes show good electrocatalytic CO_2 reduction activity, with selective production of HCOOH in DMF/H_2O mixture (FE(HCOOH) of 90%) at moderate overpotentials (500–700 mV) (Table 1, entries 121–125).[200,201] Among four complexes $[CpCo(P^R_2N_2^{R'})I]^+$, **135** with the most electron-donating phosphine ligand (R = cyclo-

DOI: 10.1016/j.enchem.2020.100034
EnergyChem **2**, 100034 (2020)

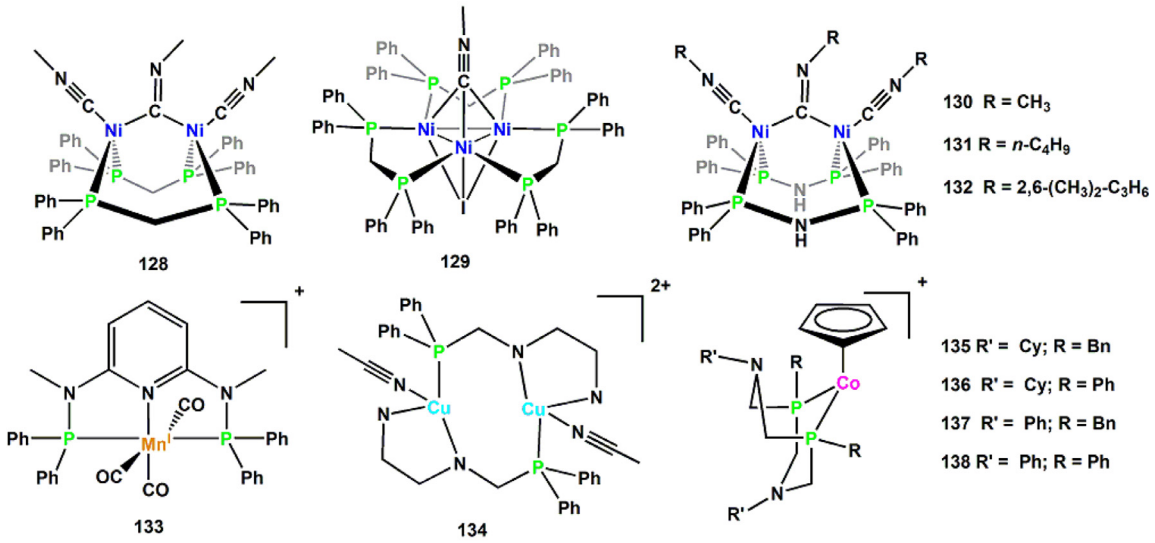

Fig. 17. Complexes based on phosphine ligands as molecular electrocatalysts for CO_2 reduction.

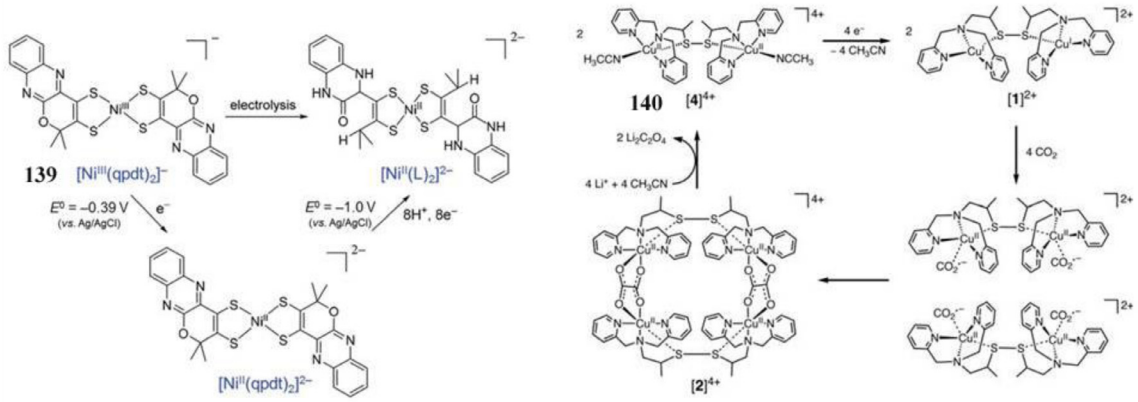

Fig. 18. Ni and Cu complexes based on sulfur ligands as molecular electrocatalysts for CO_2 reduction. Ni complex: Reproduced with permission.[205]. Copyright 2018, American Chemical Society; Cu complex: Reproduced with permission [34] Copyright 2010, AAAS.

hexyl) and the most basic amine (R' = benzyl) exhibits the best catalytic activity, with a TOF of 23 h^{-1} or 15 h^{-1} in the presence of 1.1 or 0.56 M water, respectively, after electrolysis at −2.25 V vs Fc^+/Fc for 1 h (Table 1, entries 121–122).[200] Mechanistic studies and DFT simulation results revealed that amine groups could stabilize the key intermediates through H-bonding with water molecules during the process of hydride transfer from the Co center to the CO_2 molecule.

Inspired by CO-dehydrogenase, formate dehydrogenase, [FeFe]- and [NiFe]-hydrogenases with the metal active sites chelated by S atoms,[205–209] a Ni complex $[Ni^{III}(qpdt)_2]^-$ (**139**; Fig. 18) with a quinoxaline-pyran-fused dithiolene ligand ($qpdt^{2-}$) was used as a electrocatalyst for CO_2 reduction. Using a Hg/Au amalgam electrode, formic acid was found the main product, with FE of 60% after 4 h electrolysis at −2.40 V vs Fc^+/Fc. Minor amounts of CO (19% FE) and H_2 (9% FE) were also formed, giving a total FE of nearly 90% (Table 1, entry 126).[205] During the electrolysis, a complete reduction of ligand $qpdt^{2-}$ first occurs, followed by the subsequent pyran ring open to give the real active catalyst ($[Ni^{II}(L)_2]^{2-}$.[205] Then, a Ni-hydride intermediate $[Ni^{III}(H)(L)_2]^{2-}$ is formed after an one-electron reduction process of $[Ni^{II}(L)_2]^{2-}$ and an addition with H^+.[205] The $[Ni^{III}(H)(L)_2]^{2-}$ species then reacts with CO_2, and the real electrocatalyst $[Ni^{II}(L)_2]^{2-}$ was renewed after the release of $HCOO^-$.[205] Besides, Bouwman and co-workers reported a dinuclear Cu(II) complex based on a sulfur ligand ($[4]^{4+}$, **140**; Fig. 18).[34] **140** can catalyze the one-electron reduction of CO_2 in CH_3CN in the presence of $LiClO_4$, to produce lithium oxalate at −0.72 V vs Fc^+/Fc (Table 1, entry 127).[34,210] The electrochemical reduction of $[4]^{4+}$ at a cathodic peak potential (E_{pc}) of −0.63 V vs Fc^+/Fc produces a dinuclear Cu(I) complex ($[1]^{2+}$) that is later oxidized in air selectively by CO_2 to yield a tetranuclear Cu(II) complex containing two bridging CO_2-derived oxalate groups ($[2]^{4+}$). The treatment of the Cu(II) oxalate complex in CH_3CN with a soluble lithium salt yields the initial $[4]^{4+}$ and results in the quantitative precipitation of lithium oxalate.[34] DFT calculations suggest that one CO_2 molecule is first reduced cooperatively by two Cu(I) metals to give a fully delocalized mixed-valence Cu^I/Cu^{II} ($CO_2^{\cdot-}$) radical anion intermediate, which is further partial reduction of metal-ligated CO_2 molecule and (metal-mediated) nucleophilic-like attack on the carbon atom of an incoming

DOI: 10.1016/j.enchem.2020.100034
EnergyChem 2, 100034 (2020)

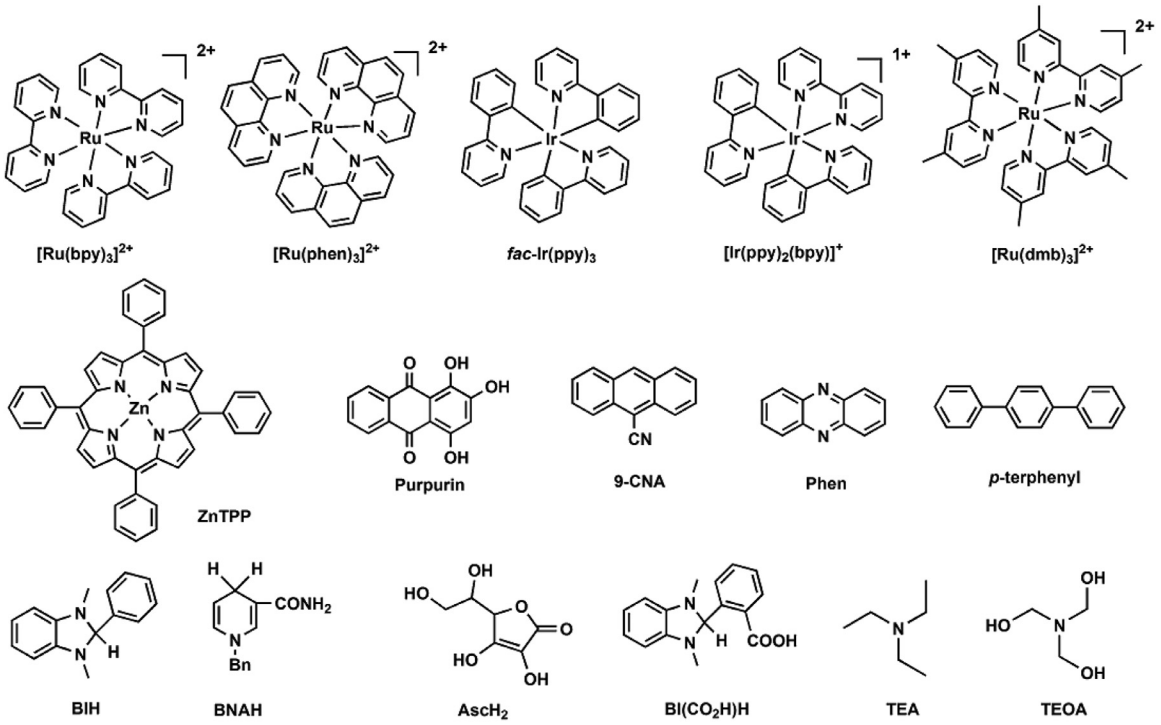

Fig. 19. Photosensitizers (PSs) and sacrificial donors (SDs) usually used for photochemical CO_2 reduction.

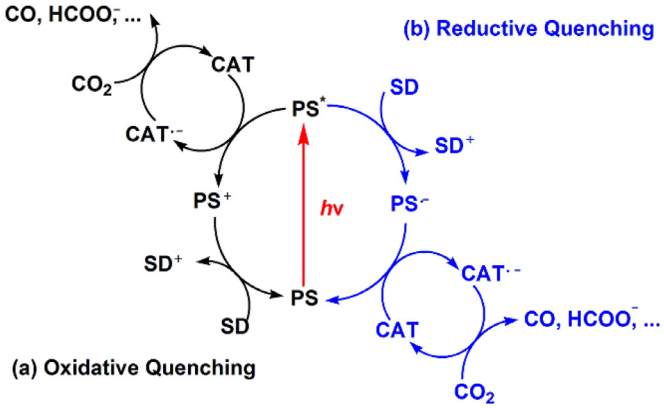

Fig. 20. Oxidative quenching and reductive quenching modes of PS* in molecular photocatalytic CO_2 reduction systems. Reproduced with permission.[16] Copyright 2018, Elsevier.

second CO_2 molecule to afford the dinuclear Cu(II)-oxalate product ($[2]^{4+}$).[211,212]

PHOTOCATALYTIC CO_2 REDUCTION

Beside electricity, solar-driven CO_2 reduction has also attracted extensive research interests. This process can not only reduce the CO_2 concentration in atmosphere, but also achieve the transfer and storage of the solar energy. Many molecular catalysts with high-performance for electrochemical CO_2 reduction are also efficient in photochemical CO_2 reduction.[11] Typically, molecular photocatalytic system for CO_2 reduction comprises a molecular catalyst (CAT), a sacrificial electron donor (SD), and a molecular photosensitizer (PS) that can photochemically mediate the transfer of electrons from SD to CAT (see Fig. 19).[11] The first step for photocatalytic CO_2 reduction is excitation of the PS to generate its lowest energy thermally equilibrated excited state (PS^*) under light irradiation. The excited PS^* should be sufficiently long-lived to facilitate a subsequent bimolecular electron-transfer reaction via two possible paths: oxidative quenching and reductive quenching (see Fig. 20). In oxidative quenching, the electron transfers from PS^* to a CAT to generate a PS^+ and a $CAT^{\cdot-}$ species. The PS^+ then reacts with a SD. The resulting $CAT^{\cdot-}$ species further gives an electron to the binding CO_2 molecule to form reduction product. To make this electron-transfer reaction thermodynamically exergonic, the $E(PS^+/PS^*)$ reduction potential should be more negative than the $E(CAT/CAT^{\cdot-})$ one. However, this is rare for CO_2 reduction catalysts which generally have very negative reduction potentials. In reductive quenching, the electron transfers from SD to PS^* to

DOI: 10.1016/j.enchem.2020.100034
EnergyChem 2, 100034 (2020)

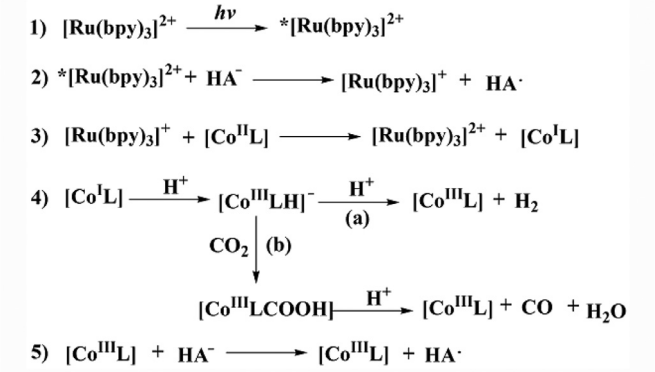

Scheme 2. Proposed mechanism of photochemical reduction of CO_2 to CO by Tinnemans et al. Reproduced with permission.[24] Copyright 1984 Wiley-VCH.

generate a strong reductant $PS^{\cdot-}$ and SD^+ species. $PS^{\cdot-}$ will then transfer one electron to CAT to produce $CAT^{\cdot-}$ species. The resulting $CAT^{\cdot-}$ species further reduces the binding CO_2 molecule to obtain corresponding reduction product. Similarly, to make this electron-transfer reaction thermodynamically exergonic, the $E(PS^*/PS^{\cdot-})$ redox potential of PS should be more positive than the $E(SD^+/SD)$ redox potential. The reductive quenching mechanism is typically kinetically favored since the concentration of SD is generally orders of magnitude greater than the catalyst concentration.[16] Although reaction paths are different, the one electron-reduced catalyst ($CAT^{\cdot-}$) is necessary in both systems. In most cases, the $CAT^{\cdot-}$ species is the active intermediate for CO_2 binding and conversion. Therefore, the generation of a reduced catalyst species ($CAT^{\cdot-}$) by photo-induced electron transfer (PET) is critical for a photocatalytic system.[4]

Similar to catalysts in electrochemical systems, the reduced CAT in photochemical systems need release a ligand and bind a CO_2 molecule to form the corresponding CO_2 adduct. However, there are some significant differences between two systems. In electrochemical conditions, many highly reducing electrons (with the same potential) are available from the electrode interface to reduce CAT and the CO_2 adduct. However, in photochemical systems, only one electron is transferred to the CAT through a bimolecular electron-transfer reaction. A second electron thus must be supplied by another source, such as the second bimolecular electron-transfer reaction, the deprotonation product of the oxidized SD (which is usually a strong reductant), or another CAT that has been reduced through disproportionation. Generally, the photochemical CO_2 reduction is likely to be less efficient than the electrochemical method due to the slow electron transfer.[11] Therefore, it is particularly significant to accelerate the electron transfer between PS and CAT by ligand design and modification. One point that needs to be mentioned is that there is a difference between photocatalyst and photosensitized catalyst. The former use light directly to perform photochemical reactions, while the latter works on the basis of a matched photosensitizer to absorb light.

In this section, non-noble metal (Ni, Co, Mn, Fe, and Cu) complexes for photocatalytic CO_2 reduction are discussed. We in particular focused on ligand design and modification of catalysts to improve their catalytic performance for photochemical CO_2 reduction. We divide the non-noble metal molecular catalysts into six major categories according to ligand types. The data discussed below for photochemical CO_2 reduction were summarized in Table 2.

Metal complexes with macrocyclic ligands

In 1984, Tinnemans et al. initially used three tetraazamacrocyclic Co complexes (**1, 141**, and **142**; Fig. 21) as CAT for photocatalytic CO_2 reduction in aqueous solution (pH 4.0).[24] $[Ru(bpy)_3]^{2+}$ and ascorbate were used as the PS and SD, respectively. **1** and **141** showed higher CO selectivity (22% for **1** and 32% for **141**, entries 1–2 in Table 2), but **142** are unsatisfied (less than 1% CO; Table 2, entry 3). The TON_{CO} was only 22 for **1** and 9.6 for **141** after irradiation for 18 h. A mechanism was proposed that the excited $[Ru(bpy)_3]^{2+}$ is reductively quenched by ascorbate to generate a more reducing species $[Ru(bpy)_3]^+$ (Scheme 2, steps 1 and 2), which then reduces $[Co^{II}L]$ (L = ligand of **1, 141**, and **142**) to form an active $[Co^{I}L]$ species (step 3). The $[Co^{I}L]$ species in protic solvent then binds a proton to form a $[Co^{III}LH]^-$ hydride (step 4), which then may undergo two different paths: reacting with another proton to give H_2 (path a) or inserting a CO_2 into its Co-H bond to release CO (path b). Finally, the resulting $[Co^{III}L]$ is reduced to $[Co^{II}L]$ by reacting with an ascorbate (step 5). The formation of $[Co^{I}L]$ and the corresponding $[CoL(CO_2)S]$ (S= solvent) adduct in photocatalytic system was evidenced by transient spectra reported later by Fujita and co-workers.[215–218]

Yanagida and Fujita et al. reported a CH_3CN/CH_3OH photocatalytic system using Co-cyclam **143** and its derivatives as the CAT (Fig. 21), *p*-terphenyl as the PS, and TEA or TEOA as the SD.[215,219–223] Irradiation with UV light ($\lambda_{ex} > 290$ nm) over this system produced CO and $HCOO^-$ (Table 2, entries 5–11). For **143**, the system showed good selectivity for CO_2 reduction and high quantum yield ($\Phi_{(CO+HCOO-)} = 25\%$ with $\lambda_{ex} = 313$ nm, entry 4 in Table 2). However, the system suffered from a limited TON ($TON_{(CO+HCOO-)} = 16.9$). Yanagida, Fujita and co-workers further investigated the structural effects of macrocycles in **143** on its catalytic performance. They found that partially unsaturated, 14-membered tetraazamacrocycles with two or four *C*-methyl groups (**141, 144, 145**; Fig. 21) gave comparable activity for CO_2 reduction.[215] **144** had the most negative $E^0(Co^{II}/Co^{I})$ and the system using **144** as catalyst exhibited the best photocatalytic performance for CO_2 reduction (Table 2, entry 6). However, catalysts (**1, 146**; Fig. 21) with more extensively *C*-methylated macrocycles had a large decrease of catalytic activity for CO_2 reduction. Interestingly, CO_2 photoreduction to CO is enhanced in the presence of TEOA using **147** supported by the 14-membered tetraazamacrocycle without N–H bond (Fig. 21; Table 2, entry 10). This implies that

DOI: 10.1016/j.enchem.2020.100034
EnergyChem **2**, 100034 (2020)

Table 2. Non-noble metal (Ni, Co, Mn, Fe and Cu) complexes as molecular catalysts for photocatalytic CO_2 reduction.

Entry	CAT	PS	SD	Solvent	Light source, irradiation time	Main Product (Yield[d]/μmol, TON[a])	TOF (s^{-1})	Φ[b] (%)	Selectivity[c] (%)	Ref
1	**1** (80 μM)	$[Ru(bpy)_3]^{2+}$ (0.5 mM)	$AscH^-$	H_2O (pH 4)	daylight lamp, 18 h	CO (26.4, 22)	nr	nr	22 (CO)	24
2	**141** (80 μM)	$[Ru(bpy)_3]^{2+}$ (0.5 mM)	$AscH^-$	H_2O (pH 4)	daylight lamp, 18 h	CO (11.52, 9.6)	nr	nr	32 (CO)	24
3	**142** (80 μM)	$[Ru(bpy)_3]^{2+}$ (0.5 mM)	$AscH^-$	H_2O (pH 4)	daylight lamp, 18 h	CO (<3.6, <3)	nr	nr	<1 (CO)	24
4	**143** (1.7 mM)	*p*-terphenyl (2 mM)	TEOA	CH_3CN/MeOH (4:1 *v*/*v*)	Hg lamp (500 W high-pressure, λ > 290 nm), 1 h	CO (52.02, 10.2) $HCOO^-$ (34.17, 6.7)	nr	15 (CO) 10 ($HCOO^-$) λ_{ex} =313 nm	nr	215,219
5	**143** (1.7 mM)	*p*-terphenyl (2 mM)	TEA	CH_3CN/MeOH (4:1 *v*/*v*)	Hg lamp (500 W high-pressure, λ > 290 nm), 1 h	CO (23.97, 4.7) $HCOO^-$ (11.73, 2.3)	nr	nr	60.5 (CO) 31.8 ($HCOO^-$)	215,219
6	**144** (1.7 mM)	*p*-terphenyl (2 mM)	TEOA	CH_3CN/MeOH (4:1 *v*/*v*)	Hg lamp (500 W high-pressure, λ > 290 nm), 1 h	CO (27.03, 5.3) $HCOO^-$ (17.85, 3.5)	nr	nr	51.6 (CO) 34.4 ($HCOO^-$)	215,219
7	**1** (1.7 mM)	*p*-terphenyl (2 mM)	TEOA	CH_3CN/MeOH (4:1 *v*/*v*)	Hg lamp (500 W high-pressure, λ > 290 nm), 1 h	CO (10.2, 2.0) $HCOO^-$ (1.53, 0.3)	nr	nr	52.4 (CO) 7.9 ($HCOO^-$)	215,219
8	**145** (1.7 mM)	*p*-terphenyl (2 mM)	TEOA	CH_3CN/MeOH (4:1 *v*/*v*)	Hg lamp (500 W high-pressure, λ > 290 nm), 1 h	CO (24.99, 4.9) $HCOO^-$ (12.75, 2.5)	nr	nr	58.5 (CO) 30.4 ($HCOO^-$)	215
9	**146** (1.7 mM)	*p*-terphenyl (2 mM)	TEOA	CH_3CN/MeOH (4:1 *v*/*v*)	Hg lamp (500 W high-pressure, λ > 290 nm), 1 hou	CO (5.1, 1.0)	nr	nr	44 (CO)	215
10	**147** (1.7 mM)	*p*-terphenyl (2 mM)	TEOA	CH_3CN/MeOH (4:1 *v*/*v*)	Hg lamp (500 W high-pressure, λ > 290 nm), 1 h	CO (13.77, 2.7) $HCOO^-$ (2.04, 0.4)	nr	nr	30.3 (CO) 4.8 ($HCOO^-$)	215
11	**148** (1.7 mM)	*p*-terphenyl (2 mM)	TEOA	CH_3CN/MeOH (4:1 *v*/*v*)	Hg lamp (500 W high-pressure, λ > 290 nm), 1 h	nd	nd	nd	nd	215
12	**7** (0.1 mM)	$[Ru(bpy)_3]^{2+}$ (0.5 mM)	$AscH_2$	H_2O (pH 4)	Xe lamp (1000 W, 600 nm > λ> 340 nm), 8 h	CO (nr, 0.1) H_2 (nr, 0.7) Adding PS: CO (6.78, 4.8)	nr	nr	12 (CO) 88 (H_2)	225
13	7 (2 mM)	$[Ru(bpy)_3]^{2+}$ (0.5 mM)	$AscH_2$	H_2O (pH 5)	Xe lamp (1000 W, λ = 440 nm), 24 h	CO (nr, 0.1)	nr	0.06 (CO) 0.003 ($HCOO^-$)	nr	224
14	**149** (2.0 mM)	$[Ru(bpy)_3]^{2+}$ (0.5 mM)	$AscH_2$	H_2O (pH 5)	Xe lamp (1000 W, λ = 440 nm), 7 h	nr	nr	CO (0.045) $HCOO^-$ (0.019)	nr	224
15	**150** (0.25 mM)	$[Ru(bpy)_3]^{2+}$ (0.5 mM)	$AscH_2$	H_2O (pH 4)	Hg lamp (460 W ultra-high-pressure), 1 h	CO (8.75, 0.7)	nr	nr	nr	226

(*continued on next page*)

DOI: 10.1016/j.enchem.2020.100034
EnergyChem 2, 100034 (2020)

Table 2 (*continued*)

16	**151** (0.25 mM)	$[Ru(bpy)_3]^{2+}$ (0.5 mM)	$AscH_2$	H_2O (pH 4)	Hg lamp (460 W ultra-high-pressure), 1 h	CO (55, 4.4)	nr	nr	94 (CO)	226
17	**152** (10 μM)	ZnSe-BF_4 (0.5 μM) combined with **143**	$AscH_2$	H_2O (pH 4)	AM 1.5 G, ($\lambda >$ 400 nm), 20 h	CO (2.42, 121)	nr	nr	8 (CO)	227
18	**152** (10 μM)	ZnSe-BF_4 (0.5 μM) combined with **143**, 25 μM MEDA	$AscH_2$	H_2O (pH 4)	simulated solar light (AM 1.5 G, $\lambda >$ 400 nm), 20 h	CO (5.66, 283)	nr	3.4 (CO)	33.8 (CO)	227
19	**29** (0.05 mM)	*fac*-Ir(ppy)$_3$ (0.2 mM)	TEA	CH_3CN	LED light ($\lambda >$ 460 nm), 22 h	CO (54, 270)	CO (0.0034)	nr	97 (CO)	12
20	**30** (2.0 μM)	*fac*-Ir(ppy)$_3$ (0.2 mM)	TEA	CH_3CN	LED light ($\lambda >$ 420 nm), 20 h	$HCOO^-$ (ca. 1, ca. 5)	nr	nr	nr	12
21	**34** (0.05 mM)	$[Ru(dmb)_3]^{2}$ (0.05 mM)	BNAH	DMF/TEOA (4:1 *v*/*v*)	LED light (λ = 480 nm), 12 h	HCOOH (29.8, 149) CO (2.4, 12) H_2 (2.8, 14)	CO (0.0034)	5.3 (HCOOH)	85 (HCOOH)	229
22	**57** (0.1 mM)	$[Ru(dmb)_3]^{2+}$ (1 mM)	BNAH	DMF/TEOA (4:1 *v*/*v*)	LED light (λ = 470 nm), 15 h	HCOOH (260, 130) CO (14.2, 7.1) H_2 (3.2, 1.6)	HCOOH (0.0024) CO (0.00013)	3.2 (HCOOH) 0.18 (CO)	93.7 (HCOOH) 5.1 (CO)	231
23	**57** (0.1 mM)	$[Ru(dmb)_3]^{2+}$ (1 mM)	BNAH	CH_3CN/TEOA (4:1 *v*/*v*)	LED light (λ = 470 nm), 15 h	HCOOH (18, 9) CO (42, 21) H_2 (2.6, 1.3)	HCOOH (0.00017) CO (0.00039)	0.22 (HCOOH) 0.53 (CO)	28.8 (HCOOH) 67.1 (CO)	231
24	**153** (0.5 mM Mn)	$[Ru(dmb)_3]^{2+}$ (0.5 mM)	BNAH	DMF/TEOA (4:1 *v*/*v*)	LED light (λ = 470 nm), 18 h	$HCOO^-$ (1100, 110) CO (45, 4.5)	$HCOO^-$ (0.0017)	6.74 ($HCOO^-$)	95.2 ($HCOO^-$)	101
25	**34** (0.5 mM)	$[Ru(dmb)_3]^{2+}$ (0.5 mM)	BNAH	DMF/TEOA (4:1 *v*/*v*)	LED light (λ = 470 nm), 18 h	$HCOO^-$ (700, 70) CO (51, 5.1)	$HCOO^-$ (0.00108)	4.27 ($HCOO^-$)	93 ($HCOO^-$)	101
26	**60** (2 mM)	ZnTPP (0.5 mM)	TEA	CH_3CN/H_2O (20:1 *v*/*v*)	Xe lamp (500 W), 3 h	CO (5950, 119) $HCOO^-$ (950, 19)	CO (0.011) $HCOO^-$ (0.0018)	nr	86 (CO) 13.8 ($HCOO^-$)	233
27	**62** (0.005 mM)	$[Ru(bpy)_3]^{2+}$ (0.3 mM)	BIH	CH_3CN/0.5 M TEOA	LED light (λ = 460 nm), 80 min	CO (26.6, 2660)	CO (0.554)	nr	98 (CO)	46
28	**62** (0.05 mM)	$[Ru(bpy)_3]^{2+}$ (0.3 mM)	BIH	CH_3CN/0.5 M TEOA	LED light (λ = 460 nm), 80 min	CO (49.7, 497) $HCOO^-$ (0.05, 5) H_2 (0.03, 3)	CO (0.104)	2.8 (CO)	98 (CO)	46
29	**62** (0.005 mM)	purpurin (2 mM)	BIH	DMF	LED light (λ = 460 nm), 11 h	CO (7.9, 790)	CO (0.0199)	0.8 (CO)	95 (CO)	46
30	**154** (0.05 mM)	$[Ru(phen)_3]^{2+}$ (0.2 mM)	BIH/TEOA	CH_3CN	LED light (λ = 460 nm), 60 h	$HCOO^-$ (82.1, 821) CO (22.1, 221) H_2 (4.0, 40)	nr	maximum 2.6 ($HCOO^-$)	75.9 (CO)	234
31	**154** (0.05 mM)	$[Ru(phen)_3]^{2+}$ (0.2 mM)	BIH	CH_3CN/1 M PhOH	LED light (λ = 460 nm), 1 h	CO (82.9, 829) $HCOO^-$ (1.2, 12) H_2 (2.2, 22)	nr	nr	96 (CO)	234

(*continued on next page*)

DOI: 10.1016/j.enchem.2020.100034
EnergyChem **2**, 100034 (2020)

Table 2 (*continued*)

32	**155** (0.18 mM)	$[Ru(bpy)_3]^{2+}$ (0.3 mM)	TEA	CH_3CN + 40 mM TTA	Xe lamp ($\lambda \geq$ 410 nm), 4 h	CO (2.5, 3.4) $HCOO^-$ (1.0, 1.4)	CO (0.00024)	nr	CO (71.4)	235
33	**156** (0.18 mM)	$[Ru(bpy)_3]^{2+}$ (0.3 mM)	TEA	CH_3CN + 40 mM TTA	Xe lamp ($\lambda \geq$ 410 nm), 4 h	CO (3.7, 5.1) H_2 (5.8, 8.1)	CO (0.00035)	nr	CO (38.9)	235
34	**157** (0.16 mM)	$[Ru(bpy)_3]^{2+}$ (2 mM)	TEOA	CH_3CN/H_2O (4:1 *v*/*v*)	Xe lamp ($\lambda \geq$ 420 nm), 0.5 h	CO (41.6, 52)	nr	1.48	58.3 (CO)	29
35	**157** (30 nmol Co^{2+})	$[Ru(bpy)_3]^{2+}$ (0.4 mM)	TEOA	CH_3CN/H_2O (4:1 *v*/*v*)	LED light (λ = 420 nm), 10 h	nr	CO (0.027)	0.9 (CO)	63.1 (CO)	243
36	**158** (30 nmol Co^{2+})	$[Ru(bpy)_3]^{2+}$ (0.4 mM)	TEOA	CH_3CN/H_2O (4:1 *v*/*v*)	LED light (λ = 420 nm), 10 h (1 atm CO_2)	nr	CO (0.0063)	0.21 (CO)	63.6 (CO)	243
37	**159** (30 nmol Co^{2+})	$[Ru(bpy)_3]^{2+}$ (0.4 mM)	TEOA	CH_3CN/H_2O (4:1 *v*/*v*)	LED light (λ = 420 nm), 10 h (1 atm CO_2)	nr	CO (0.028)	0.93 (CO)	98.2 (CO)	243
38	**159** (30 nmol Co^{2+})	$[Ru(bpy)_3]^{2+}$ (0.4 mM)	TEOA	CH_3CN/H_2O (4:1 *v*/*v*)	LED light (λ = 420 nm), 10 h (0.1 atm CO_2)	nr	CO (0.023)	nr	98.2 (CO)	243
39	**160** (30 nmol Co^{2+})	$[Ru(bpy)_3]^{2+}$ (0.4 mM)	TEOA	CH_3CN/H_2O (4:1 *v*/*v*)	LED light (λ = 420 nm), 10 h (1 atm CO_2)	nr	CO (0.012)	0.39 (CO)	66.7 (CO)	243
40	**161** (30 nmol Co^{2+})	$[Ru(bpy)_3]^{2+}$ (0.4 mM)	TEOA	CH_3CN/H_2O (4:1 *v*/*v*)	LED light (λ = 420 nm), 10 h (1 atm CO_2)	nr	CO (0.059)	2.0 (CO)	98.2 (CO)	243
41	**161** (30 nmol Co^{2+})	$[Ru(bpy)_3]^{2+}$ (0.4 mM)	TEOA	CH_3CN/H_2O (4:1 *v*/*v*)	LED light (λ = 420 nm), 10 h (0.1 atm CO_2)	nr	CO (0.049)	nr	97.8 (CO)	243
42	**162** (1 μM)	$[Ru(bpy)_3]^{2+}$ (2 mM)	TEOA/BIH	CH_3CN + 3% H_2O	white light ($\lambda >$ 420 nm), 3 h	CO (31.2, 12,487) H_2 (1.0, 411)	CO (1.16)	1.2 (CO)	97 (CO)	244
43	**162** (1 μM)	$[Ru(bpy)_3]^{2+}$ (2 mM)	TEOA/BIH	CH_3CN	white light ($\lambda >$ 420 nm), 3 h	CO (7.4, 2939) H_2 (0.2, 93)	CO (0.222)	nr	97 (CO)	244
44	**163** (0.05 μM)	$[Ru(phen)_3]^{2+}$ (0.4 mM)	TEOA	CH_3CN/H_2O (4:1 *v*/*v*)	LED light (λ = 450 nm) 10 h	CO (2.48, 9900)	CO (0.275)	nr	98 (CO)	245
45	**164** (0.05 mM)	$Cu^I(dmp)(P)_2^+$ (0.5 mM)	BIH, 50 mM	CH_3CN/TEOA (5:1 *v*/*v*)	Hg lamp (λ = 435.8 nm), 12 h	CO (54.5, 273)	CO (0.0063)	nr	78 (CO)	246
46	**63** (0.005 mM)	$[Ru(bpy)_3]^{2+}$ (0.3 mM)	BIH	CH_3CN/TEOA (4:1, *v*/*v*)	LED light (λ = 460 nm), 3 h	CO (38.44, 3844) $HCOO^-$ (3.34, 534) H_2 (1.18, 118)	CO (0.366)	1.45 for the first 45 min (CO)	85 (CO)	46
47	**63** (0.05 mM)	$[Ru(bpy)_3]^{2+}$ (0.3 mM)	BIH	C CH_3CN/TEOA (4:1, *v*/*v*)	LED light (λ = 460 nm), 3 h	CO (18.79, 1879) $HCOO^-$ (0.48, 48) H_2 (0.15, 15)	CO (0.174)	8.8 (CO)	97 (CO)	46
48	**63** (0.005 mM)	purpurin (0.02 mM)	BIH	DMF	LED lihgt (λ = 460 nm), 12 h	CO (13.65, 1365)	CO (0.0316)	1.1 (CO)	92 (CO)	46
49	**63** (20 μM)	mpg-C_3N_4 (8 mg)	TEOA	CH_3CN/TEOA (4:1 *v*/*v*)	Hg lamp (400 W high-pressure, $\lambda \geq$ 400), 17 h	CO (12.4, 155)	CO (0.0025)	4.2 (CO)	97 (CO)	251

(*continued on next page*)

DOI: 10.1016/j.enchem.2020.100034
EnergyChem 2, 100034 (2020)

Table 2 (*continued*)

50	**165** (10 μmol)	CdS (50 mg)	TEOA	CH_3CN/H_2O (4:1 *v*/*v*)	non-focus 300 W LED light, 2 h	nr	nr	1.68 (CO)	81.25 (CO)	[252]
51	**78** (0.01 mM)	–	TEA	DMF	Xe lamp (300 W), 15 min	CO (nr, ca. 70)	nr	5 (CO)	nr	[254]
52	**78** (10–50 μM)	–	TEA	CH_3CN	visible light (BG40-type optical filter), 10 h	CO (0.51 based 10 μM **78**, 17)	nr	nr	8 for 1 h (CO)	[257]
53	**79** (10–50 μM)	–	TEA	CH_3CN	visible light (BG40-type optical filter), 10 h	CO (0.84 based 10 μM **79,** 28)	CO (0.0021 for 1 h)	nr	93 for 1 h (CO)	[257]
54	**79** (2 μM)	9-CNA (0.2 mM)	TEA	CH_3CN	Xe lamp ($\lambda >$ 420 nm), 45 h	CO (nr, 40–60)	nr	0.08 (CO)	ca. 100 (CO)	[259]
55	**79** (2 μM)	*fac*-Ir(ppy)$_3$ (0.2 mM)	TEA	CH_3CN	Xe lamp ($\lambda >$ 420 nm), 55 h	CO (nr, 140)	CO (0.039 for 1 h)	0.13 (CO)	93 (CO)	[259]
56	**81** (10–50 μM)	–	TEA	CH_3CN	visible light (BG40-type optical filter), 10 h	CO (0.69 based 10 μM **81**, 23)	CO (0.0019 for 1 h)	nr	76 for 1 h (CO)	[257]
57	**82** (2 μM)	*fac*-Ir(ppy)$_3$ (0.2 mM)	TEA	CH_3CN	simulated solar light ($\lambda >$ 420 nm), 102 h	CO (2.57, 367) CH_4 (0.55, 79) H_2 (0.18, 26)	CO (0.001) CH_4 (0.0002)	nr	78 (CH_4) 17 (CO) 5 (H_2)	[47]
58	**82** (2 μM)	Purpurin (0.2 mM)	TEA	CH_3CN/H_2O (1:9 *v*/*v*), 0.1 M NaHCO3	simulated solar light ($\lambda >$ 420 nm), 47 h	CO (0.42, 60) H_2 (0.035, 5)	CO (0.00035)	nr	95 (CO)	[260]
59	**82** (2 μM)	*fac*-Ir(ppy)$_3$ (0.2 mM)	TEA	CH_3CN/H_2O (3:7 *v*/*v*)	simulated solar light ($\lambda >$ 420 nm), 47 h	CO (0.168, 24) CH_4 (0.021, 3) H_2 (0.035, 5)	CO (0.00014) CH_4 (0.000018)	nr	75 (CO) 9 (CH_4) 16 (H_2)	[261]
60	**170** (0.15 mM)	–	TEA	CH_3CN	Xe lamp ($\lambda >$ 310 nm), 6 h	CO (47.25, 9)	nr	nr	nr	[262]
61	**170** (0.15 mM)	*p*-terphenyl (3 mM)	TEA	CH_3CN	Xe lamp ($\lambda >$ 310 nm), 6 h	CO (472.5, 90)	nr	nr	nr	[262]
62	**171** (0.048 mM)	*p*-terphenyl (3 mM)	TEA	CH_3CN	Xe lamp ($\lambda >$ 310 nm), ca. 6 h	CO (73.58, 43.8)	nr	nr	nr	[263]
63	**172** (0.045 mM)	*p*-terphenyl (3 mM)	TEA	CH_3CN	Xe lamp ($\lambda >$ 310 nm), ca. 6 h	CO (80.48, 51.1)	nr	nr	nr	[263]
64	**98** (10 μM)	–	TEA	CH_3CN	Xe lamp ($\lambda >$ 320 nm), 200 h	$HCOO^- + CO$ (105, 300)	nr	nr	nr	[265]
65	**173** (ca. 0.05 mM)	*p*-terphenyl (3 mM)	TEA	CH_3CN	Xe lamp ($\lambda >$ 320 nm), 20 h	CO (108.5, 62)	nr	nr	nr	[255]
66	**169** (0.034 mM)	*p*-terphenyl (3 mM)	TEA	CH_3CN	Xe lamp (300 W), 20 h	CO (73.54, 61.8)	nr	nr	nr	[256]
67	**174** (0.04 mM)	*p*-terphenyl (3 mM)	TEA	CH_3CN	Xe lamp ($\lambda >$ 310 nm), 6 h	CO (66.5, 47.5)	nr	nr	nr	[262]
68	**175** (2 mg)	–	TEOA	MeCN	Xe lamp (400 nm $< \lambda <$ 800 nm), 6 h	nr	CO (200.6 μmol/(g*h)) CH_4 (36.76 μmol/(g*h))	nr	15.4 (CH_4)	[268]
69	MOF-525 (2 mg)	–	TEOA	MeCN	Xe lamp (400 nm $< \lambda <$ 800 nm), 6 h	nr	CO (64.02 μmol/(g*h)) CH_4 (6.2 μmol/(g*h))	nr	8.83 (CH_4)	[268]

(*continued on next page*)

DOI: 10.1016/j.enchem.2020.100034
EnergyChem **2**, 100034 (2020)

Table 2 (*continued*)

70	**176** (0.1 mg)	*g*-C_3N_4 (50 mg)	TEOA	CH_3CN/H_2O (3:1 *v*/*v*)	Xe lamp (400 nm < λ < 780 nm), 6 h	CO (0.65, 5.7) CH_4 (trace)	CO (1.09 mmol/(g*h))	nr	98 (CO)	[269]
71	**177** (22 and 65 mg)	Graphene sheets 100 mL (0.2 mg/mL)	–	H_2O	Xe lamp (λ > 400 nm), 6 h	nr	CH_4 (57.38 μmol/(m*h)) C_2H_2 (112.89 μmol/(m*h))	nr	nr	[271]
72	**178** (5 μM)	*fac*-Ir(ppy)$_3$ (0.4 mM)	TEA	CH_3CN	LED light (λ_{max} = 460 nm), 70 h	CO (19.06, 953)	CO (0.0139 for 8 h)	nr	85 (CO)	[272]
73	**179** (10 μM)	*fac*-Ir(ppy)$_3$ (0.4 mM)	TEA	CH_3CN/H_2O (5:1 *v*/*v*)	LED light (λ_{max} = 450 nm), 60 h	CO (2.85, 56.9) $HCOO^-$ (3.21, 64.2) H_2 (9.08, 181.6)	CO (0.00026) $HCOO^-$ (0.0003)	nr	18.8 (CO) 21.2 ($HCOO^-$) 60 (H_2)	[275]
74	**180** (0.01 mM)	*fac*-Ir(ppy)$_3$ (0.5 mM)	TEA	DMF	LED light (λ_{max} = 460 nm), 60 h	CO (14.72, 368)	CO (0.0017)	nr	ca. 95 (CO)	[276]
75	**180** (0.01 mM)	*fac*-Ir(ppy)$_3$ (0.5 mM)	TEA	DMF	LED light (λ_{max} = 460 nm), 15 h	CO (3.36, 84)	CO (0.0016)	nr	89 (CO)	[276]
76	**181** (0.01 mM)	*fac*-Ir(ppy)$_3$ (0.5 mM)	TEA	DMF	LED light (λ_{max} = 460 nm), 15 h	nd	nd	nd	nd	[276]
77	**182** (0.01 mM)	*fac*-Ir(ppy)$_3$ (0.5 mM)	TEA	DMF	LED light (λ_{max} = 460 nm), 15 h	CO (0.52, 13)	CO (0.00024)	nr	65 (CO)	[276]
78	**183** (0.01 mM)	*fac*-Ir(ppy)$_3$ (0.5 mM)	TEA	DMF	LED light (λ_{max} = 460 nm), 15 h	nd	nd	nd	nd	[276]
79	**184** (0.01 mM)	*fac*-Ir(ppy)$_3$ (0.5 mM)	TEA	DMF	LED light (λ_{max} = 460 nm), 12 h	CO (2.8, 56)	CO (0.0013)	nr	86 (CO)	[277]
80	**184** (0.01 mM)	*fac*-Ir(ppy)$_3$ (0.5 mM)	TEA	DMF	LED light (λ_{max} = 460 nm), 48 h	CO (23.5, 470)	CO (0.0027)	nr	87 (CO)	[277]
81	**185** (0.01 mM)	*fac*-Ir(ppy)$_3$ (0.5 mM)	TEA	DMF	LED light (λ_{max} = 460 nm), 12 h	CO (5.1, 102)	CO (0.0024)	nr	88 (CO)	[277]
82	**185** (0.01 mM)	*fac*-Ir(ppy)$_3$ (0.5 mM)	TEA	DMF	LED light (λ_{max} = 460 nm), 48 h	CO (21.05, 403)	CO (0.0023)	nr	89 (CO)	[277]
83	**186** (2 μM)	$[Ru(phen)_3]^{2+}$ (0.4 mM)	TEOA	CH_3CN/H_2O (4:1 *v*/*v*)	LED light (λ = 450 nm), 10 h	CO (11.79, 1179)	CO (0.032)	0.22 (CO)	97 (CO)	[173]
84	**178** (2 μM)	$[Ru(phen)_3]^{2+}$ (0.4 mM)	TEOA	CH_3CN/H_2O (4:1 *v*/*v*)	LED light (λ = 450 nm), 10 h	CO (6.86, 686)	CO (0.019)	0.13 (CO)	97 (CO)	[173]
85	**187** (0.01 μM)	$[Ru(phen)_3]^{2+}$ (0.4 mM)	TEA	CH_3CN/H_2O (4:1 *v*/*v*)	LED light (λ = 450 nm), 10 h	CO (2.24, 44,800)	CO (1.24)	0.27 at 2.0 μM CAT (CO)	97 (CO)	[174]

(*continued on next page*)

DOI: 10.1016/j.enchem.2020.100034
EnergyChem 2, 100034 (2020)

Table 2 (*continued*)

86	**187** (0.05 μM)	$[Ru(phen)_3]^{2+}$ (0.4 mM)	TEA	CH_3CN/H_2O (4:1 v/v)	LED light ($\lambda = 450$ nm), 10 h	CO (2.9, 11,600)	CO (0.32)	nr	97 (CO)	174
87	**188** (0.05 μM)	$[Ru(phen)_3]^{2+}$ (0.4 mM)	TEOA	CH_3CN/H_2O (4:1 v/v)	LED light ($\lambda = 450$ nm), 10 h	CO (0.4, 1600)	CO (0.04)	0.007 (CO)	85 (CO)	174
88	**189** (0.01 μM)	$[Ru(phen)_3]^{2+}$ (0.4 mM)	TEOA	CH_3CN/H_2O (4:1 v/v)	LED light ($\lambda = 450$ nm), 10 h	CO (2.9, 58,000)	CO (1.61)	0.19 at 2.0 μM CAT (CO)	97 (CO)	280
89	**190** (0.01 μM)	$[Ru(phen)_3]^{2+}$ (0.4 mM)	TEOA	CH_3CN/H_2O (4:1 v/v)	LED light ($\lambda = 450$ nm), 10 h	CO (2.46, 49,200)	CO (1.37)	0.17 at 2.0 μM CAT (CO)	98 (CO)	280
90	**191** (0.01 μM)	$[Ru(phen)_3]^{2+}$ (0.4 mM)	TEOA	CH_3CN/H_2O (4:1 v/v)	LED light ($\lambda = 450$ nm), 10 h	nd	nd	0.04 at 2.0 μM Cat (CO)	nd	280
91	**102** (2.0 μM)	$[Ru(phen)_3]^{2+}$ (0.4 mM)	TEOA	CH_3CN/H_2O (4:1 v/v)	LED light ($\lambda = 450$ nm), 12 h	CO (7.9, 790)	CO (0.021 for 8 h)	0.16 (CO)	98 (CO)	175
92	**103** (2.0 μM)	$[Ru(phen)_3]^{2+}$ (0.4 mM)	TEOA	CH_3CN/H_2O (5:1 v/v)	LED light ($\lambda = 450$ nm), 12 h	CO (10.7, 1070)	CO (0.031 for 8 h)	0.22 (CO)	98 (CO)	175
93	**104** (2.0 μM)	$[Ru(phen)_3]^{2+}$ (0.4 mM)	TEOA	CH_3CN/H_2O (5:1 v/v)	LED light ($\lambda = 450$ nm), 12 h	CO (13.3, 1330)	CO (0.038 for 8 h)	0.27 (CO)	98 (CO)	175
94	**104** (0.04 μM)	$[Ru(phen)_3]^{2+}$ (0.4 mM)	TEOA	CH_3CN/H_2O (4:1 v/v)	LED light ($\lambda = 450$ nm), 12 h	CO (2.11, 10,650)	CO (0.32 for 8 h)	nr	99 (CO)	175
95	**105** (1.0 μM)	$[Ru(phen)_3]^{2+}$ (0.4 mM)	TEOA	CH_3CN/H_2O (5:1 v/v)	LED light ($\lambda = 450$ nm), 12 h	CO (9.5, 950)	CO (0.028 for 8 h)	0.19 (CO)	98 (CO)	175
96	**192** (0.025 μM)	$[Ru(phen)_3]^{2+}$ (0.4 mM)	TEOA	CH_3CN/H_2O (4:1 v/v)	LED light ($\lambda = 450$ nm), 10 h	CO (2.11, 16,896)	CO (0.47)	0.04 (CO)	98 (CO)	14
97	**192** (0.025 μM)	$[Ru(phen)_3]^{2+}$ (0.4 mM)	TEOA	CH_3CN/H_2O (4:1 v/v)	LED light ($\lambda = 450$ nm), 10 h	CO (2.11, 17,000)	CO (0.47)	0.04 (CO)	98 (CO)	30
98	**193** (0.025 μM)	$[Ru(phen)_3]^{2+}$ (0.4 mM)	TEOA	CH_3CN/H_2O (4:1 v/v)	LED light ($\lambda = 450$ nm), 10 h	CO (8.10, 65,000)	CO (1.8)	0.15 (CO)	98 (CO)	30
99	**188** (0.025 μM)	$[Ru(phen)_3]^{2+}$ (0.4 mM)	TEOA	CH_3CN/H_2O (4:1 v/v)	LED light ($\lambda = 450$ nm), 10 h	CO (0.18, 1500)	CO (0.04)	nr	74 (CO)	30
100	**194** (0.025 μM)	$[Ru(phen)_3]^{2+}$ (0.4 mM)	TEOA	CH_3CN/H_2O (4:1 v/v)	LED light ($\lambda = 450$ nm), 10 h	CO (4.22, 33,792)	CO (0.94)	0.15 at 1.0 μM CAT (CO)	98 (CO)	281
101	**194** (0.5 μM)	$[Ru(phen)_3]^{2+}$ (0.4 mM)	TEOA	CH_3CN/H_2O, (4:1 v/v), $CO_2/Ar = 10/90$	LED light ($\lambda = 450$ nm), 10 h	CO (1.50, 600)	CO (0.017)	nr	95 (CO)	281
102	**195** (0.025 μM)	$[Ru(phen)_3]^{2+}$ (0.4 mM)	TEOA	CH_3CN/H_2O (4:1 v/v)	LED light ($\lambda = 450$ nm), 10 h	CO (2.33, 18,656)	CO (0.52)	nr	97 (CO)	281
103	**110** (2 nM)	*fac*-$Ir(ppy)_3$ (0.2 mM)	TEA	CH_3CN	Xe lamp (150 W, AM 1.5 filter), 7 h	CO (1.96, 98,000)	CO (3.9)	0.01 (CO)	ca. 100 (CO)	28
104	**196** (0.1 mM)	*fac*-$Ir(ppy)_3$ (0.1 mM)	BIH	CH_3CN/TEA (19:1 v/v)	Xe lamp (150 W, AM 1.5 filter), 6 h	CO (2.12, 10.6)	CO (0.006 for 4 h)	nr	nr	283
105	**120** (0.1 mM)	*fac*-$Ir(ppy)_3$ (0.1 mM)	BIH	CH_3CN/TEA (19:1 v/v)	Xe lamp (150 W, AM 1.5 filter), 6 h	CO (0.018, 0.09)	nr	nr	nr	283
106	**197** (30 μM)	$[Ru(bpy)_3]^{2+}$ (0.50 mM)	BIH	DMA/H_2O (9:1 v/v)	LED light (6 W, $\lambda = 450$ nm), 55 h	CO (86, 713)	CO (0.0052)	1.42 (CO)	>99 (CO)	285
107	**197** (30 μM)	$[Ru(bpy)_3]^{2+}$ (0.50 mM)	BIH	DMA/H_2O (9:1 v/v)	LED light (6 W, $\lambda = 450$ nm), 4 h	CO (10.32, 86)	CO (0.006)	nr	>99 (CO)	32

(*continued on next page*)

DOI: 10.1016/j.enchem.2020.100034
EnergyChem 2, 100034 (2020)

Table 2 (*continued*)

108	**197** (30 μM), Mg^{2+} (5 mM)	$[Ru(bpy)_3]^{2+}$ (0.50 mM)	BIH	DMA/H_2O (9:1 v/v)	LED light (6 W, $\lambda = 450$ nm), 4 h	CO (20.64, 172)	CO (0.012)	3.3 (CO)	>99 (CO)	32
109	**198** (30 μM)	$[Ru(bpy)_3]^{2+}$ (0.50 mM)	BIH	DMA/H_2O (9:1 v/v)	LED light (6 W, $\lambda = 450$ nm), 4 h	CO (10.08, 84)	CO (0.006)	nr	>99 (CO)	32
110	**198** (30 μM), Mg^{2+} (5 mM)	$[Ru(bpy)_3]^{2+}$ (0.50 mM)	BIH	DMA/H_2O (9:1 v/v)	LED light (6 W, $\lambda = 450$ nm), 4 h	CO (40.8, 340)	CO (0.024)	11.1 (CO)	>99 (CO)	32
111	**199** (0.5 mM)	–	$AscH_2$	H_2O (pH 4)	Xe lamp (500 W, $\lambda > 450$ nm), 44 h	CO (0.157, <1)	nr	nr	72 (CO)	40
112	$[Ni(cyclam)]^{2+}$ (0.5 mM)	$[Ru(phen)_3]^{2+}$ (0.5 mM)	$AscH_2$	H_2O (pH 4)	Xe lamp (500 W, $\lambda > 450$ nm), 44 h	CO (0.058, <1)	nr	nr	36 (CO)	40
113	**200** (0.01 mM)	–	$AscH_2$	H_2O (pH 5.1)	Xe lamp (500 W, $\lambda > 450$ nm), 2 h	CO (<0.179, 1)	nr	nr	11 (CO)	288
114	**205** (30 μM)	–	$AscH_2$	H_2O (pH 6.5)	halogen lamp ($\lambda >$ 435 nm), 60 h	CO (3.1, 5.2)	nr	nr	nr	289
115	**206** (0.5 mM)	–	TEOA	DMF/H_2O (3:1 v/v)	Xe lamp (500 W, $750 > \lambda >$ 400 nm), 29 h	CO (29, 2) H_2 (29, 2)	nr	nr	50 (CO)	290
116	$[Ni(bpy)_3]^{2+}$ (0.5 mM)	$[Ru(bpy)_3]^{2+}$ (0.5 mM)	TEOA	DMF/H_2O (3:1 v/v)	Xe lamp (500 W, $750 > \lambda >$ 400 nm), 29 h	CO (30, 2) H_2 (8, <1)	nr	nr	79 (CO)	290
117	**207** (0.5 mM)	–	TEOA	DMF/H_2O (3:1 v/v)	Xe lamp (500 W, $750 > \lambda >$ 400 nm), 29 h	CO (49, 3) H_2 (18, 1)	nr	nr	9.3 (CO)	290
118	**208** (0.5 mM)	–	TEOA	DMF/H_2O (3:1 v/v)	Xe lamp (500 W, $750 > \lambda >$ 400 nm), 29 h	CO (77, 5) H_2 (20, 1)	nr	nr	12.7 (CO)	290
119	$[Co(bpy)_3]^{3+}$ (0.5 mM)	$[Ru(bpy)_3]^{2+}$ (0.5 mM)	TEOA	DMF/H_2O (3:1 v/v)	Xe lamp (500 W, $750 > \lambda >$ 400 nm), 29 h	CO (130, 9) H_2 (240, 16)	nr	nr	44 (CO)	290
120	**209** (0.1 mM)	–	BIH	CH_3CN/TEOA (5:1 v/v)	Xe lamp (300 W, $\lambda > 415$ nm), 8 h	CO (30.6, 51) H_2 (7.8, 13)	CO (0.0018)	nr	79.6 (CO)	291
121	**210** (0.1 mM)	–	BIH	CH_3CN/TEOA (5:1 v/v)	Xe lamp (300 W, $\lambda > 415$ nm), 8 h	CO (8.4, 14) H_2 (3.6, 6)	CO (0.0005)	nr	69.7 (CO)	291
122	**211** (0.1 mM)	–	BIH	CH_3CN/TEOA (5:1 v/v)	Xe lamp (300 W, $\lambda > 415$ nm), 8 h	CO (32.4, 54) H_2 (4.8, 8)	CO (0.0019)	nr	87.2 (CO)	291
123	**212** (0.1 mM)	–	BIH	CH_3CN/TEOA (5:1 v/v)	Xe lamp (300 W, $\lambda > 415$ nm), 8 h	CO (1.2, 2) H_2 (0.6, 1)	CO (0.00007)	nr	66.7 (CO)	291
124	**213** (0.1 mM)	–	BIH	CH_3CN/TEOA (5:1 v/v)	Xe lamp (300 W, $\lambda > 415$ nm), 16 h	CO (42, 70) H_2 (23.4, 39)	CO (0.0018)	nr	64.3 (CO)	291
125	$[Co(phen)_3]^{2+}$ (0.1 mM)	$[Ru(bpy)_3]^{2+}$ (0.1 mM)	BIH	CH_3CN/TEOA (5:1 v/v)	Xe lamp (300 W, $\lambda > 415$ nm), 2 h	CO (17.4, 29) H_2 (15, 25)	CO (0.004)	nr	54.5 (CO)	291

(*continued on next page*)

DOI: 10.1016/j.enchem.2020.100034
EnergyChem 2, 100034 (2020)

Table 2 (*continued*)

126	**214** (0.05 mM)	–	BIH	DMA/TEOA (4:1 *v*/*v*)	high-pressure Hg lamp or Xe lamp (λ_{ex} = 546 nm), 6 h	HCOOH (19.5, 98) CO (5.8, 29)	HCOOH (0.0045) CO (0.0013)	HCOOH (14) CO (0.64)	HCOOH (77)	[292]
127	**215** (0.05 mM)	–	BIH	DMA/TEOA (4:1 *v*/*v*)	high-pressure Hg lamp or Xe lamp (λ_{ex} = 546 nm), 6 h	HCOOH (6.7, 33) CO (3.5, 18)	HCOOH (0.0015) CO (0.0008)	HCOOH (5.4) CO (0.43)	HCOOH (65)	[292]
128	[Mn(MeRes)(CO)$_3$Br] (0.05 mM)	[Ru(dmb)$_3$]$^{2+}$ (0.05 mM)	BIH	DMA/TEOA (4:1 *v*/*v*)	high-pressure Hg lamp or Xe lamp (λ_{ex} = 546 nm), 6 h	HCOOH (18.1, 90) CO (2.2, 11)	HCOOH (0.0042) CO (0.0005)	HCOOH (11) CO (0.24)	HCOOH (89.1)	[292]
129	**216** (34 μmol Co^{2+})	[Ru(phen)$_3$]$^{2+}$ (0.4 mM)	TEOA	CH$_3$CN/H$_2$O (4:1 *v*/*v*)	LED light (λ = 450 nm), 10 h	CO (3.33, 97,941)	CO (2.72)	0.06 (CO)	98 (CO)	[31]

[a] Turnover number based on the amount of CAT.
[b] Quantum yield for product formation.
[c] Selectivity = targeted CO_2 reduction products/all products (including hydrogen).
[d] The amount of CO_2 reduction product reported, some of them were calculated using the reported catalytic data. nd = not detected, nr = not reported.

the presence of N–H group in 14-membered tetraazamacrocycles is not always a requisite for effective CO_2 binding. With regard to the N-methylated cyclam, **148** can not mediate the photoreduction of CO_2 (Fig. 21; Table 2, entry 11). This inactivity may be explained as the steric hindrance of the four N-methyl groups, which impedes the catalytic center from binding CO_2 substrate molecules.[215]

As mentioned in the electrocatalytic CO_2 reduction section, the $[Ni^I(cyclam)]^+$ complex shows good activity for electrochemical reduction of CO_2 to CO.[60] Ni-cyclam complexes were also studied as catalysts for photocatalytic CO_2 reduction. Spreer and Otvos et al. built an effective photocatalytic system using $[Ni(cyclam)]^{2+}$ (**7**; Fig. 2 and 22) as the CAT, $[Ru(bpy)_3]^{2+}$ as the PS, and $AscH_2$ as the SD. The total TON_{CO} reaches 4.8, and the quantum yield for CO formation is 0.06% (Table 2, entries 12 and 13).[224,225] When the cyclam ligand was replaced with a 12-membered-ring macrocycle, the corresponding Ni complex **149** exhibits lower photocatalytic activity in CO_2-to-CO conversion (Table 2, entry 14).[224] Later, two dimerized Ni-cyclam complexes were further investigated by Mochizuki and co-workers. They found that dimerized Ni-cyclam **151** (Fig. 22) improved both efficiency and selectivity in CO_2-to-CO reduction when compared to the monomacrocyclic complex **150** (Table 2, entries 15 and 16).[226] **151** produced 6 times and 8 times as much CO as **150** and the parent complex **7**, respectively. A surprising result is that Ni(II) complex **25**, with the same bimacrocyclic skeleton as **151** but without the methyl groups (Fig. 3 and 22), generates only 60% of the CO amount **151** generated.[226]

Immobilization of molecular catalysts onto 2D layer materials or 3D porous materials is a traditional approach to prepare heterogeneous catalysts. Hybrid photocatalysts for CO_2 reduction can also be prepared by depositing molecular catalysts such as macrocyclic complexes on semiconductor materials.[227,228] Recently, Reisner et al. developed a precious metal-free photocatalytic system consisting of a phosphonic acid-functionalised Ni(cyclam) catalyst (**152**; Fig. 23) and ligand-free ZnSe quantum dots (QDs) as a visible-light PS. The catalytic system shows a high activity for CO_2 reduction to CO, with the TON_{CO} of over 120 (Table 2, entry 17). In contrast, the anchor-free catalyst **7** produces three times less CO.[227] Further modification of ZnSe surface with 2-(dimethylamino)ethanethiol (MEDA) partially suppresses H_2 generation and enhances CO production, with the TON_{CO} of over 280 after irradiation for 20 h with visible light ($\lambda > 400$ nm, AM 1.5G, 1 sun) (Table 2, entry 18). The external quantum efficiency of 3.4% at 400 nm is comparable to state-of-the-art precious metal catalysts.[227]

Co catalyst **29** supported on N_5-macrocycle and its Fe analogue **30** (Fig. 4) reported by Lau, Robert and coworkers for electrocatalytic CO_2 reduction were also found activity for photocatalytic CO_2 reduction.[12] Interestingly, the reduction products are dependent on the catalytic centers. Using *fac*-$Ir(ppy)_3$ as PS and TEA as SD, the photocatalytic CO_2 reduction system by **29** produced CO with a TON of 270 and a selectivity of up to 97% (Table 2, entry 19), while the same reaction system by **30** mainly produced formate (TON = 5) (Table 2, entry 20).[204]

Metal complexes with polypyridine ligands

The aforementioned electrocatalyst *fac*-Mn(bpy)(CO)$_3$Br (**34**; Figs. 5 and 24) was also active for photocatalytic CO_2 reduction. A DMF/TEOA (v/v = 4:1) solution containing **34**, $[Ru(dmb)_3]^{2+}$, and BNAH was irradiated by 480 nm light under a CO_2 atmosphere, producing HCOOH with Φ_{HCOOH} of 5.3%. A TON_{HCOOH} of 149 was obtained after 12 h irradiation

DOI: 10.1016/j.enchem.2020.100034
EnergyChem **2**, 100034 (2020)

(Table 2, entry 21).[229] Such performance is comparable to the photocatalytic system using the noble metal complex *fac*-*Re*(dmb)$(CO)_3Cl$ (Φ_{CO} = 6.2%) under similar reaction conditions.[230] Note that the photocatalytic product was HCOOH, which is different from the electrocatalytic result that CO was the main product.[35,90] The electrochemically active complex (**57**; Fig. 6 and 24) similar to **34** was also used as CAT to construct a photocatalytic system consisting of $[Ru(dmb)_3]^{2+}$, BNAH, and DMF/TEOA (4:1 *v*/*v*). [231] **57** exhibited more stable photochemically than **34**. This system also produced HCOOH as the main product with a Φ_{HCOOH} of 3.2% and a TON_{HCOOH} of 130 (Table 2, entry 22) under a 470 nm light irradiation for 15 h.[231] However, when the solvent was changed to CH_3CN/TEOA (*v*/*v* = 4:1), Kubiak and co-workers found that this solvent system favored CO formation (TON_{CO} = 21, Φ_{CO} = 0.53%) over HCOOH (TON_{HCOOH} = 9, Φ = 0.22%) and H_2 (TON_{H2} = 1.3) (Table 2, entry 23). The two-electron reduction product, i.e., $[Mn(bpy)(CO)_3]^-$ produced by disproportionation of the one-electron-reduced species $[Mn(bpy)(CO)_3(CN)]^{\cdot-}$ was proposed as an active species for CO_2 reduction.[106,232] In 2018, a MOF (**153**; Fig. 24) consisting of **34** as unit and Zn(IV) as bridges was used as CAT in a DMF/TEOA (*v*/*v* = 4:1) photocatalytic system for CO_2 reduction in the presence of $[Ru(dmb)_3]^{2+}$ as PS and BNAH as SD.[101] This system produced HCOOH with a high selectivity of 95.2% and a Φ_{HCOOH} of 6.74% at λ_{ex} = 470 nm (Table 2, entry 24). The TON_{HCOOH} reaches 110, larger than that of the corresponding homogeneous systems (**70**, Φ_{HCOOH} = 4.27% with **34** as CAT) under similar reaction conditions (Table 2, entry 25). The MOF was suggested to inhibit the Mn complexes from forming Mn dimer. The catalyst could be easily recovered by decantation from the dispersed solution after the photocatalytic reaction and could be reused. The photocatalytic activity of the system gradually decreased because of partial decomposition of the *fac*-$Mn(CO)_3$ structure, despite that the Mn content itself did not decrease in the MOF, yielding a total TON_{HCOOH} of 170 after 4 recycling steps. Recently, Bian et al. built a photocatalytic system using **60** (Figs. 6 and 24) as CAT, ZnTPP as PS and TEA as SD.[233] In CH_3CN/H_2O (*v*/*v* = 20:1), the main product is CO with a TON_{CO} of 119 and TON_{HCOOH} of 19 based on the Mn complex (Table 2, entry 26).

The electrochemically active Co quaterpyridine complex **62** (Fig. 7) is also active for photocatalytic CO_2 reduction.[46,117] Lau and Robert et al. found that in CH_3CN/TEOA solvent system with **62** as the CAT, $[Ru(bpy)_3]^{2+}$ as the PS and BIH as the SD, a TON_{CO} as high as 2660 with 98% selectivity and 6.74% Φ_{CO} can be achieved (Table 2, entries 27–28).[46] An organic PS purpurin could also be employed in this photocatalytic system instead of $[Ru(bpy)_3]^{2+}$. Irradiation (λ_{ex} = 460 nm) on a DMF solution consisting of **62** (0.005 mM), purpurin (2 mM), BIH (0.1 M) and saturated CO_2 led to the selective formation of CO with TON_{CO} of 790 (Table 2, entry 29).[46] In 2019, Lau and Robert et al. further reported a binuclear Co complex $[Co_2biqpy]^{4+}$ (**154;** Fig. 25) bearing a bi-quaterpyridine ligand. They found that **154** can selectively reduce CO_2 to $HCOO^-$ or CO under visible light irradiation (λ_{ex} = 460 nm).[234] In basic CH_3CN solution, $HCOO^-$ was observed with a selectivity of 75.9% and a TON of 821 respectively under irradiation for 60 h (Table 2, entry 30). When phenol was used as a co-substrate, CO was afforded with a high selectivity of 96% and a TON of 829 (Table 2, entry 31) under irradiation for 1 h. Electrochemical experiments and DFT calculations indicated that the catalytic process is controlled by the two Co atoms acting synergistically.[234]

In 2018, two Co complexes (**155** and **156**; Fig. 25) with pentadentate polypyridine ligands were synthesized for photocatalytic CO_2 reduction.[235,236] The Co(II) is pentacoordinated with pentadentate polypyridine ligands to form trigonalbipyramidal geometry, obviously different from commonly observed hexacoordinated Co complexes. In photochemical system using **155** as CAT, $[Ru(bpy)_3]^{2+}$ as PS, TEA as SD and *tri*-p-tolylamine (TTA) as a reversible quencher, CO (TON_{CO} = 3.4) and $HCOO^-$ (TON_{CO} = 1.4) were produced under visible-light irradiation (Table 2, entry 32). While for **156** with methoxy groups attached to the terminal pyridines of ligand, CO and H_2 (TON_{CO} = 5.1 and TON_{H2} = 8.1) were detected in the catalytic system (Table 2, entry 33).[235]

Recently, MOFs have attracted enormous attention in CO_2 reduction owing to their unique merits such as excellent CO_2 adsorption capacities and tailorable light-absorption abilities.[237–239] A number of Co-based MOFs bearing polypyridine ligands have been designed and used for photocatalytic CO_2 reduction.[240–242] In 2014, Wang and co-workers reported a Co-based zeolitic imidazolate framework (**157**; Fig. 25), which can serve as a robust MOF catalyst to reduce CO_2 by visible light.[29] **157** is an insoluble zeolitic solid with micropores. Irradiation of a CH_3CN/H_2O (4:1 *v*/*v*) suspension containing the powder of **157**, $[Ru(bpy)_3]^{2+}$ and TEOA with visible light (λ_{ex} = 420 nm) produced CO and H_2, with a Φ_{CO} of 1.48% (Table 2, entry 34). Repeated use of the CAT powder (5 times) gave a total TON_{CO} of 450. Besides, Zhang and Liao et al. designed and synthesized a series of Co-based MOFs, $[Co_2(\mu\text{-Cl})_2(bbta)]$ (**158**), $[Co_2(\mu\text{-OH})_2(bbta)]$ (**159**), $[Co_2(\mu\text{-Cl})_2(btdd)]$ (**160**) and $[Co_2(\mu\text{-OH})_2(btdd)]$ (**161**) supported by pyridine derivatives (H_2bbta =1*H*,5*H*-benzo-(1,2-d:4,5-d′)bistriazole, H_2btdd = bis(1*H*-1,2,3-triazolo-[4,5-*b*,4′,5′-*i*])dibenzo[1,4]dioxin); Fig. 25).[243] The catalytic performances of **158–161** for photocatalytic CO_2 reduction were studied under visible light irradiation in a 4:1 (*v*:*v*) CH_3CN/H_2O solution containing $[Ru(bpy)_3]^{2-}$ and TEOA. The results revealed that **159** and **161** (Table 2, entries 37 and 40) with μ-OH^- ligands bind with the open Co centers showed higher efficiency for CO_2-to-CO conversion than **158, 160** (Table 2, entries 36 and 39) and the zeolitic imidazolate framework **157** (Table 2, entry 35). The CO selectivity up to 98.2% and TOF of 0.059 s^{-1} of **161** (Table 2, entry 40) are much higher than most of reported heterogeneous catalysts.[29] More importantly, the TOFs of **159** and **161** reduced only about 20% in a low CO_2 concentration (1:9 CO_2/Ar mixture, entries 38 and 41 in Table 2), while other MOFs reduce by at least 90%.[243] Periodic DFT calculations and isotope tracing experiments showed that the μ-OH^- ligands serve not only as strong H-bonding donors to stabilize the initial Co-CO_2 adduct but also as local proton sources to facilitate the C—O bond cleavage, which greatly boosts the photocatalytic CO_2-to-CO conversion.

Cu complexes with polypyridine ligands active for photocatalytic CO_2 reduction are relatively rare. In 2017, a quaterpyridine Cu complex $[Cu(qpy)]^{2+}$ (**162**; qpy = 2,2′:6′,2″:6″,2‴-quaterpyridine; Fig. 25) was firstly reported as a selective catalyst for CO_2 reduction in a photocatalytic system containing 2 mM $[Ru(bpy)_3]^{2+}$, BIH/TEOA and CH_3CN.[244] This reaction is greatly enhanced by addition of H_2O (1–4% *v*/*v*), obtaining a TON of >12,400 for CO production and a selectivity of 97% (Table 2, entries 42–43).[244] Besides, we developed a new Cu^{II} complex $(Et_4N)[Cu(pyN_2Me_2)(HCO_2)]$ (**163**; Fig. 25) based on a NNN-pincer ligand bis(2,6-dimethylphenyl)-2,6-pyri-dinedicarbox-amidate(2-) (pyN_2Me_2).[245] We found that

DOI: 10.1016/j.enchem.2020.100034
EnergyChem **2**, 100034 (2020)

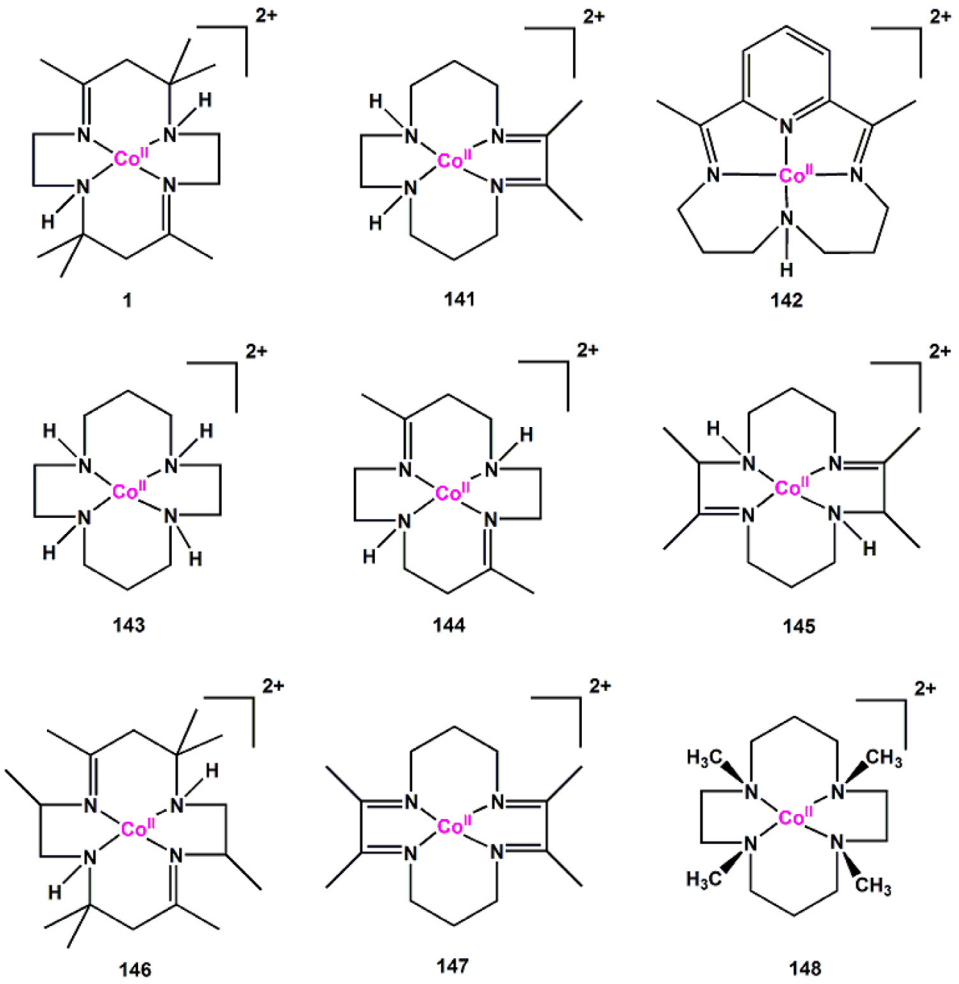

Fig. 21. Co macrocyclic complexes as molecular catalysts for photochemical CO_2 reduction.

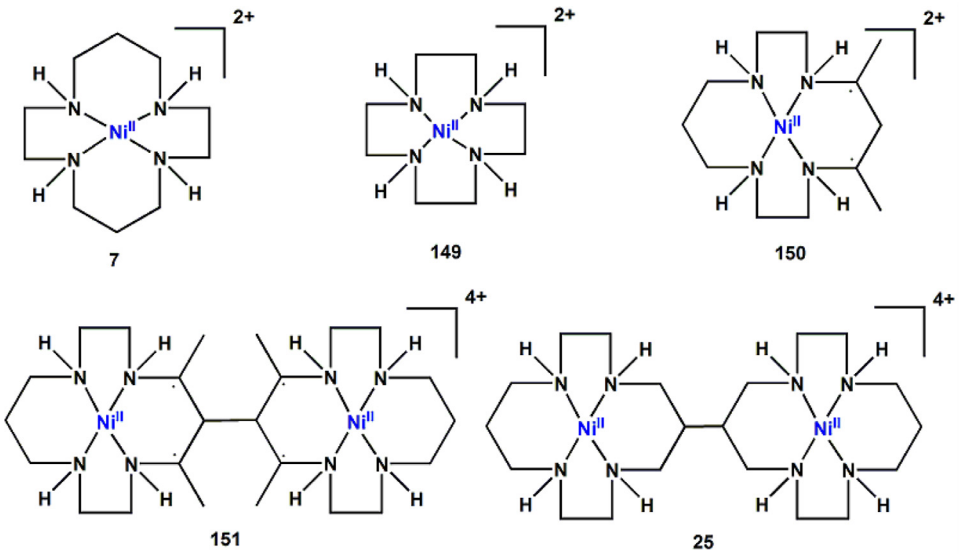

Fig. 22. Ni macrocyclic complexes as molecular catalysts for photochemical CO_2 reduction.

DOI: 10.1016/j.enchem.2020.100034
EnergyChem **2**, 100034 (2020)

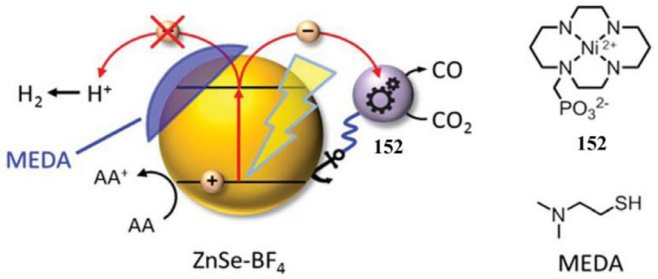

Fig. 23. Schematic representation of the photocatalytic system consisting of catalyst **152**, and ligand-free ZnSe QDs (ZnSe-BF_4) for CO_2 reduction. Reproduced with permission.[227] Copyright 2018, Royal Society of Chemistry.

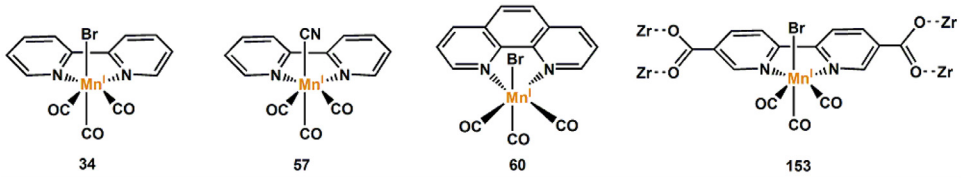

Fig. 24. Mn complexes based on polypyridine ligands as molecular catalysts for photochemical CO_2 reduction.

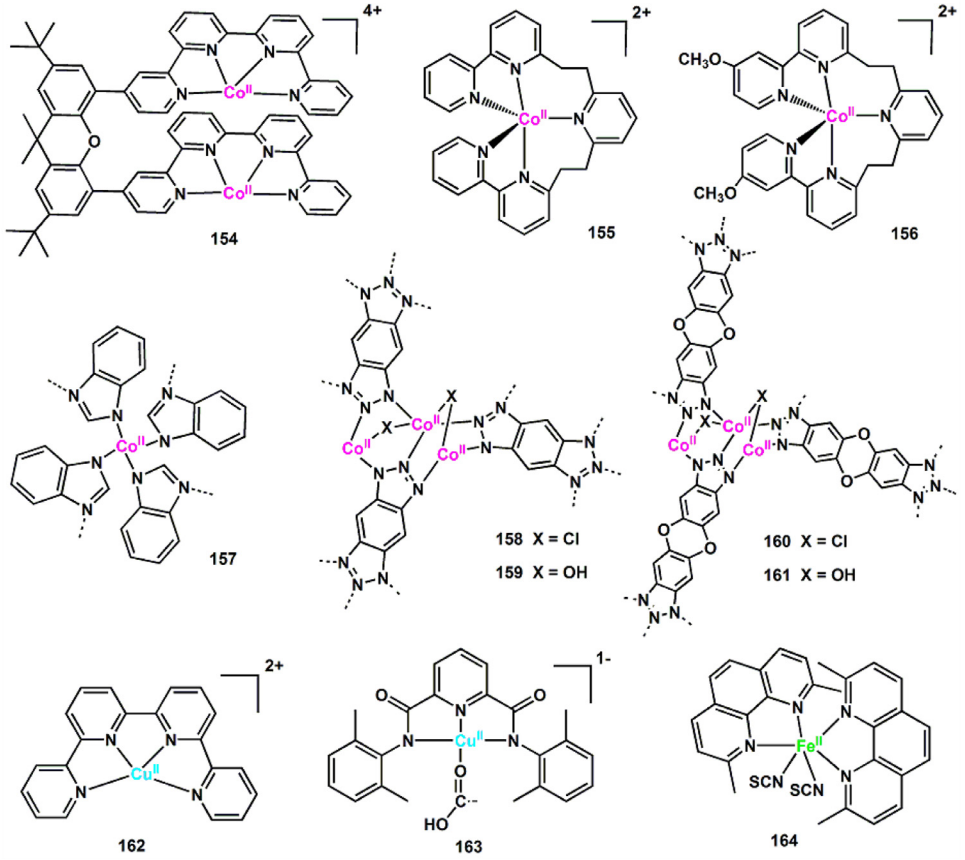

Fig. 25. Complexes and MOFs based on polypyridine ligands as molecular catalysts for photochemical CO_2 reduction.

163 (0.05 μM) possesses excellent photocatalytic performance for CO_2-to-CO conversion in the presence of $[Ru(phen)_3]^{2+}$ and TEOA in CH_3CN/H_2O (v:v = 4:1) solution, giving a high TON of 9900 and a TOF of 0.275 s^{-1}, as well as a high CO selectivity of 98% under irradiation of visible light for 10 h (Table 2, entry 44).

Fe polypyridine complexes were also employed as catalysts for photochemical CO_2 reduction.[246–250] Ishitani and co-workers reported an efficient and durable photocatalytic system for CO_2 reduction, where Fe polypyridine complex $Fe^{II}(dmp)_2(NCS)_2$ (**164**; Fig. 25) served as CAT, heteroleptic complex $Cu^{I}(dmp)(P)_2^{+}$ (dmp =2,9-dimethyl-1,10-phenanthroline; P = phosphine ligand) acted as PS, and BIH served as SD, from which CO was produced as the main product with a TON and quantum yield of 273 and 6.7%, respectively (Table 2,

DOI: 10.1016/j.enchem.2020.100034
EnergyChem **2**, 100034 (2020)

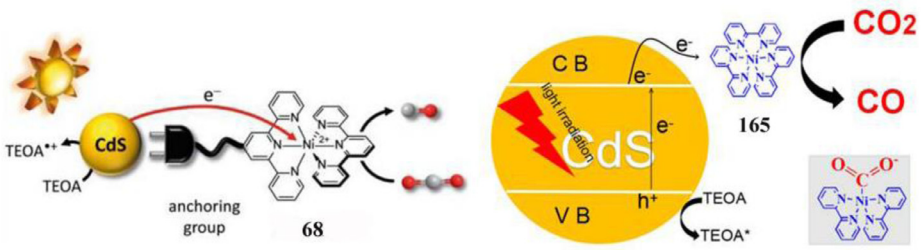

Fig. 26. Anchoring Ni polypyridine complexes onto CdS quantum dots photosensitizer. Reproduced with permission.[125] Copyright 2017, American Chemical Society.

entry 45).[246] In addition, the above-mentioned electroactive Fe quaterpyridine complex **63** (Fig. 7) can also serve as catalyst for photocatalytic CO_2 reduction.[46,117] Ishitani and co-workers found that in CH_3CN/TEOA solvent system with $[Ru(bpy)_3]^{2+}$ as the PS and BIH as the SD, a TON_{CO} of over 3000 with 85% selectivity can be realized for **63** (Table 2, entry 46).[46] The quantum yields of CO formation can reach 8.8% (Table 2, entry 47). The PS $[Ru(bpy)_3]^{2+}$ can be replaced with an organic PS purpurin. Irradiation of a DMF solution consisting of purpurin (2 mM), **63** (0.005 mM), and BIH (0.1 M) with visible light ($\lambda_{ex} = 460$ nm) led to the conversion of CO_2 to CO with TON of 1365 based on **63** (Table 2, entry 48).[46] In 2018, Ishitani and co-workers further developed an efficient and selective photocatalytic system for CO_2 reduction, which consisted of **63** catalyst and mesoporous graphitic carbon nitride (mpg-C_3N_4) redox photosensitizer.[251] After irradiation ($\lambda \geq 400$) in an CH_3CN/TEOA (v/v 4:1) mixed solution for 17 h, 12.4 μmol CO was detected as the major product, corresponding to a selectivity of 97%, a TON_{CO} of 155, and an apparent quantum yield of 4.2% (Table 2, entry 49).

The Ni-bis(tpy) complex (**68**; Fig. 7 and 26) could be anchored on CdS quantum dots for photochemical CO_2 reduction.[125] This combined system affords a visible-light-driven catalytic system for CO_2-to-CO conversion in a near-neutral aqueous solution with a selectivity of over 90%. The control experiments revealed that the strong attachment between the Ni molecular catalyst and the quantum dots is essential. Lin and co-workers developed a facile photocatalytic system consisting of a nickel complex $Ni(bpy)_3Cl_2$ as CAT (**165**; Fig. 26) and CdS as PS.[252–253] The main product CO was obtained under visible-light irradiation for 2 h. The selectivity reached as high as 81.25%, approximately six times more than that without **165** (Table 2, entry 50). A quantum yield of 1.68% was achieved under $\lambda = 420$ nm light irradiation.[252]

Metal complexes with porphyrin and porphyrin-like ligands

As described in the section of electrochemical CO_2 reduction, metal porphyrins, especially Fe porphyrins, have been extensively investigated as electrocatalysts for CO_2 reduction. Because they show strong absorption in visible light region, which is sensitive to the oxidation states of the metals and ligands, metalloporphyrins are suitable for the detection of reactive intermediates in catalytic CO_2 reduction cycle by electronic absorption spectroscopy.[10] In the past decades, scientists have systematically studied the effect of the substituents on the phenyl groups of porphyrin complexes on the photocatalytic efficiency. Many effective porphyrin complexes, in particular Fe tetraphenylporphyrin complexes and its derivatives with modified ligands, were designed for photochemical CO_2 reduction under visible light irradiation.

The first Fe porphyrins for photocatalytic CO_2 reduction was reported by Neta et al. in 1997.[254] Photoexcitation of a DMF/TEA (5%) solution containing photocatalysts **78** (Fig. 8 and 27) led one-electron reduction of Fe^{III} to Fe^{II}. The Fe^{II} species could be further reduced to Fe^{I} by TEA. Disproportionation of two Fe^{I} intermediates produces Fe^{III} and the catalytically active Fe^0 species, by which the main product of photochemical CO_2 reduction is CO, with a TON of 70 (Table 2, entry 51). However, the porphyrin ring rapidly converted into the corresponding chlorin structure, which is followed by further photochemical decomposition. Neta and co-workers then synthesized a cationic Fe porphyrin (**166**; Fig. 27) in which N-methyl was attached to four benzene rings. By **166**, the reduction of CO_2 generated CO in an pH 8.8 aqueous solution containing $NaHCO_3$ and TEA.[254] However, the whole CO_2 photoreduction proceeds with extremely low efficiency because photochemical reduction of the Fe porphyrins was very slow. To address this problem, Neta and co-workers introduced *p*-terphenyl as the PS to the system.[255] The standard reduction potential of the one-electron reduced species (OERS) of *p*-terphenyl was negative enough (−2.45 V vs SCE in dimethylamine) to reduce the $Fe^{II}P$ species (−1.05 V vs SCE for **78**, −1.02 V vs SCE for **167**, and −1.00 V vs SCE for **168**) and $Fe^{I}P$ (−1.66 V vs SCE for **78**, −1.61 V vs SCE for **167**, and −1.55 V vs SCE for **168**; Fig. 27) to form the corresponding Fe^0P species. The FeP system exhibits 10 times higher photocatalytic efficiency than those without *p*-terphenyl. By using *p*-terphenyl as PS, Fe tetrakis(3-methylphenyl)porphyrin (**169**; Fig. 27) was also able to photochemically reduce CO_2 in homogeneous solutions.[255,256]

In 2014, Robert and co-workers reported two ligand-modified Fe porphyrins (**79** and **81**; Fig. 8 and 27). They are derived from the parent catalyst **78** (Fig. 27). Both catalysts are active for photochemical ($\lambda > 280$ nm) CO_2 reduction in CH_3CN solution. After photocatalysis for 1 h, the CO selectivity reaches 93% for **79** and 76% for **81** (Table 2, entries 53 and 56). These results demonstrate the crucial role of the phenol substituents on phenyl rings in orienting the photocatalysis toward CO_2 reduction.[257] In contrast, for **78**, H_2 is the main reduction product under the same irradiation conditions (Table 2, entry 52),[257] probably owing to its much more negative standard redox potentials ($E^0(Fe^I/Fe^0) = -1.67$ V vs SCE in DMF)[258] and the absence of phenyl ring substituents to stabilize intermediate species involved in hydrocarbon production. The better catalytic performance of **79** and **81** for CO formation may be owing to their internal phenolic groups which can stabilize and protonate the CO_2 adduct formed with Fe(0) via intramolecular H-bonds. Robert and co-workers further explored the influence of PS

DOI: 10.1016/j.enchem.2020.100034
EnergyChem **2**, 100034 (2020)

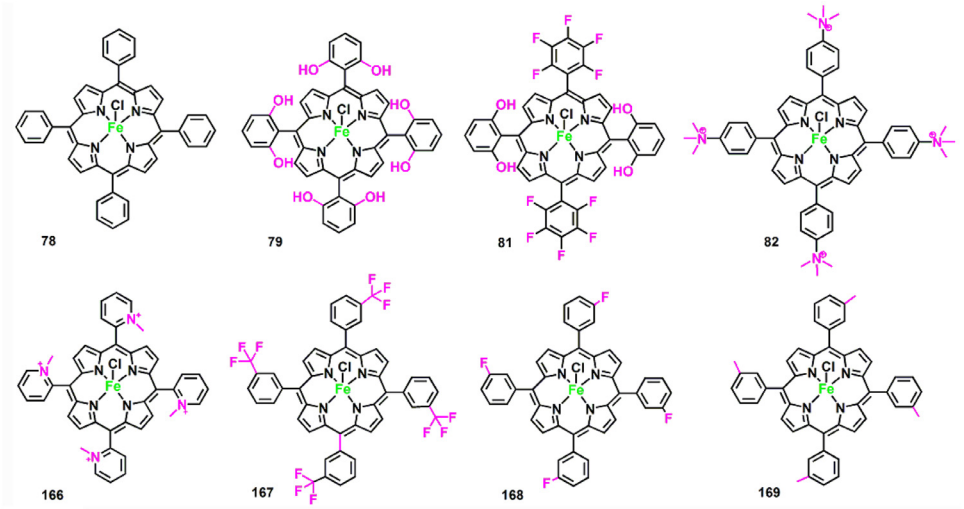

Fig. 27. Fe complexes based on porphyrin ligands as molecular catalysts for photochemical CO_2 reduction.

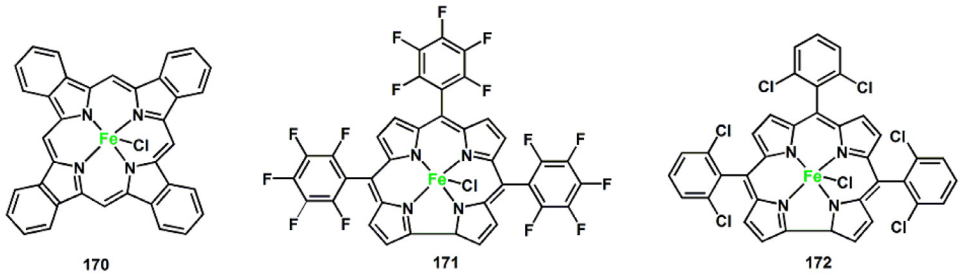

Fig. 28. Fe phthalocyanine and corroles as molecular catalysts for photochemical CO_2 reduction.

on photocatalytic performance. Using complex **79** as CAT, 9-cyanoanthracene (9-CNA; Fig. 19) as an inexpensive organic photosensitizer, the conversion of CO_2 to CO showed 100% selectivity and a maximum TON of 60 (Table 2, entry 54).[259] When 9-CNA was replaced with $Ir(ppy)_3$, a TON of 140 and selectivity of 93% for CO were obtained (Table 2, entry 55). Moreover, the catalyst and sensitizer are robust for a long period ($t > 50$ h).[259]

In 2017, Robert group further found that the Fe tetraphenylporphyrin **82** (Fig. 8 and 27) functionalized with four trimethylammonium groups at the *para* positions of the phenyls is an efficient and selective molecular electrocatalyst for CO_2 reduction.[27,176] In the presence of *fac*-$Ir(ppy)_3$ and TEA, the reduction of CO_2 by **82** produces CO, CH_4 and H_2 with TONs (selectivity) of 367 (78%), 79 (17%) and 26 (5%), respectively (Table 2, entry 57). Besides, Robert and co-workers found that **82** is water soluble and acts as a homogeneous molecular catalyst to selectively reduce CO_2 to CO with the assistance of an organic photosensitizer purpurin.[260] In this system, CO is produced with a selectivity of 95% and TON_{CO} of 60 (Table 2, entry 58), illustrating the possibility of photocatalyzing CO_2 reduction in aqueous solution using visible light. Recently, upon visible light irradiation, Robert and co-workers found that photochemical reduction of CO_2 has also been achieved using **82** as CAT, $[Ir(ppy)_2bpy]^+$ as PS in aqueous conditions (CH_3CN/H_2O v:v = 3:7). The main product was again CO while 9% of CH_4 was produced simultaneously (Table 2, entry 59).[261]

Fe phthalocyanine (**170**; Fig. 28) and Fe corroles (**171** and **172**) also exhibited photocatalytic activity for CO_2-to-CO conversion.[262–264] For **170**, the TON_{CO} was not as high as that of other Fe porphyrin derivatives even in the presence of *p*-terphenyl as PS (entries 60–61 in Table 2).[262] For **171** and **172** (entries 62–63 in Table 2), the photocatalytic activities (TONs = 40–100) were comparable to that of **78** under the same conditions (Table 2, entry 51).[263]

Co porphyrin **98** (Fig. 12 and 29) and its derivatives **173** and analogues Co phthalocyanine **174** (Fig. 29) were studied for photocatalytic CO_2 reduction by Neta, Fujita, Gross, and co-workers (Table 2, entries 64–66).[255,262–263,265,266] In 1998, they reported that Co porphyrin **98** was able to convert CO_2 into CO and formate in the presence of TEA as the SD in CH_3CN under UV/Vis light irradiation ($\lambda > 320$ nm).[265] After irradiation of 200 h, the system produced formate (TON > 220) and CO (TON = 80) with a total TON of more than 300 (Table 2, entry 64).[265] Electrochemical, photochemical and spectroscopic studies revealed that the $[Co^0P]$ species (P = porphyrin) was the active intermediate towards CO_2 binding and transformation. The Co^0P species is generated through successive photoreduction of $[Co^{II}P]$ and $[Co^{I}P]$ by TEA. The Co porphyrin **173** can also be used to produce CO, and its photocatalytic efficiency was comparable to that of the corresponding Fe porphyrin **169** (Table 2, entries 65 and 66).[255,256]

In 2016, Ye and co-workers selected $Zr_6O_4(OH)_4(TCPP\text{-}H_2)_3$ [MOF-525, TCPP = 4,4′,4″,4‴-(porphyrin-5,10,15,20-

DOI: 10.1016/j.enchem.2020.100034
EnergyChem **2**, 100034 (2020)

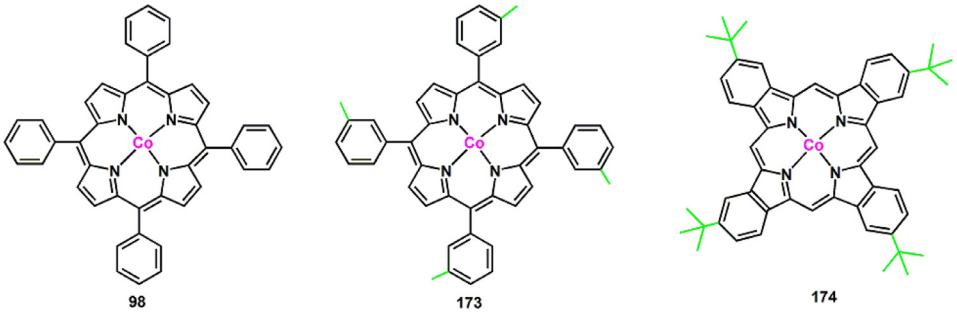

Fig. 29. Co porphyrin and its derivatives as molecular catalysts for photochemical CO_2 reduction.

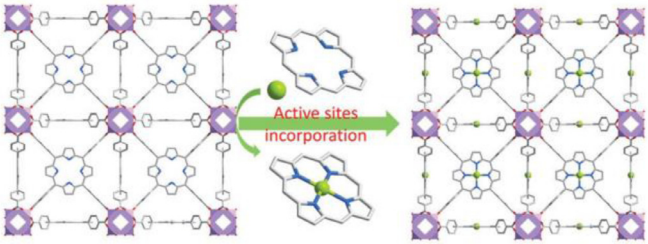

Fig. 30. 3D network of MOF-525-Co (**175**) featuring a highly porous framework and incorporated active Co sites. Reproduced with permission.[268] Copyright 2016, Wiley-VCH.

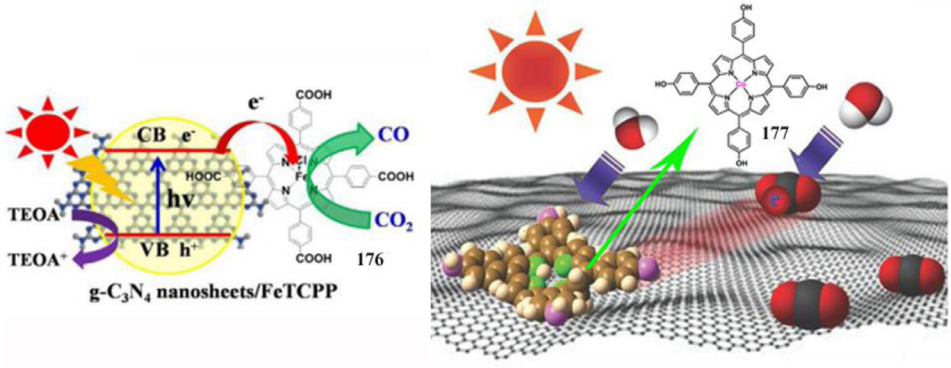

Fig. 31. Left: Structure of g-C_3N_4/FeTCPP heterogeneous catalyst system. Reproduced with permission.[269] Copyright 2018, Elsevier. Right: Proposed transfer process of photogenerated electrons for the porphyrin-graphene composite. Reproduced with permission.[270,271] Copyright 2014, Royal Society of Chemistry.

tetrayl) tetrabenzoate] as a MOF matrix.[267] After incorporation of Co, the resulting MOF-525-Co (**175**; Fig. 30) can selectively capture and reduce CO_2 to CO by visible light.[268] **175** comprises atomically dispersed catalytic centers and thus exhibits significantly enhanced photocatalytic conversion of CO_2, a 3.13-fold improvement in CO evolution rate (200.6 μmolg^{-1} h^{-1}) and a 5.93-fold improvement in CH_4 generation rate (36.67 μmol g^{-1} h^{-1}) compared with the empty matrix MOF-525 (Table 2, entries 68–69).[268] Experimental and theoretical investigations revealed that the single Co atoms in the MOF greatly boost the electron-hole separation efficiency in porphyrin units and therefore dramatically improve the photocatalytic performance of CO_2 reduction.

Recently, He and co-workers reported that the integration of carbon nitride nanosheet (g-C_3N_4) and Fe tetra(4-carboxylphenyl)porphyrin chloride (FeTCPP **176**; Fig. 31) molecular catalyst achieved CO generation with selectivity up to 98% by visible-light driven CO_2 reduction (Table 2, entry 70).[269] More interestingly, thin film photocatalysts constructed by merging Co tetrahydroxyphenyl porphyrin **177** and graphene proceeded well for CO_2 reduction under visible light, yielding CH_4 and C_2H_2 through selectively transfer of photogenerated electrons from graphene to CO_2 rather than to H_2O (Fig. 31; Table 2, entry 71).[270,271] The cooperation effect of graphene and Co complex provides a potential approach for generating multicarbon chemicals from CO_2 reduction.

Metal complexes with nonplanar N_4 ligands

Besides Co complexes featuring planar *trans* structures such as Co-macrocycle, Co-quaterpyridine, and Co-porphyrin complexes, Co complexes supported by nonplanar tetradentate N_4 ligands were also reported for photocatalytic CO_2-to-CO conversion with high TON and selectivity. In 2015, Chan et al. found [Co(TPA)Cl]$^+$ (**178**; Fig. 32) containing a tetradentate

DOI: 10.1016/j.enchem.2020.100034
EnergyChem **2**, 100034 (2020)

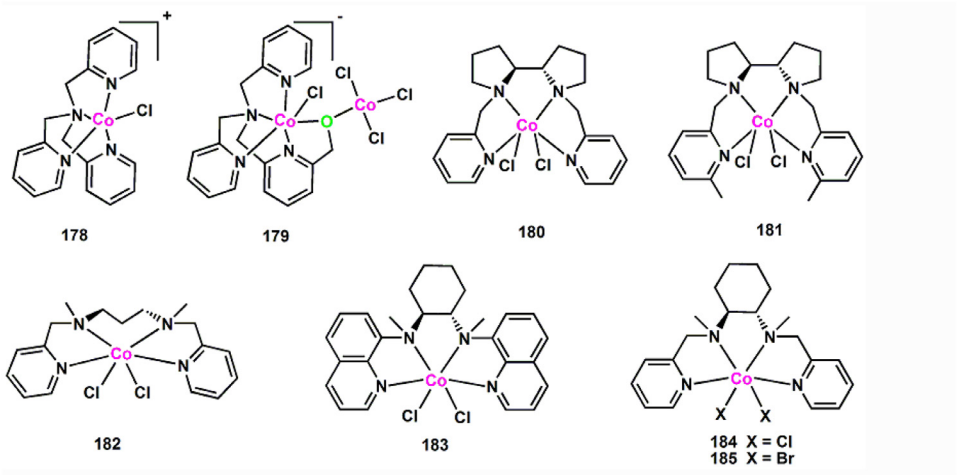

Fig. 32. Co complexes based on nonplanar N_4 ligands as molecular catalysts for photochemical CO_2 reduction.

tripodal ligand (TPA = tris(2-pyridylmethyl)amine) was able to catalyze CO_2-to-CO conversion using *fac*-Ir(ppy)$_3$ as the PS and TEA as the SD in CH_3CN, with a selectivity of 85% and a TON_{CO} of 953 (Table 2, entry 72).[272–274] Then, a novel dinuclear *cis*-Co^{II} complex **179** (Fig. 32) supported by a modified N_4 ligand derived with TPA was reported in 2018.[275] In contrast to **178, 179** contains an oxygen atom at the *cis*-coordination site. Experiments on the photocatalytic reduction of CO_2 revealed that **179** as the CAT can convert CO_2 to CO and formate (Table 2, entry 73).[275] DFT calculations revealed that the oxygen atom at the cis-coordination site plays an important role in CO_2-to-CO and CO_2-to-HCOOH conversions during photocatalysis.

In 2016, Che and co-workers reported a series of novel *cis*-[Co(N_4)Cl_2] complexes (**180–183**; N_4 = nonplanar N_4 ligands; Fig. 32) for photocatalytic CO_2 reduction (Table 2, entries 74–78).[276] These complexes adopt octahedral *cis*-coordination geometry in the solid state with two chloride ligands at *cis* positions. They found the photocatalytic performance of these Co complexes for CO_2 reduction was highly affected by the N_4 ligand structure. Complex **180** with a more flexible tetradentate ligand (PDP = 1,1′-bis(2-pyridinylmethyl)−2,2′-bipyrrolidine showed the highest activity and selectivity for photocatalytic CO_2-to-CO conversion in a DMF system containing *fac*-Ir(ppy)$_3$ as the PS and TEA as the SD. A TON_{CO} of 368 and selectivity of 95% were obtained after 60 h of visible light irradiation (Table 2, entry 74).[276] Electrochemical and spectroscopic studies demonstrated that the Co^{I} species generated by photoinduced electron transfer from excited *fac*-Ir(ppy)$_3$ to **180** is the active species for CO_2 binding. DFT calculations revealed that the protonation process of $[Co(CO_2)LCl]^0$ to give $[Co(COOH)LCl]^+$ is exothermic ($\triangle G^0 = -2.9$ kcal mol^{-1}) in comparison to the same process in the absence of chloride at Co ($\triangle G^0 = +24.1$ kcal mol^{-1}). The findings highlight the important role of *cis*-chloride at the Co center for CO_2 transformation. In addition, Wang and co-workers investigated the catalytic performance of two *cis*-Co complexes (**184** and **185**; Fig. 32) in a photocatalytic CO_2 reduction system using *fac*-Ir(ppy)$_3$ as the PS and TEA as the SD.[277,278] Both complexes were based on the same N_4 ligand but different halide ligands from complex **185** (Fig. 32). They found that two catalysts exhibited different performance in catalyzing CO_2-to-CO conversion under the same conditions. The rate of CO production by **185** (TON_{CO} = 102, entry 82 in Table 2) was faster than that by **184** (TON_{CO} = 56, entry 79 in Table 2) in the first 12 h of irradiation, indicating the influence of halogen ligands on CO formation. However, **184** was more stable and obtained a higher total TON_{CO} of 470 than **185** with a TON_{CO} of 403 after 48 h of photocatalysis (Table 2, entries 80 and 82).[277] Spectroscopic and electrochemical studies revealed that the rate constant and free energy change of the photoinduced electron transfer (PET) process by **185** are larger than those by **184**.

Tetradentate tripodal compounds, typical nonplanar N_4 ligands with C_3 symmetric axes, usually bind metals to form five-coordinated mononuclear metal complex.[172,173,279] The solvent molecule at the axial position can be replaced by a CO_2 molecule during the catalytic process. Thus, complexes with tetradentate tripodal ligands can act as catalysts for photocatalytic CO_2 reduction. Recently, our group developed a series of Co complexes with tetradentate tripodal ligands (**186–195**; Fig. 33) through ligand modification and constructed efficient and durable photocatalytic systems for CO_2 reduction.[14,30,31,174,280,281] Initially, a Co(II)-based mononuclear catalyst [Co(NTB)CH_3CN](ClO_4)$_2$ (**186**; Fig. 33) supported by a new tetradentate tripodal ligand NTB (NTB = tris-(benzimidazolyl-2-methyl)amine) with electron-rich benzimidazol groups was developed, which yields a TON_{CO} of 1179 and selectivity of 97% in a water-containing (CH_3CN/H_2O, v/v = 4:1) system using 0.4 mM [Ru(phen)$_3$](PF_6)$_2$ as the PS and TEOA/TEA as the SD (Table 2, entry 83).[173] **186** exhibits a better catalytic activity than the previously reported catalyst **178** (TON_{CO} = 686; Table 2, entry 84) under the same conditions, which is explained by electrochemical results that **186** has a more positive onset potential for electrochemical CO_2 reduction (−0.65 V vs NHE) than **178** (−0.92 V vs NHE). This is probably because the benzimidazol group of NTB in **186** is more electronic donating than the pyridyl group of TPA in **178**. Later, we designed another tripodal ligand complex [CoL(CH_3CN)](ClO_4)$_2$ (**187**; (L = tris[2-(*iso*-propylamino)ethyl]amine; Fig. 33), by which the reduction of CO_2 yielded a TON_{CO} of 44,800 and a CO selectivity of 97% with TEA as the SD (Table 2, entry 85).[174] It is noteworthy that the catalytic efficiency of the photocatalytic reduction of CO_2 by **187** is over seven-fold compared with that by **188** (Fig. 33) based on a similar tripodal ligand (Table 2, entries 86–87). This is presumably due to the smaller steric hindrance of isopropyl groups in **187** compared with benzyl

DOI: 10.1016/j.enchem.2020.100034
EnergyChem **2**, 100034 (2020)

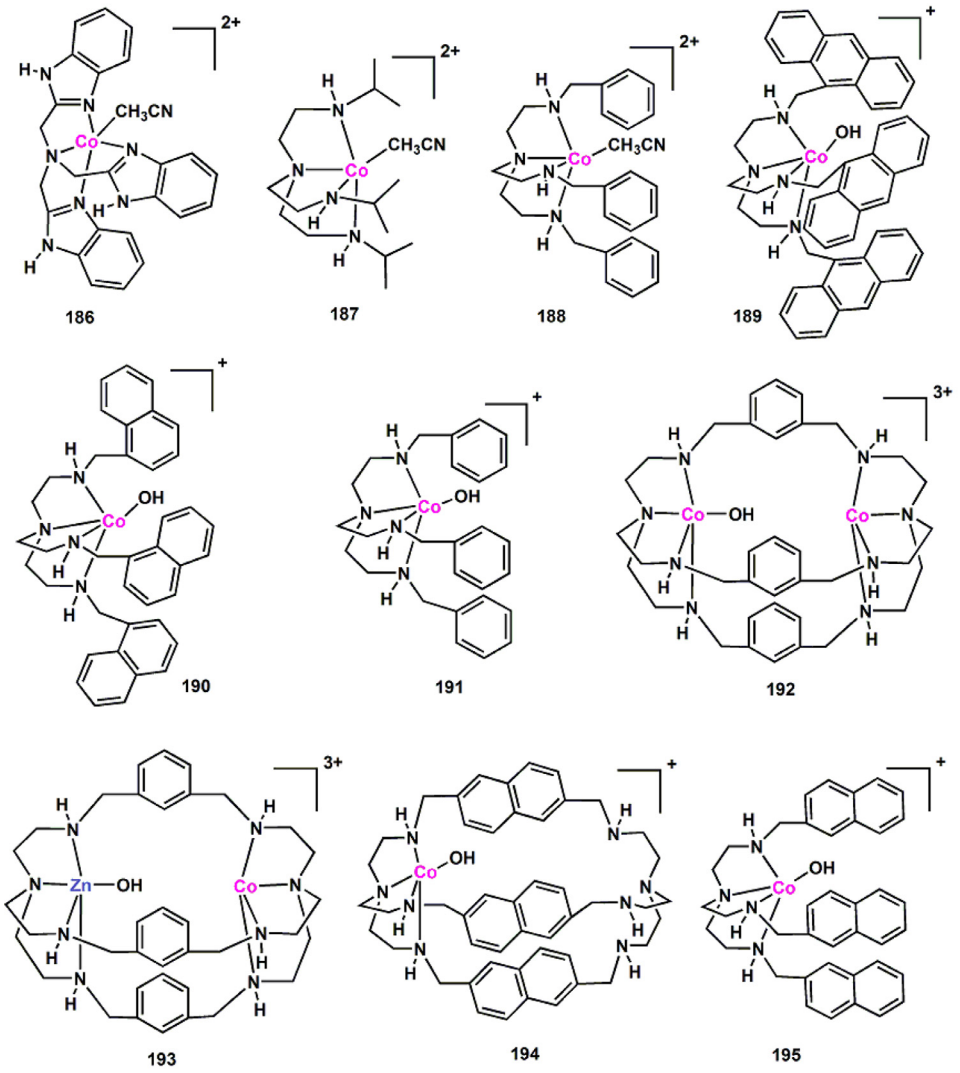

Fig. 33. Co complexes based on nonplanar N_4 ligands as molecular catalysts for photochemical CO_2 reduction.

groups in **188**. Small steric hindrance is beneficial for both CO_2 binding to catalytic center Co^{II} in **187** and electron transfer between the excited PS and catalyst **187**.[215-216,282] Based on the above-mentioned works, we further designed and synthesized three tripodal ligands with different conjugate groups and their corresponding Co complexes (**189–191**; Fig. 33).[280] Anthrylmethyl-substituted **189** and naphthylmethyl-substituted **190** possess higher efficiency than phenyl-methyl-substituted **191** for photocatalytic CO_2-to-CO conversion (Table 2, entries 88–90), with TON and TOF of 58,000 and 1.61 s^{-1} for **189**, and 49,200 and 1.37 s^{-1} for **190**, respectively. Complexes **189** and **190** also display higher CO selectivity ($\geq$ 97%) than **191**.[280] Control experiments and DFT calculations revealed that the excellent catalytic performances of **189** and **190** can be ascribed to the extended conjugation substituents in ligands, which endow the Co^{II} catalytic center with low reduction potential, accelerate the intermolecular electron transfer, and thus dramatically boost the CO_2-to-CO conversion.

With excellent electrocatalytic performance, the electrocatalysts **102–105** (Fig. 13) reported by our group were also active for photocatalytic CO_2 reduction (Table 2, entries 91–95).[175] **102–105** can reduce CO_2 to CO with high selectivity over 97%. More importantly, the catalytic efficiency of **102–104** was gradually improved with the increase of quinolinyl group and **104** possesses the highest TON value of 10,650 and CO selectivity of nearly 100% (Table 2, entry 94). The slightly lower catalytic efficiency of **105** may be attributed to the steric hindrance of quinolinyl groups.

Besides mononuclear Co(II) complexes, we also tried to develop dinuclear Co(II) complexes to exploit the dinuclear metal synergistic catalysis (DMSC) for CO_2 reduction. Recently, we designed a dinuclear Co cryptate complex (**192**; Fig. 33).[14] In **192**, two Co centers are confined within a bis-N_4 cryptand ligand by coordination. Due to the DMSC effect between two Co(II) centers, **192** exhibits a strong ability to absorb and fix CO_2, and shows outstanding activity for photochemical CO_2-to-CO conversion, with a high TON_{CO} value of 16,896 and a selectivity of 98% (Table 2, entry 96). These values are much higher than those of the corresponding mononuclear analogue **188** under the same conditions (Table 2, entry 87). The experimental results and DFT calculations showed that the excited state $[Ru(phen)_3]^{2+*}$ in the catalytic system was effectively oxidatively quenched by **192** and the high catalytic efficiency is attributed to the synergistic catalysis effect between two Co^{II} ions in **192**. A reaction pathway was proposed in Fig. 34. Firstly, **192** fixes CO_2 to form **192a** which then undergoes a

DOI: 10.1016/j.enchem.2020.100034
EnergyChem **2**, 100034 (2020)

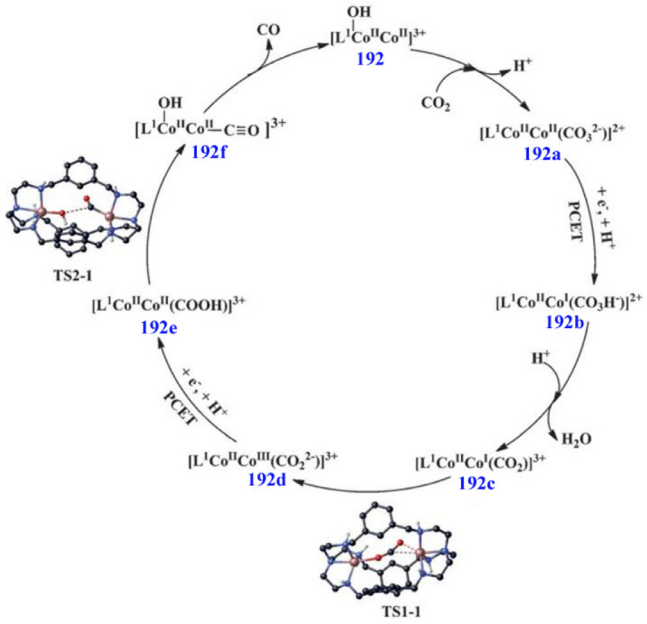

Fig. 34. Catalytic mechanism of **192** for the visible-light driven reduction of CO_2 to CO. Reproduced with permission.[14] Copyright 2017, Wiley-VCH.

proton-coupled electron transfer (PCET) to generate $Co^{II}Co^{I}$ species **192b**. Next, **192b** is protonated and then releases H_2O to give **192c. 192c** is converted into **192d** via transition state TS1-1. Then, **192d** undergoes a second PCET process to give **192e**. The C–OH bond in **192e** is cleaved via TS2-1 to form **192f**. Finally, the catalytic cycle completes via **192f** releasing a CO. The electrons of two PCET processes are delivered by photogenerated $[Ru^{I}(phen)_3]^{+}$ ($E^0 = -1.16$ V vs NHE). Based on these results, we proposed that during the photochemical CO_2-to-CO conversion by **192**, the two Co(II) centers work synergistically, where one acts as a catalytic center to reduce CO_2, and the other serves as an assistant catalytic site to facilitate the removal of the OH group.

To further confirm and take advantage of the DMSC, we designed a dinuclear hetero-metallic cryptate complex (**193**; Fig. 33), in which one Co^{II} in **193** was replaced by a Zn^{II}.[30] We have found that the dinuclear heterometallic complex **193** has an even larger TON_{CO} value of 65,000 (Table 2, entry 98) than **192** (TON_{CO} = 17,000, entry 97 in Table 2) and **188** (TON_{CO} = 1500, entry 99 in Table 2) for photocatalytic CO_2 reduction under the same conditions.[30] The greatly enhanced catalytic activity of **193** can be ascribed to significantly strengthened DMSC effect between Co^{II} and Zn^{II}, where the stronger binding affinity to OH^- of Zn^{II} greatly promotes the C−OH cleavage of the O=C−OH intermediate and thus significantly enhances the photocatalytic activity of **193** for CO_2 reduction to CO. These results provide a new strategy for the design and synthesis of outstanding catalysts for CO_2-to-CO conversion, and the concept of DMSC will greatly boost the developments of "artificial photosynthesis" and other catalytic fields.

To further improve the catalytic performance for CO_2 reduction via DMSC, we designed and synthesized a new cryptand to tune the distance between the two metal centers in dinuclear cryptate complexes. Unexpectedly, only a mononuclear cryptate (**194**; Fig. 33), rather than dinucelar cryptate, was obtained.[281] For comparison, a corresponding tripodal complex (**195**; Fig. 33) was also synthesized. It was found that cryptate complex **194**, with the active Co^{II} center encapsulated within its cavity, possesses higher catalytic activity than the tripodal complex **195** for photocatalytic CO_2-to-CO conversion, with the TON_{CO} and CO selectivity of 33,792 and 98% for **194** (Table 2, entry 100), and 18,656 and 97% for **195** (Table 2, entry 102), respectively.[281] Even under flue-gas condition (CO_2/Ar = 10/90), **194** still exhibits high activity (TON_{CO} = 600) and selectivity (95%) for photochemical CO_2-to-CO conversion (Table 2, entry 101). Control experiments and DFT calculation results demonstrate that the enhanced catalytic activity of **194** can be ascribed to its unique structure, which provides the low reduction potential of the catalytic center Co^{II} and the low energy barrier of catalytic transition states.

Metal complexes with N-heterocyclic carbene ligands

The electrochemically active N-heterocyclic carbene complexes (**110**–**114**; Fig. 14) have also been found photochemical catalytic conversion of CO_2 into CO.[28] Systematic changes in the carbene and amine donors of the ligand have been surveyed through ligand modification. Encouraged by the high performance in electrocatalysis, Chang et al. also utilized the aforementioned Ni N-heterocyclic carbene-isoquinoline complex **110** as a catalyst for photochemical CO_2-to-CO conversion in the presence of a large excess *fac*-Ir(ppy)$_3$ ($E_{1/2}^{red} = -1.73$ V vs SCE) as the PS (0.2 mM) and TEA as the SD under a simulated solar light irradiation in CH_3CN solution. **110** exhibits high selectivity to CO, as no H_2 and only a small quantity of CH_4 were detected. The TON of **110** for CO is significantly enhanced with decreasing catalyst concentrations and reaches a maximum value of 98,000 based on 2 nM CAT (Table 2, entry 103). [28] The mechanistic studies revealed oxidative quenching of photoexcited *fac*-Ir(ppy)$_3$ by **110**.

Recently, Papish et al. designed and synthesized a Ni(II) complex (**196**; Fig. 35) supported by CNC pincer ligand.[283] They found that a single remote atom change from H (**120**;

DOI: 10.1016/j.enchem.2020.100034
EnergyChem **2**, 100034 (2020)

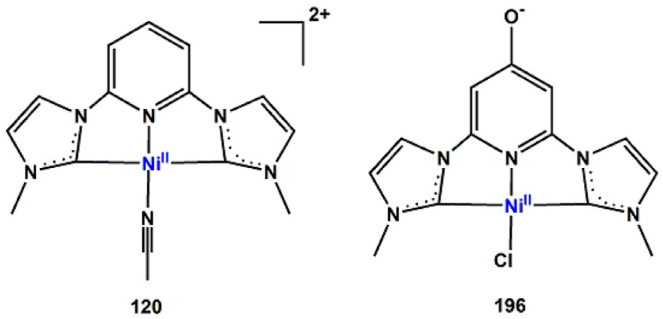

Fig. 35. Ni complexes based on N-heterocyclic carbene ligands as molecular catalysts for photochemical CO_2 reduction.

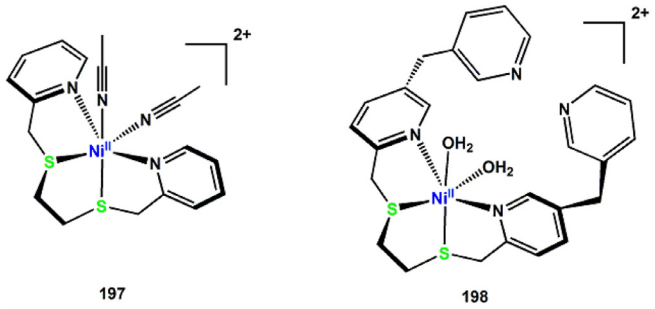

Fig. 36. Ni complexes (**197** and **198**) based on sulfur ligands as molecular catalysts for photochemical CO_2 reduction. Left: Reproduced with permission.[285] Copyright 2017, American Chemical Society. Right: Reproduced with permission.[32] Copyright 2019, American Chemical Society.

Figs. 15 and 35) to O (**196**) on the pincer CNC ligand resulted in a dramatic increase in catalytic activity for CO_2 reduction. In CH_3CN solution with $Ir(ppy)_3$, BIH, and TEA saturated with CO_2, **196** gives a TON_{CO} of 10.6 when irradiated with approximate natural sunlight over 6 h (Table 2, entry 104). Under identical conditions, **120** gives a TON_{CO} of only 0.09 (Table 2, entry 105). This efficiency difference highlights the critical role of a remote O^- group on catalytic activity. This study shows that remote atom substitution on a ligand can greatly influence catalytic performance. Furthermore, **196** was found to be protonated or deprotonated reversibly in situ to switch on or off the photocatalytic performance towards CO_2 reduction.[283]

Metal complexes with sulfur/bridging ligands

Metal complexes based on multidentate ligands containing thioether-sulfur atoms as metal-binding sites can be expected to improve activity for CO_2 reduction by stabilizing both intermediate and products in the catalytic cycle. With this idea, Kojima and co-workers developed a Ni complex $[Ni(bpet)(CH_3CN)_2]^{2+}$ (**197**; bpet = bis(2-pyridylmetyl)-1,2-ethanedithiol; Fig. 36), in which the Ni center and the S-coordinating sites resemble the $NiFe_4S_4$ cluster as in natural CO dehydrogenases (CODHs).[284] It was found that **197** can be used as a molecular catalyst for highly selective photochemical CO_2-to-CO conversion in the presence of $[Ru(bpy)_3]Cl_2$ as the PS and BIH as the SD in a DMA/H_2O solution mixture (9:1 v/v) under a CO_2 atmosphere, with a TON of over 700, a CO selectivity of > 99% and a quantum yield of 1.42% (Table 2, entry 106).[285] Further investigations indicated that the photo-excited PS is reductively quenched by BIH to generate the $[Ru(bpy)_3]^+$ species which drives the $Ni^{II/0}$ reduction. Electrochemistry result shows that the small potential difference between Ni^I and Ni° could be attributed to the stabilization of Ni^0 species by the S coordination. In 2019, Kojima and co-workers developed a novel Ni complex $[Ni(bpet\text{-}py_2)(H_2O)_2]^{2+}$ (**198**, Fig. 36)) supported by a S_2N_2-tetradentate ligand (bpet-py_2 = Bis-[5-(3-pyridylmethyl)-2-pyridylmethyl]-1,2-ethanedithiol) with two noncoordinating pyridine groups (bpet-py_2 = Bis-[5-(3-pyridylmethyl)−2-pyridylmethyl]−1,2-ethanedithiol).[32] They found that complexes **197** and **198** displayed a similar activity for photocatalytic CO_2 reduction in the absence of Mg^{2+} ions (Table 2, entries 107 and 109). However, the addition of Lewis-acidic Mg^{2+} ions greatly boosted the CO_2-to-CO conversion. Particularly for **198**, the activity was 4 times higher in the presence of Mg^{2+} ions than that in the absence of Mg^{2+} ions (Table 2, entries 109–110). The quantum yield of **198** for CO formation reached 11.1%, over 3 times higher than that of **197** (3.3%). The experimental and DFT calculation results indicated that the better catalytic activity of **198** over **197** derived from the noncoordinating pyridine arms in the ligand of **198**, which could capture Mg^{2+} ions. The Ni(II) and Mg(II) centers cooperately contribute to stabilize the Ni-CO_2 intermediate, leading to the improvement of CO_2 reduction.[32]

Coupling the catalyst with the PS via a bridging ligand to obtain supramolecular photocatalysts is an effective approach to accelerate energy and electron transmission, thus boosting the catalytic activity towards CO_2 reduction.[17,286–287] Several supramolecular photocatalysts have been reported. The first one, $Ru(phen)_2(phen\text{-}Ni(cyclam))(ClO_4)_4$ (**199**; Fig. 37), was reported by Kimura et al. in 1992.[40] **199** is a typical example of supramolecular photocatalyst composed of a $[Ru(phen)_3]^{2+}$ derivative as the PS unit and $[Ni(cyclam)]^{2+}$ as the CAT unit. This combined Ru-Ni supramolecular photocatalyst shows good

DOI: 10.1016/j.enchem.2020.100034
EnergyChem **2**, 100034 (2020)

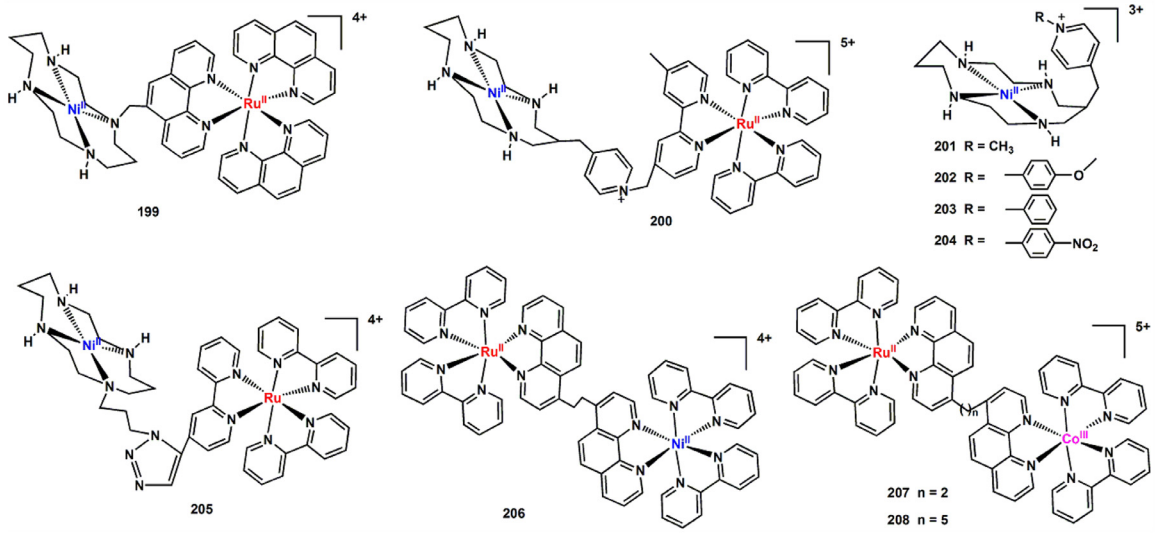

Fig. 37. Supramolecular photocatalysts for photochemical CO_2 reduction.

stability and catalytic activity for photocatalytic CO_2 reduction.[40] The selectivity for CO of 72% (Table 2, entry 111) was higher than that of the physically mixed system comprising the corresponding model complexes $[Ru(phen)_3]^{2+}$ and $[Ni(cyclam)]^{2+}$ (36%, Table 2, entry 112).[17,40] However, the productivity and selectivity are still modest, presumably because the introduction of a methyl in the periphery of $Ni(cyclam)^{2+}$significantly decreases the catalytic efficiency. Therefore, another Ru-Ni supramolecular photocatalyst where the 3′-position of cyclam was substituted by a pyridinium derived $[Ru(bpy)_3]^{2+}$ (**200**; Fig. 37) was developed (Table 2, entry 113), and four other monomeric pyridinium derivatives of $Ni(cyclam)^{2+}$ (**201–204**; Fig. 37) were also synthesized for comparison.[288] Photocatalytic experiments demonstrated that Ru-Ni complex **200** is not an efficient catalyst for CO_2 reduction as it is cleaved in the presence of a reductant and light. However, surprisingly, monomeric $Ni(cyclam)^{2+}$ species with pyridinium pendants (**201–204**) display significantly better activity and selectivity than the parent $Ni(cyclam)^{2+}$ (**7**; Fig. 2), with the order of **7 < 201 < 202 < 204 < 203**, presumably because the pendant pyridinium groups can serve as the electron acceptor and/or the electron storage during catalysis. In order to further activate the cyclam-nickel centers by visible light, Aukauloo et al. developed a new supramolecular photocatalysts (**205**; Fig. 37) for CO_2 reduction in 2014. In **205**, a ruthenium trisbipyridyl-like unit covalently attaches to a nickel cyclam via a triazole ring.[289] In aqueous solutions (pH = 6.5), activation of the Ru^{II}–Ni^{II} modular assembly with 450 nm visible light in the presence of ascorbate as a SD accomplishes the reduction of CO_2 and yields CO and H_2 in a ratio of 2.7 to 1 with a TON_{CO} of 5.2 and a TON_{H2} of 2 (Table 2, entry 114).[289]

In 1999, Komatsuzaki et al. reported three bimetallic supramolecular photocatalysts (**206–208**; Fig. 37), which consist of a $[Ru(bpy)_2(phen)]^{2+}$-type complex as the PS unit and a Ni(II) or Co(III) polypyridyl complex as the CAT unit.[290] **206** produced almost equivalent amounts of CO and H_2 (TON_{CO} = TON_{H2} = 2; Table 2, entry 115), whereas the mixed system ($[Ru(bpy)_3]^{2+}$ + $[Ni(bpy)_3]^{2+}$) mainly produced CO (TON_{CO} = 2, TON_{H2} < 1; Table 2, entry 116). The photocatalytic performance of the Ru(II)-Co(III) supramolecular photocatalysts (**207**, TON_{CO} = 3, TON_{H2} = 1, entry 117, Table 2; **208**, TON_{CO} = 5, TON_{H2} = 1, Table 2, entry 118) were lower than that of a mixed system of the corresponding model complexes, $[Ru(bpy)_3]^{2+}$ and $[Co(bpy)_3]^{3+}$ (TON_{CO} = 9, TON_{H2} = 16; Table 2, entry 119). Although the stability and selectivity are slightly superior to systems based on physically mixing of PS and CAT complexes, these three bimetallic systems catalyze the photoreduction of CO_2 to CO very inefficiently. In 2017, a series of Ru-Co supramolecular photocatalysts (**209–213**; Fig. 38) were synthesized and tested for photochemical reduction of CO_2 to CO.[291] As shown in Fig. 38, these five Ru-Co complexes differ from each other in the Co coordination sphere, Ru coordination sphere, or the linker between Ru and Co units. The best systems are those using a CAT unit in which the Co center is coordinated by three diimine ligands, such as **209, 211** and **213**, with TON values of about 50–70 for CO after 8 h irradiation using a 300 W Xe lamp (λ > 415 nm) in the presence of BIH as the SD in a CH_3CN/TEOA (*v*/*v* = 5:1) solvent mixture (Table 2, entries 120, 122 and 124).[291] Interestingly, when the aromatic linker is a *t*Bu-phenol (**213**), slightly better stability was observed as compared to **209** and **211** with a phenyl linker, since CO and H_2 formation were still observed after 16 h of reaction (TON_{CO} = 70 and TON_{H2}= 39; Table 2, entry 124). In contrast, when the Co center is penta-coordinated with a terpyridine ligand as in complexes **210** and **212**, poor catalytic efficiency was observed (Table 2, entry 121 and 123). The physically mixed system consisting of $[Ru(bpy)_3]^{2+}$ as the PS and $[Co(phen)_3]^{2+}$ as the CAT gives larger TOF values but it is much less selective and stable under the same conditions (Table 2, entry 125). Very recently, Ishitani, Fabry and co-workers reported a binuclear and a trinuclear Ru(II)-Mn(I) supramolecular photocatalysts for CO_2 reduction (**214–215**, Fig. 38).[292] They found that **214** with one Ru(II) PS unit and Mn(I) CAT unit showed higher efficiency for HCOOH formation (TON_{HCOOH} = 98 and TON_{CO}= 29; Table 2, entry 126) than the corresponding mixed system containing $[Mn(MeRes)(CO)_3Br]$ and $[Ru(dmb)_3]^{2+}$ (TON_{HCOOH} = 90 and TON_{CO}= 11; Table 2, entry 128). In marked contrast, **215** with two Ru(II) PS unit and Mn(I) CAT unit displayed lower efficiency (TON_{HCOOH} = 33 and TON_{CO}= 18; Table 2, entry 127) due to slow intramolecular electron transfer from the PS unit to the CAT unit.[292]

DOI: 10.1016/j.enchem.2020.100034
EnergyChem **2**, 100034 (2020)

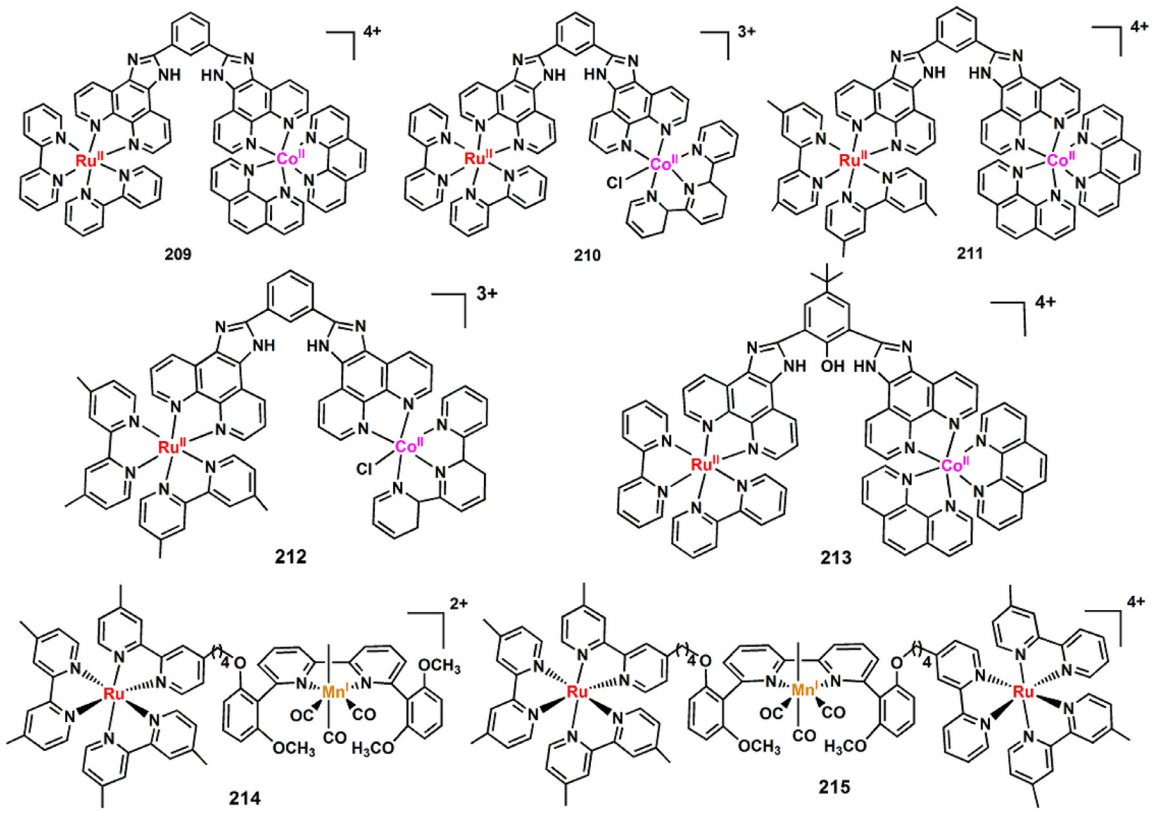

Fig. 38. Ru-Co and Ru-Mn supramolecular photocatalysts for photochemical CO_2 reduction.

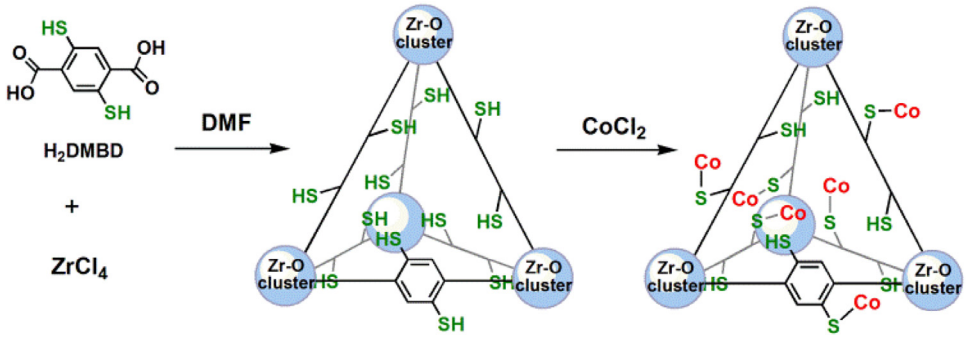

Fig. 39. Synthesis of the Zr-DMBD-Co-x catalysts for photochemical CO_2 reduction. Reproduced with permission.[31] Copyright 2019, Wiley-VCH.

MOFs could be used as supports to anchor active sites for photocatlaytic CO_2 reduction. We developed a series of catalysts Zr-DMBD-Co-x (**216**; x is the weight percentage of Co(II) ions; Fig. 39) by anchoring active Co(II) centers into a robust Zr-based MOF (Zr-DMBD) with self-standing thiol (−SH) groups.[31] The loading amounts of Co(II) ions in Zr-DMBD is tunable (8.69, 3.11, 1.00, 0.30, 0.02, 0.002, wt%). The pores of the prepared **216** are modified by well-defined Co-thiolate units (Co−S) and possess suitable pores capable of CO_2 adsorption. In the optimized photocatalytic system,[14,30,175] the sample Zr-DMBD-Co-0.002% displays highly efficient and selective photocatalytic CO_2-to-CO conversion in the presence of $[Ru(phen)_3](PF_6)_2$ as the PS and TEOA as the SD under visible-light irradiation in a water-containing system (CH_3CN/H_2O, v/v = 4:1). The TON_{CO} and CO selectivity reach as high as 97,941 and 98%, respectively (Table 2, entry 129).[31] Compared with previous reported MOF-based catalysts for photochemical CO_2 reduction, this catalyst exhibits the highest efficiency, activity, as well as atomic economy.

Hundreds of molecular catalysts for photocatalytic CO_2 reduction have been introduced above. It is necessary to point out that the photocatalytic activity belongs to the result of synergistic effect among catalyst, photosensitizer, and sacrificial agent in a catalytic system. Therefore, any description that only emphasizes the activity of catalysts may not be suitable. In addition, many researchers often use high TON values to evaluate the performance of catalysts. In fact, almost all the photocatalytic systems listed in Table 2 contain large excess amounts of photosensitizer. In this case, the TON values are less meaningful for the catalysts. Just reporting high TONs and at the same time ignoring the concept of photocatalysis highly mislead for the community. The comparison of TONs is meaningful only

DOI: 10.1016/j.enchem.2020.100034
EnergyChem **2**, 100034 (2020)

for the similar catalytic systems, by which the relative activity of catalysts can be distinguished.

CONCLUSION AND OUTLOOK

In this review, from the ligand perspective, we have discussed current development of non-noble metal molecular catalysts for both electrochemical and photochemical CO_2 reduction. It can be seen that the catalytic performance of a large number of non-noble metal complexes can be improved via ligand modification, which strongly evidenced that the ligand modification is an effective strategy to enhance the catalytic performance of molecular catalysts. Although an applicable catalytic system with perfect performance has not been reported, with continuous efforts of researchers, the way to get so perfect catalysts is closer and closer. To obtain ideal molecular catalysts for CO_2 reduction, several aspects could be suggested based on the above discussion. Firstly, strengthening the binding of catalysts to CO_2 molecules is very necessary. Without binding sites to CO_2 molucules, CO_2 can not be concentrated around the catalysts, and it is difficult for the catalytic centers to contact, activate and convert the CO_2 molecules. Therefore, catalysts with ligands containing functional groups for capturing CO_2 are much needed. Especically, if the steric hindrance could be negeligible, such functional groups are expected to be near the metal centers. The closer, the better. The ligands with –OH and $–NH_2$ groups have been reported to be beneficial for CO_2 capture. Secondly, the Lewis basicity of the coordination atoms on ligand around the metal centers should be suitable. In principle, weak Lewis basicity of the coordination atoms leads to the easy reduction of the metal center, which will decrease the overpotential of electrochemical CO_2 reduction. However, the weaker basicity also induces the unstability of the metal complex catalysts. Thirdly, functional groups around the catalytic centers that can contribute to the stability of the reaction intermediate are also desired. These groups may generate weak interaction with the intermediate binding with the catalytic centers, by which the reaction intermediate may further proceed along the expected reaction direction. In addition, confinement of the ligand is also found to be beneficial for the stability of the reaction intermediate. Finally, we have put forward and definitely evidenced that the dinuclear metal synergistic catalysis can greatly boost the photochemical CO_2-to-CO conversion. Therefore, multidentate ligands that can bind two or more metal centers to form compounds with conformations suitable for synergistically catalyzing CO_2 reduction are much expected. Multidentate ligands are potential to extend molecular catalysts with single metal sites to dinuclear or polynuclear metal sites, which can cooperate to activate and convert CO_2 molecules.

With definite molecular structures and designability, metal complexes have provided a perfect research platform for developing CO_2 reduction catalysts. The studies on molecular catalysis for CO_2 reduction, not only aim at applicable catalysts, but also devote to understanding activity-structure relationship to give fundamental undstanding to the catalytic reaction process at a molecular level. In this sense, the investigation on molecular catalysis of CO_2 redcution, in spite of challenging and difficult, is greatly significant and meaningful. This review has thoroughly discussed the relationship between activity and structures of molecular complexes in CO_2 reduction catalysts. We believe that this review will give researchers new insights in catalyzing CO_2 reduction, and more efforts will be devoted to deeply studying the catalytic mechanism of CO_2 reduction. In near future, the ligand modification strategy will be dominant in development of CO_2 reduction catalysts, especially non-noble metal catalysts.

ACKNOWLEDGMENTS

This work was supported by the National Key R&D Program of China (2017YFA0700104), the National Natural Science Foundation of China (21931007, 21790052 and 21861001), 111 Project of China (D17003), and the Science & Technology Development Fund of Tianjin Education Commission for Higher Education (2018KJ129).

AUTHOR CONTRIBUTIONS

Dong Cheng Liu: Writing original draft; Writing review & editing. **Di Chang Zhong:** Writing rev iew & editing. **Tong Bu Lu:** Writing review & editing.

CONFLICT OF INTEREST

The authors declare no conflict of interest.

REFERENCES

1. Spurgeon, J. M., Kumar, B. A comparative technoeconomic analysis of pathways for commercial electrochemical CO_2 reduction to liquid products. *Energy Environ. Sci.* **11**, 1536–1551 (2018).
2. Dalle, K. E., Warnan, J., Leung, J. J., Reuillard, B., Karmel, I. S., Reisner, E. Electro- and solar-driven fuel synthesis with first row transition metal complexes. *Chem. Rev.* **119**, 2752–2875 (2019).
3. Artz, J., Muller, T. E., Thenert, K., Kleinekorte, J., Meys, R., Sternberg, A., Bardow, A., Leitner, W. Sustainable conversion of carbon dioxide: an integrated review of catalysis and life cycle assessment. *Chem. Rev.* **118**, 434–504 (2018).
4. Wang, F. Artificial photosynthetic systems for CO_2 reduction: progress on higher efficiency with cobalt complexes as catalysts. *ChemSusChem* **10**, 4393–4402 (2017).
5. Francke, R., Schille, B., Roemelt, M. Homogeneously catalyzed electroreduction of carbon dioxide-methods, mechanisms, and catalysts. *Chem. Rev.* **118**, 4631–4701 (2018).
6. Bose, P., Mukherjee, C., Golder, A. K. A Ni^{II} complex of the tetradentate salen ligand H_2LNH_2 comprising an anchoring $–NH_2$ group: synthesis, characterization and electrocatalytic CO_2 reduction to alcohols. *Inorg. Chem. Front.* **6**, 1721–1728 (2019).
7. Morris, A. J., Meyer, G. J., Fujita, E. Molecular approaches to the photocatalytic reduction of carbon dioxide for solar fuels. *Acc. Chem. Res.* **42**, 1983–1994 (2009).
8. Wang, W. H., Himeda, Y., Muckerman, J. T., Manbeck, G. F., Fujita, E. CO_2 hydrogenation to formate and methanol as an alternative to photo- and dlectrochemical CO_2 reduction. *Chem. Rev.* **115**, 12936–12973 (2015).
9. Qiao, J., Liu, Y., Hong, F., Zhang, J. A review of catalysts for the electroreduction of carbon dioxide to produce low-carbon fuels. *Chem. Soc. Rev.* **43**, 631–675 (2014).
10. Fukuzumi, S., Lee, Y.-. M., Ahn, H. S., Nam, W. Mechanisms of catalytic reduction of CO_2 with heme and nonheme metal complexes. *Chem. Sci.* **9**, 6017–6034 (2018).
11. Takeda, H., Cometto, C., Ishitani, O., Robert, M. Electrons, photons, protons and earth-abundant metal complexes for molecular catalysis of CO_2 reduction. *ACS Catal* **7**, 70–88 (2017).
12. Chen, L., Guo, Z., Wei, X. G., Gallenkamp, C., Bonin, J., Anxolabehere-Mallart, E., Lau, K. C., Lau, T. C., Robert, M. Molecular catalysis of the electrochemical and photochemical reduction of CO_2 with earth-abundant metal complexes. selective production of CO vs HCOOH by switching of the metal center. *J. Am. Chem. Soc.* **137**, 10918–10921 (2015).

DOI: 10.1016/j.enchem.2020.100034
EnergyChem **2**, 100034 (2020)

13. Volpe, M., Hartnett, H., Leeland, J. W., Wills, K., Ogunshun, M., Duncombe, B. J., Wilson, C., Blake, A. J., McMaster, J., Love, J. B. Binuclear cobalt complexes of schiff-base calixpyrroles and their roles in the catalytic reduction of dioxygen. *Inorg. Chem.* **48**, 5195–5207 (2009).
14. Ouyang, T., Huang, H. H., Wang, J. W., Zhong, D. C., Lu, T. B. A dinuclear cobalt cryptate as a homogeneous photocatalyst for highly selective and efficient visible-light driven CO_2 reduction to CO in CH_3CN/H_2O solution. *Angew. Chem. Int. Ed.* **56**, 738–743 (2017).
15. Barlow, J. M., Yang, J. Y. Thermodynamic considerations for optimizing selective CO_2 reduction by molecular catalysts. *ACS Cent. Sci.* **5**, 580–588 (2019).
16. Grills, D. C., Ertem, M. Z., McKinnon, M., Ngo, K. T., Rochford, J. Mechanistic aspects of CO_2 reduction catalysis with manganese-based molecular catalysts. *Coord. Chem. Rev.* **374**, 173–217 (2018).
17. Tamaki, Y., Ishitani, O. Supramolecular photocatalysts for the reduction of CO_2. *ACS Catal* **7**, 3394–3409 (2017).
18. Cao, L.-. M., Huang, H.-. H., Wang, J.-. W., Zhong, D.-. C., Lu, T.-. B. The synergistic catalysis effect within a dinuclear nickel complex for efficient and selective electrocatalytic reduction of CO_2 to CO. *Green Chem* **20**, 798–803 (2018).
19. Costentin, C., Drouet, S., Robert, M., Saveant, J. M. Turnover numbers, turnover frequencies, and overpotential in molecular catalysis of electrochemical reactions. Cyclic voltammetry and preparative-scale electrolysis. *J. Am. Chem. Soc.* **134**, 11235–11242 (2012).
20. Yamazaki, Y., Takeda, H., Ishitani, O. Photocatalytic reduction of CO_2 using metal complexes. *J. Photochem. Photobiol. C* **25**, 106–137 (2015).
21. Tamaki, Y., Koike, K., Morimoto, T., Ishitani, O. Substantial improvement in the efficiency and durability of a photocatalyst for carbon dioxide reduction using a benzoimidazole derivative as an electron donor. *J. Catal.* **304**, 22–28 (2013).
22. Fisher, B. J., Eisenberg, R. Electrocatalytic reduction of carbon dioxide by using macrocycles of nickel and cobalt. *J. Am. Chem. Soc.* **102**, 7361–7363 (1980).
23. Bujno, K., Bilewicz, R., Siegfried, L., Kaden, T. Electroreduction of CO_2 catalyzed by Ni(II) tetraazamacrocyclic complexes - reasons of poisoning of the catalytic surfaces. *Electrochim. Acta* **42**, 1201–1206 (1997).
24. Tinnemans, A. H. A., Koster, T. P. M., Thewissen, D. H. M. W., Mackor, A. Tetraaza-macrocyclic cobalt(II) and nickel(II) complexes as electron-transfer agents in the photo(electro)chemical and electrochemical reduction of carbon dioxide. *Recl. Trav. Chim. Pays-Bas* **103**, 288–295 (1984).
25. Lehn, J. M., Ziessel, R. Photochemical generation of carbon monoxide and hydrogen by reduction of carbon dioxide and water under visible light irradiation. *Proc. Natl. Acad. Sci. USA* **79**, 701–704 (1982).
26. Costentin, C., Robert, M., Saveant, J. M. Current issues in molecular catalysis illustrated by iron porphyrins as catalysts of the CO_2-to-CO electrochemical conversion. *Acc. Chem. Res.* **48**, 2996–3006 (2015).
27. Azcarate, I., Costentin, C., Robert, M., Saveant, J. M. Through-space charge interaction substituent effects in molecular catalysis leading to the design of the most efficient catalyst of CO_2-to-CO electrochemical conversion. *J. Am. Chem. Soc.* **138**, 16639–16644 (2016).
28. Thoi, V. S., Kornienko, N., Margarit, C. G., Yang, P., Chang, C. J. Visible-light photoredox catalysis: selective reduction of carbon dioxide to carbon monoxide by a nickel N-heterocyclic carbene-isoquinoline complex. *J. Am. Chem. Soc.* **135**, 14413–14424 (2013).
29. Wang, S., Yao, W., Lin, J., Ding, Z., Wang, X Cobalt imidazolate metal-organic frameworks photosplit CO_2 under mild reaction conditions. *Angew. Chem. Int. Ed.* **53**, 1034–1038 (2014).
A Co-based zeolitic imidazolate framework was employed as efficient catalyst for photoreduction of CO_2 to CO under mild reaction conditions
30. Ouyang, T., Wang, H. J., Huang, H. H., Wang, J. W., Guo, S., Liu, W. J., Zhong, D. C., Lu, T. B. Dinuclear metal synergistic catalysis boosts photochemical CO-to-CO conversion. *Angew. Chem. Int. Ed.* **57**, 16480–16485 (2018).
The concept of dinuclear metal synergistic catalysis (DMSC) effect was firstly put forward and achieved in photochemical CO_2-to-CO conversion, to significantly improved the catalytic activity and selectivity
31. Liu, D. C., Ouyang, T., Xiao, R., Liu, W. J., Zhong, D. C., Xu, Z., Lu, T. B. Anchoring Co(II) Ions into a thiol-laced metal-organic framework for efficient visible-light-driven conversion of CO_2 into CO. *ChemSusChem* **12**, 2166–2170 (2019).
32. Hong, D., Kawanishi, T., Tsukakoshi, Y., Kotani, H., Ishizuka, T., Kojima, T. Efficient photocatalytic CO_2 reduction by a Ni(II) complex having pyridine pendants through capturing a Mg^{2+} ion as a lewis-acid cocatalyst. *J. Am. Chem. Soc.* **141**, 20309–20317 (2019).
33. Finn, C., Schnittger, S., Yellowlees, L. J., Love, J. B. Molecular approaches to the electrochemical reduction of carbon dioxide. *Chem. Commun.* **48**, 1392–1399 (2012).
34. Angamuthu, R., Byers, P., Lutz, M., Spek, A. L., Bouwman, E. Electrocatalytic CO_2 conversion to oxalate by a copper complex. *Science* **327**, 313–315 (2010).
A sulfur-ligand-based dinuclear Cu(II) complex can catalyze the one-electron reduction of CO_2 in CH_3CN to produce oxalate
35. Bourrez, M., Molton, F., Chardon-Noblat, S., Deronzier, A. [Mn(bipyridyl)CO_3Br]: an abundant metal carbonyl complex as efficient electrocatalyst for CO_2 reduction. *Angew. Chem., Int. Ed.* **50**, 9903–9906 (2011).
Two manganese complexes bearing bipyridine ligands were firstly reported as high-performance electrocatalysts for CO2 reduction
36. Costentin, C., Drouet, S., Robert, M., Saveant, J. M. A local proton source enhances CO_2 electroreduction to CO by a molecular Fe catalyst. *Science* **338**, 90–94 (2012).
The electrocatalytic efficiency of CO_2 reduction to CO was greatly enhanced by the introduction of phenolic groups on the phenyl groups of Fe tetraphenylporphyrin
37. Maurin, A., Robert, M. Noncovalent Immobilization of a Molecular Iron-Based Electrocatalyst on Carbon Electrodes for Selective, Efficient CO_2-to-CO Conversion in Water. *J. Am. Chem. Soc.* **138**, 2492–2495 (2016).
38. Maurin, A., Robert, M. Catalytic CO_2-to-CO conversion in water by covalently functionalized carbon nanotubes with a molecular iron catalyst. *Chem. Commun.* **52**, 12084–12087 (2016).
39. Smith, P. T., Benke, B. P., Cao, Z., Kim, Y., Nichols, E. M., Kim, K., Chang, C. J. Iron porphyrins embedded into a supramolecular porous organic cage for electrochemical CO_2 reduction in water. *Angew. Chem. Int. Ed.* **57**, 9684–9688 (2018).
An efficient supramolecular electrocatalyst was synthesized by embedding iron tetraphenylporphyrin into a supramolecular porous organic cage
40. Kimura, E., Bu, X., Shionoya, M., Wada, S., Maruyama, S A new nickel(II) cyclam (cyclam = 1,4,8,11-tetraazacyclotetradecane) complex covalently attached to $Ru(phen)_3^{2+}$ (phen=1,10-Phenanthroline). A new candidate for the catalytic photoreduction of carbon dioxide. *Inorg. Chem.* **31**, 4542–4546 (1992).
41. Liang, Z., Zhao, R., Qiu, T., Zou, R., Xu, Q. Metal-organic framework-derived materials for electrochemical energy applications. *EnergyChem* **1**, 100001 (2019).
42. Li, D., Xu, H.-. Q., Jiao, L., Jiang, H.-. L. Metal-organic frameworks for catalysis: state of the art, challenges, and opportunities. *EnergyChem* **1**, 100005 (2019).
43. Luo, Y.-. H., Dong, L.-. Z., Liu, J., Li, S.-. L., Lan, Y.-. Q. From molecular metal complex to metal-organic framework: the CO_2

DOI: 10.1016/j.enchem.2020.100034
EnergyChem **2**, 100034 (2020)

reduction photocatalysts with clear and tunable structure. *Coord. Chem. Rev.* **390**, 86–126 (2019).
44. Zhou, D.-. D., Zhang, X.-. W., Mo, Z.-. W., Xu, Y.-. Z., Tian, X.-. Y., Li, Y., Chen, X.-. M., Zhang, J.-. P. Adsorptive separation of carbon dioxide: from conventional porous materials to metal–organic frameworks. *EnergyChem* **1**, 100016 (2019).
45. Wang, Q., Zhang, Y., Lin, H., Zhu, J. Recent advances in metal-organic frameworks for photo-/electrocatalytic CO_2 reduction. *Chem. Eur. J.* **25**, 14026–14035 (2019).
46. Guo, Z., Cheng, S., Cometto, C., Anxolabehere-Mallart, E., Ng, S. M., Ko, C. C., Liu, G., Chen, L., Robert, M., Lau, T. C. Highly efficient and selective photocatalytic CO_2 reduction by iron and cobalt quaterpyridine complexes. *J. Am. Chem. Soc.* **138**, 9413–9416 (2016).
Two Fe and Co quaterpyridine complexes show highly efficient and selective for photocatalytic CO_2 reduction even using organic dye purpurin as the photosensitizer
47. Rao, H., Schmidt, L. C., Bonin, J., Robert, M. Visible-light-driven methane formation from CO_2 with a molecular iron catalyst. *Nature* **548**, 74–77 (2017).
An iron tetraphenylporphyrin complex with functionalized ligand was reported as an efficient photocatalyst not only for the conversion of CO_2 to CO, but also for the reduction of CO_2 to methane
48. Costentin, C., Robert, M., Saveant, J. M. Catalysis of the electrochemical reduction of carbon dioxide. *Chem. Soc. Rev.* **42**, 2423–2436 (2013).
49. Wang, J.-. W., Liu, W.-. J., Zhong, D.-. C., Lu, T.-. B. Nickel complexes as molecular catalysts for water splitting and CO_2 reduction. *Coord. Chem. Rev.* **378**, 237–261 (2019).
50. Wang, J.-. W., Zhong, D.-. C., Lu, T.-. B. Artificial photosynthesis: catalytic water oxidation and CO_2 reduction by dinuclear non-noble-metal molecular catalysts. *Coord. Chem. Rev.* **377**, 225–236 (2018).
51. Bonin, J., Maurin, A., Robert, M. Molecular catalysis of the electrochemical and photochemical reduction of CO_2 with Fe and Co metal based complexes. Recent advances. *Coord. Chem. Rev.* **334**, 184–198 (2017).
52. Kang, P., Chen, Z., Brookhart, M., Meyer, T. J. Electrocatalytic reduction of carbon dioxide: let the molecules do the work. *Top. Catal.* **58**, 30–45 (2014).
53. Elgrishi, N., Chambers, M. B., Wang, X., Fontecave, M. Molecular polypyridine-based metal complexes as catalysts for the reduction of CO_2. *Chem. Soc. Rev.* **46**, 761–796 (2017).
54. Sahara, G., Ishitani, O. Efficient photocatalysts for CO_2 reduction. *Inorg. Chem.* **54**, 5096–5104 (2015).
55. Neri, G., Donaldson, P. M., Cowan, A. J. The role of electrode-catalyst interactions in enabling efficient CO_2 Reduction with $Mo(bpy)(CO)_4$ as revealed by vibrational sum-frequency generation spectroscopy. *J. Am. Chem. Soc.* **139**, 13791–13797 (2017).
56. Clark, M. L., Grice, K. A., Moore, C. E., Rheingold, A. L., Kubiak, C. P. Electrocatalytic CO_2 reduction by $M(bpy\text{-}R)(CO)_4$ (M = Mo, W; R = H, tBu) complexes. Electrochemical, spectroscopic, and computational studies and comparison with group 7 catalysts. *Chem. Sci.* **5**, 1894–1900 (2014).
57. Saravanakumar, D., Song, J., Jung, N., Jirimali, H., Shin, W. Reduction of CO_2 to CO at Low overpotential in neutral aqueous solution by a Ni(cyclam) complex attached to poly(allylamine). *ChemSusChem* **5**, 634–636 (2012).
58. Benson, E. E., Kubiak, C. P., Sathrum, A. J., Smieja, J. M. Electrocatalytic and homogeneous approaches to conversion of CO_2 to liquid fuels. *Chem. Soc. Rev.* **38**, 89–99 (2009).
59. Che, C.-. M., Mak, S.-. T., Lee, W.-. O., Fung, K.-. W., Mak, T. C. W. Electrochemical studies of nickel(II) and cobalt(II) complexes of tetra-azamacrocycles bearing a pyridine functional group and X-ray structures of $[NiII(L^3)Cl]ClO_4$ and $[Ni^{II}(L^3)][ClO_4]_2 \cdot H_2O$ {L^3=*meso*-2,3,7,11,12-pentamethyl-3,7,11,17-tetra-azabicyclo[11.3.1]heptadeca-1(17),13,15-triene}. *J. Chem. Soc., Dalton Trans.*, 2153–2159 (1988).
60. Beley, M., Collin, J. P., Ruppert, R., Sauvage, J. P. Electrocatalytic reduction of carbon dioxide by nickel $cyclam^{2+}$ in water: study of the factors affecting the efficiency and the selectivity of the process. *J. Am. Chem. Soc.* **108**, 7461–7467 (1986).
61. Collin, J. P., Jouaiti, A., Sauvage, J. P. Electrocatalytic properties of $Ni(cyclam)^{2+}$ and and $Ni_2(biscyclam)^{4+}$ with respect to carbon dioxide and water reduction. *Inorg. Chem.* **27**, 1986–1990 (1988).
62. Schneider, C. R., Shafaat, H. S. An internal electron reservoir enhances catalytic CO_2 reduction by a semisynthetic enzyme. *Chem. Commun.* **52**, 9889–9892 (2016).
63. Nichols, E. M., Chang, C. J. Urea-based multipoint hydrogen-bond donor additive promotes electrochemical CO_2 reduction catalyzed by nickel cyclam. *Organometallics* **38**, 1213–1218 (2018).
64. Schneider, C. R., Lewis, L. C., Shafaat, H. S. The good, the neutral, and the positive: buffer identity impacts CO_2 reduction activity by nickel(II) cyclam. *Dalton Trans* **48**, 15810–15821 (2019).
65. Beley, M., Collin, J.-. P., Ruppert, R., Sauvage, J.-. P. Nickel(II)-cyclam: an extremely selective electrocatalyst for reduction of CO_2 in water. *J. Chem. Soc., Chem. Commun.*, 1315 (1984).
66. Smith, C. I., Crayston, J. A., Hay, R. W. Reduction of carbon dioxide by nickel macrocyclic catalysts adsorbed on a mercury electrode or a copper rotating disk electrode. *J. Chem. Soc., Dalton Trans.*, 3267–3269 (1993).
67. Murase, M., Kitahara, G., Suzuki, T. M., Ohta, R. Efficient catalytic electrode for CO_2 reduction realized by physisorbing Ni(cyclam) molecules with hydrophobicity based on hansen's theory. *ACS Appl. Mater. Interfaces* **8**, 24315–24318 (2016).
68. Balazs, G. B., Anson, F. C. The adsorption of $nickel(cyclam)^{1+}$ at mercury electrodes and its relation to the electrocatalytic reduction of carbon dioxide. *J. Electroanal. Chem. Interfacial Electrochem.* **322**, 325–345 (1992).
69. Schneider, J., Jia, H., Kobiro, K., Cabelli, D. E., Muckerman, J. T., Fujita, E. Nickel(II) macrocycles: highly efficient electrocatalysts for the selective reduction of CO_2 to CO. *Energy Environ. Sci.* **5**, 9502–9510 (2012).
70. Neri, G., Aldous, I. M., Walsh, J. J., Hardwick, L. J., Cowan, A. J. A highly active nickel electrocatalyst shows excellent selectivity for CO_2 reduction in acidic media. *Chem. Sci.* **7**, 1521–1526 (2016).
71. Fujita, E., Haff, J., Sanzenbacher, R., Elias, H. High electrocatalytic activity of RRSS-$[Ni^{I}HTIM](ClO_4)_2$ and $[Ni^{II}DMC](ClO_4)_2$ for carbon dioxide reduction (HTIM = 2,3,9,10-Tetramethyl-1,4,8,11-tetraazacyclotetradecane, DMC = C-meso-5,12-Dimethyl-1,4,8,11-tetraazacyclotetradecane). *Inorg. Chem.* **33**, 4627–4628 (1994).
72. Bujno, K., Bilewicz, R., Siegfried, L., Kaden, T. A. Effects of ligand structure on the adsorption of nickel tetraazamacrocyclic complexes and electrocatalytic CO_2 reduction. *J. Electroanal. Chem.* **445**, 47–53 (1998).
73. Song, J., Klein, E. L., Neese, F., Ye, S. The mechanism of homogeneous CO_2 reduction by Ni(cyclam): product selectivity, concerted proton-electron transfer and C-O bond cleavage. *Inorg. Chem.* **53**, 7500–7507 (2014).
74. Christensen, P. A., Hamnett, A., Higgins, S. J., Timney, J. A. An in-situ Fourier transform infrared study of CO_2 electroreduction catalyzed by Ni(0)-4,4′-dimethyl 2,2′-bipyridine and Ni(0)-1,10-phenanthroline complexes. *J. Electroanal. Chem.* **395**, 195–209 (1995).
75. Froehlich, J. D., Kubiak, C. P. The homogeneous reduction of CO_2 by $[Ni(cyclam)]^+$: increased catalytic rates with the addition of a CO scavenger. *J. Am. Chem. Soc.* **137**, 3565–3573 (2015).
76. Hay, R. W., Crayston, J. A., Cromie, T. J., Lightfoot, P., De Alwis, D. C. L. The preparation, chemistry and crystal structure of the nickel(II) complex of N-hydroxyethylazacyclam [3-(2′-hydroxyethyl)-1,3,5,8,12-penta-azacyclotetradecane nickel(II) perchlorate]. A new electrocatalyst for CO_2 reduction. *Polyhedron* **16**, 3557–3563 (1997).

DOI: 10.1016/j.enchem.2020.100034
EnergyChem **2**, 100034 (2020)

77. Fujita, E., Creutz, C., Sutin, N., Szalda, D. J. Carbon dioxide activation by cobalt(I) macrocycles: factors affecting carbon dioxide and carbon monoxide binding. *J. Am. Chem. Soc.* **113**, 343–353 (1991).
78. Rudolph, M., Dautz, S., Jaeger, E.-. G. Macrocyclic $[N_4^{2-}]$ coordinated nickel complexes as catalysts for the formation of oxalate by electrochemical reduction of carbon dioxide. *J. Am. Chem. Soc.* **122**, 10821–10830 (2000).
79. Khoshro, H., Zare, H. R., Namazian, M., Jafari, A. A., Gorji, A. Synthesis of cyclic carbonates through cycloaddition of electrocatalytic activated CO_2 to epoxides under mild conditions. *Electrochim. Acta* **113**, 263–268 (2013).
80. Khoshro, H., Zare, H. R., Gorji, A., Namazian, M. A study of the catalytic activity of symmetric and unsymmetric macrocyclic $[N_4^{2-}]$ coordinated nickel complexes for electrochemical reduction of carbon dioxide. *Electrochim. Acta* **117**, 62–67 (2014).
81. Cook, T. D., Tyler, S. F., McGuire, C. M., Zeller, M., Fanwick, P. E., Evans, D. H., Peters, D. G., Ren, T. Nickel complexes of C-substituted cyclams and their activity for CO_2 and H^+ reduction. *ACS Omega* **2**, 3966–3976 (2017).
82. Froehlich, J. D., Kubiak, C. P. Homogeneous CO_2 reduction by Ni(cyclam) at a glassy carbon electrode. *Inorg. Chem.* **51**, 3932–3934 (2012).
83. De Alwis, C., Crayston, J. A., Cromie, T., Eisenblatter, T., Hay, R. W., Lampeka, Y. D., Tsymbal, L. V. Cyclic voltammetry study of the electrocatalysis of carbon dioxide reduction by bis(polyazamacrocyclic) nickel complexes. *Electrochim. Acta* **45**, 2061–2074 (2000).
84. Lee, E. Y., Hong, D., Park, H. W., Suh, M. P. Synthesis, properties, and reactions of trinuclear macrocyclic nickel(II) and nickel(I) complexes: electrocatalytic reduction of CO_2 by nickel(II) complex. *Eur. J. Inorg. Chem.*, 3242–3249 (2003).
85. Chapovetsky, A., Do, T. H., Haiges, R., Takase, M. K., Marinescu, S. C. Proton-assisted reduction of CO_2 by cobalt aminopyridine macrocycles. *J. Am. Chem. Soc.* **138**, 5765–5768 (2016).
86. Chapovetsky, A., Welborn, M., Luna, J. M., Haiges, R., Miller, T. F. III, Marinescu, S. C. Pendant hydrogen-bond donors in cobalt catalysts independently enhance CO_2 reduction. *ACS Cent. Sci.* **4**, 397–404 (2018).
87. Kaes, C., Katz, A., Hosseini, M. W. Bipyridine: the most widely used ligand. A review of molecules comprising at least two 2,2′-bipyridine units. *Chem. Rev.* **100**, 3553–3590 (2000).
88. Rawat, K. S., Mandal, S. C., Pathak, B. A computational study of electrocatalytic CO_2 reduction by Mn(I) complexes: role of bipyridine substituents. *Electrochim. Acta* **297**, 606–612 (2019).
89. Hawecker, J., Lehn, J.-. M., Ziessel, R. Efficient photochemical reduction of CO_2 to CO by visible light irradiation of systems containing $Re(bipy)(CO)_3X$ or $Ru(bipy)_3^{2+}$-Co^{2+} combinations as homogeneous catalysts. *J. Chem. Soc., Chem. Commun.*, 536–538 (1983).
90. Bourrez, M., Orio, M., Molton, F., Vezin, H., Duboc, C., Deronzier, A., Chardon-Noblat, S. Pulsed-EPR evidence of a manganese(II) hydroxycarbonyl intermediate in the electrocatalytic reduction of carbon dioxide by a manganese bipyridyl derivative. *Angew. Chem. Int. Ed.* **53**, 240–243 (2014).
91. McKinnon, M., Ngo, K. T., Sobottka, S., Sarkar, B., Ertem, M. Z., Grills, D. C., Rochford, J. Synergistic metal–ligand redox cooperativity for electrocatalytic CO_2 reduction promoted by a ligand-based redox couple in Mn and Re tricarbonyl complexes. *Organometallics* **38**, 1317–1329 (2018).
92. Fokin, I., Denisiuk, A., Wuertele, C., Siewert, I. The impact of a proton relay in binuclear α-diimine-$Mn(CO)_3$ complexes on the CO_2 reduction catalysis. *Inorg. Chem.* **58**, 10444–10453 (2019).
93. Taylor, J. O., Wang, Y., Hartl, F. Photo-assisted electrocatalytic reduction of CO_2: a new strategy for reducing catalytic overpotentials. *ChemCatChem* **12**, 386–393 (2019).
94. Smieja, J. M., Sampson, M. D., Grice, K. A., Benson, E. E., Froehlich, J. D., Kubiak, C. P. Manganese as a substitute for rhenium in CO_2 reduction catalysts: the importance of acids. *Inorg. Chem.* **52**, 2484–2491 (2013).
95. Sampson, M. D., Nguyen, A. D., Grice, K. A., Moore, C. E., Rheingold, A. L., Kubiak, C. P. Manganese catalysts with bulky bipyridine ligands for the electrocatalytic reduction of carbon dioxide: eliminating dimerization and altering catalysis. *J. Am. Chem. Soc.* **136**, 5460–5471 (2014).
96. Sampson, M. D., Kubiak, C. P. Manganese electrocatalysts with bulky bipyridine ligands: utilizing lewis acids to promote carbon dioxide reduction at low overpotentials. *J. Am. Chem. Soc.* **138**, 1386–1393 (2016).
97. Sun, C., Rotundo, L., Garino, C., Nencini, L., Yoon, S. S., Gobetto, R., Nervi, C. Electrochemical CO_2 reduction at glassy carbon electrodes functionalized by Mn^I and Re^I organometallic complexes. *ChemPhysChem* **18**, 3219–3229 (2017).
98. Zhanaidarova, A., Steger, H., Reineke, M. H., Kubiak, C. P., Chelated, P. Chelated $[Zn(cyclam)]^{2+}$ Lewis acid improves the reactivity of the electrochemical reduction of CO_2 by Mn catalysts with bulky bipyridine ligands. *Dalton Trans* **46**, 12413–12416 (2017).
99. Spall, S. J. P., Keane, T., Tory, J., Cocker, D. C., Adams, H., Fowler, H., Meijer, A. J. H. M., Hartl, F., Weinstein, J. A. Manganese tricarbonyl complexes with asymmetric 2-iminopyridine ligands: toward decoupling steric and electronic factors in electrocatalytic CO_2 reduction. *Inorg. Chem.* **55**, 12568–12582 (2016).
100. Steinlechner, C., Roesel, A. F., Oberem, E., Paepcke, A., Rockstroh, N., Gloaguen, F., Lochbrunner, S., Ludwig, R., Spannenberg, A., Junge, H., Francke, R., Beller, M. Selective earth-abundant system for CO_2 reduction: comparing photo- and electrocatalytic processes. *ACS Catal* **9**, 2091–2100 (2019).
101. Fei, H., Sampson, M. D., Lee, Y., Kubiak, C. P., Cohen, S. M. Photocatalytic CO_2 reduction to formate using a Mn(I) molecular catalyst in a robust metal-organic framework. *Inorg. Chem.* **54**, 6821–6828 (2015).
102. Walsh, J. J., Smith, C. L., Neri, G., Whitehead, G. F. S., Robertson, C. M., Cowan, A. J. Improving the efficiency of electrochemical CO_2 reduction using immobilized manganese complexes. *Faraday Discuss* **183**, 147–160 (2015).
103. Rosser, T. E., Windle, C. D., Reisner, E. Electrocatalytic and solar-driven CO_2 reduction to CO with a molecular manganese catalyst immobilized on mesoporous TiO_2. *Angew. Chem., Int. Ed.* **55**, 7388–7392 (2016).
104. Torralba-Peñalver, E., Luo, Y., Compain, J.-. D., Chardon-Noblat, S., Fabre, B. Selective catalytic electroreduction of CO_2 at silicon nanowires (SiNWs) photocathodes using non-noble metal-based manganese carbonyl bipyridyl molecular catalysts in solution and grafted onto SiNWs. *ACS Catal* **5**, 6138–6147 (2015).
105. Dutta, B., Maity, S., Ghosh, S., Sinha, C., Mir, M. H. An acetylenedicarboxylato-bridged Mn(II)-based 1D coordination polymer: electrochemical CO_2 reduction and magnetic properties. *New J. Chem.* **43**, 5167–5172 (2019).
106. Machan, C. W., Stanton, C. J. III, Vandezande, J. E., Majetich, G. F., Schaefer, H. F. III, Kubiak, C. P., Agarwal, J. Electrocatalytic reduction of carbon dioxide by $Mn(CN)(2,2'\text{-bipyridine})(CO)_3$: CN coordination alters mechanism. *Inorg. Chem.* **54**, 8849–8856 (2015).
107. Ngo, K. T., McKinnon, M., Mahanti, B., Narayanan, R., Grills, D. C., Ertem, M. Z., Rochford, J. Turning on the protonation-first pathway for electrocatalytic CO_2 reduction by manganese bipyridyl tricarbonyl complexes. *J. Am. Chem. Soc.* **139**, 2604–2618 (2017).
Introducing four pendant methoxy groups in a bipyridyl ligand to obtain a modified Mn(I) catalyst, the required overpotential for electrocatalytic CO_2-to-CO conversion was greatly decreased
108. Ronne, M. H. H., Cho, D., Madsen, M. R., Jakobsen, J. B., Eom, S., Escoude, E., Hammershoj, H. C. D., Nielsen, D. U., Pedersen, S. U., Baik, M. H., Skrydstrup, T., Daasbjerg, K. Ligand

DOI: 10.1016/j.enchem.2020.100034
EnergyChem **2**, 100034 (2020)

controlled product selectivity in the electrochemical carbon dioxide reduction using manganese bipyridine catalysts. *J. Am. Chem. Soc.* **142**, 4265–4275 (2020).
109. Franco, F., Cometto, C., Nencini, L., Barolo, C., Sordello, F., Minero, C., Fiedler, J., Robert, M., Gobetto, R., Nervi, C. Local proton source in electrocatalytic CO_2 reduction with $[Mn(bpy\text{-}R)(CO)_3Br]$ complexes. *Chem. Eur. J.* **23**, 4782–4793 (2017).
110. Franco, F., Cometto, C., Ferrero Vallana, F., Sordello, F., Priola, E., Minero, C., Nervi, C., Gobetto, R. A local proton source in a $[Mn(bpy\text{-}R)(CO)_3Br]$-type redox catalyst enables CO_2 reduction even in the absence of Bronsted acids. *Chem. Commun.* **50**, 14670–14673 (2014).
111. Agarwal, J., Shaw, T. W., Schaefer, H. F., Bocarsly, A. B. Design of a catalytic active site for electrochemical CO_2 reduction with Mn(I)-tricarbonyl species. *Inorg. Chem.* **54**, 5285–5294 (2015).
112. Machan, C. W., Kubiak, C. P. Electrocatalytic reduction of carbon dioxide with Mn(terpyridine) carbonyl complexes. *Dalton Trans* **45**, 17179–17186 (2016).
113. Walsh, J. J., Neri, G., Smith, C. L., Cowan, A. J. Water-soluble manganese complex for selective electrocatalytic CO_2 reduction to CO. *Organometallics* **38**, 1224–1229 (2018).
114. Tignor, S. E., Kuo, H.-. Y., Lee, T. S., Scholes, G. D., Bocarsly, A. B. Manganese-based catalysts with varying ligand substituents for the electrochemical reduction of CO_2 to CO. *Organometallics* **38**, 1292–1299 (2018).
115. Kuo, H. Y., Lee, T. S., Chu, A. T., Tignor, S. E., Scholes, G. D., Bocarsly, A. B. A cyanide-bridged di-manganese carbonyl complex that photochemically reduces CO to CO. *Dalton Trans* **48**, 1226–1236 (2019).
116. Lin, J., Liao, R., Xu, J. High-efficiency photocatalytic CO_2 reduction in organic–aqueous system: a new insight into the role of water. *RSC Adv* **8**, 3798–3802 (2018).
117. Lam, K.-. M., Wong, K.-. Y., Yang, S.-. M., Che, C.-. M. Cobalt and nickel complexes of 2,2′:6′,2":6",2"'-quaterpyridine as catalysts for electrochemical reduction of carbon dioxide. *J. Chem. Soc., Dalton Trans.*, 1103–1107 (1995).
118. Cometto, C., Chen, L., Lo, P.-. K., Guo, Z., Lau, K.-. C., Anxolabehere-Mallart, E., Fave, C., Lau, T.-. C., Robert, M. Highly selective molecular catalysts for the CO_2-to-CO electrochemical conversion at very low overpotential. Contrasting Fe vs Co quaterpyridine complexes upon mechanistic studies. *ACS Catal* **8**, 3411–3417 (2018).
119. Cometto, C., Chen, L., Anxolabéhère-Mallart, E., Fave, C., Lau, T.-. C., Robert, M. Molecular electrochemical catalysis of the CO_2-to-CO conversion with a Co complex: a cyclic voltammetry mechanistic investigation. *Organometallics* **38**, 1280–1285 (2018).
120. Nie, W., McCrory, C. C. L. Electrocatalytic CO_2 reduction by a cobalt bis(pyridylmonoimine) complex: effect of acid concentration on catalyst activity and stability. *Chem. Commun.* **54**, 1579–1582 (2018).
121. Nichols, A. W., Chatterjee, S., Sabat, M., Machan, C. W. Electrocatalytic reduction of CO_2 to formate by an iron schiff base complex. *Inorg. Chem.* **57**, 2111–2121 (2018).
122. Wang, M., Chen, L., Lau, T.-. C., Robert, M. A hybrid Co quaterpyridine complex/carbon nanotube catalytic material for CO_2 reduction in water. *Angew. Chem. Int. Ed.* **57**, 7769–7773 (2018).
123. Elgrishi, N., Chambers, M. B., Artero, V., Fontecave, M. Terpyridine complexes of first row transition metals and electrochemical reduction of CO_2 to CO. *Phys. Chem. Chem. Phys.* **16**, 13635–13644 (2014).
124. Garnier, L., Rollin, Y., Perichon, J. Electrosynthesis of symmetrical ketones from organic halides and carbon dioxide catalyzed by 2,2′-bipyridine-nickel complexes. *J. Organomet. Chem.* **367**, 347–358 (1989).
125. Kuehnel, M. F., Orchard, K. L., Dalle, K. E., Reisner, E. Selective photocatalytic CO_2 reduction in water through anchoring of a molecular Ni catalyst on CdS nanocrystals. *J. Am. Chem. Soc.* **139**, 7217–7223 (2017).
126. Arana, C., Keshavarz, M., Potts, K. T., Abruna, H. D. Electrocatalytic reduction of CO_2 and O_2 with electropolymerized films of vinyl-terpyridine complexes of Fe, Ni and Co. *Inorg. Chim. Acta* **225**, 285–295 (1994).
127. Elgrishi, N., Chambers, M. B., Fontecave, M. Turning it off! Disfavouring hydrogen evolution to enhance selectivity for CO production during homogeneous CO_2 reduction by cobalt-terpyridine complexes. *Chem. Sci.* **6**, 2522–2531 (2015).
128. Arana, C., Yan, S., Keshavarz-K, M., Potts, K. T., Abruna, H. D. Electrocatalytic reduction of carbon dioxide with iron, cobalt, and nickel complexes of terdentate ligands. *Inorg. Chem.* **31**, 3680–3682 (1992).
129. Liu, F.-. W., Bi, J., Sun, Y., Luo, S., Kang, P. Cobalt complex with redox-active imino bipyridyl ligand for electrocatalytic reduction of carbon dioxide to formate. *ChemSusChem* **11**, 1656–1663 (2018).
130. Simpson, T. C., Durand, R. R. Jr. Ligand participation in the reduction of carbon dioxide catalyzed by complexes of 1,10 *o*-phenanthroline. *Electrochim. Acta* **33**, 581–583 (1988).
131. Isaacs, M., Canales, J. C., Aguirre, M. J., Estiu, G., Caruso, F., Ferraudi, G., Costamagna, J. Electrocatalytic reduction of CO_2 by aza-macrocyclic complexes of Ni(II), Co(II), and Cu(II). Theoretical contribution to probable mechanisms. *Inorg. Chim. Acta* **339**, 224–232 (2002).
132. Costamagna, J., Canales, J., Vargas, J., Ferraudi, G. Electrochemical reduction of carbon dioxide by hexaazamacrocyclic complexes. *Pure Appl. Chem.* **67**, 1045–1052 (1995).
133. Muena, J. P., Villagran, M., Costamagna, J., Aguirre, M. J. Dinaphthotetraaza[14]annulene copper(II) complexes in the electrocatalytic reduction of carbon dioxide and bisulfite anion. *J. Coord. Chem.* **61**, 479–489 (2008).
134. Isaacs, M., Canales, J. C., Riquelme, A., Lucero, M., Aguirre, M. J., Costamagna, J. Contribution of the ligand to the electroreduction of CO_2 catalyzed by a cobalt(II) macrocyclic complex. *J. Coord. Chem.* **56**, 1193–1201 (2003).
135. Huan, T. N., Andreiadis, E. S., Heidkamp, J., Simon, P., Derat, E., Cobo, S., Royal, G., Bergmann, A., Strasser, P., Dau, H., Artero, V., Fontecave, M. From molecular copper complexes to composite electrocatalytic materials for selective reduction of CO_2 to formic acid. *J. Mater. Chem. A* **3**, 3901–3907 (2015).
136. Varela, A. S., Kroschel, M., Reier, T., Strasser, P. Controlling the selectivity of CO_2 electroreduction on copper: the effect of the electrolyte concentration and the importance of the local pH. *Catal. Today* **260**, 8–13 (2016).
137. Kas, R., Kortlever, R., Milbrat, A., Koper, M. T., Mul, G., Baltrusaitis, J. Electrochemical CO_2 reduction on Cu_2O-derived copper nanoparticles: controlling the catalytic selectivity of hydrocarbons. *Phys. Chem. Chem. Phys.* **16**, 12194–12201 (2014).
138. Ren, D., Deng, Y., Handoko, A. D., Chen, C. S., Malkhandi, S., Yeo, B. S. Selective electrochemical reduction of carbon dioxide to ethylene and ethanol on copper(I) oxide catalysts. *ACS Catal* **5**, 2814–2821 (2015).
139. Montoya, J. H., Peterson, A. A., Nørskov, J. K. Insights into C-C coupling in CO_2 electroreduction on copper electrodes. *ChemCatChem* **5**, 737–742 (2013).
140. Sieh, D., Lacy, D. C., Peters, J. C., Kubiak, C. P. Reduction of CO_2 by pyridine monoimine molybdenum carbonyl complexes: cooperative metal-ligand binding of CO_2. *Chem. Eur. J.* **21**, 8497–8503 (2015).
141. Taylor, J. O., Leavey, R. D., Hartl, F. Solvent and ligand substitution effects on the electrocatalytic reduction of CO_2 with $[Mo(CO)_4(x,x'\text{-dimethyl-2,2'-bipyridine})]$ (x = 4-6) enhanced at a gold cathodic surface. *ChemElectroChem* **5**, 3155–3161 (2018).
142. Franco, F., Cometto, C., Sordello, F., Minero, C., Nencini, L., Fiedler, J., Gobetto, R., Nervi, C. Electrochemical reduction of CO_2 by $M(CO)_4$(diimine) complexes (M = Mo, W): catalytic

DOI: 10.1016/j.enchem.2020.100034
EnergyChem **2**, 100034 (2020)

activity improved by 2,2′-dipyridylamine. *ChemElectroChem* **2**, 1372–1379 (2015).
143. Saveant, J. M. Molecular catalysis of electrochemical reactions. mechanistic aspects. *Chem. Rev.* **108**, 2348–2378 (2008).
144. Sen, P., Mondal, B., Saha, D., Rana, A., Dey, A. Role of 2nd sphere H-bonding residues in tuning the kinetics of CO_2 reduction to CO by iron porphyrin complexes. *Dalton Trans* **48**, 5965–5977 (2019).
145. Hammouche, M., Lexa, D., Savéant, J. M., Momenteau, M. Catalysis of the electrochemical reduction of carbon dioxide by iron(0) porphyrins. *J. Electroanal. Chem.* **249**, 347–351 (1988).
146. Roemelt, C., Song, J., Tarrago, M., Rees, J. A., van Gastel, M., Weyhermueller, T., DeBeer, S., Bill, E., Neese, F., Ye, S. Electronic structure of a formal iron(0) porphyrin complex relevant to CO_2 reduction. *Inorg. Chem.* **56**, 4745–4750 (2017).
147. Costentin, C., Drouet, S., Passard, G., Robert, M., Saveant, J. M. Proton-coupled electron transfer cleavage of heavy-atom bonds in electrocatalytic processes. Cleavage of a C-O bond in the catalyzed electrochemical reduction of CO_2. *J. Am. Chem. Soc.* **135**, 9023–9031 (2013).
148. Weng, Z., Jiang, J., Wu, Y., Wu, Z., Guo, X., Materna, K. L., Liu, W., Batista, V. S., Brudvig, G. W., Wang, H. Electrochemical CO_2 reduction to hydrocarbons on a heterogeneous molecular Cu catalyst in aqueous solution. *J. Am. Chem. Soc.* **138**, 8076–8079 (2016).
149. Weng, Z., Wu, Y., Wang, M., Jiang, J., Yang, K., Huo, S., Wang, X. F., Ma, Q., Brudvig, G. W., Batista, V. S., Liang, Y., Feng, Z., Wang, H. Active sites of copper-complex catalytic materials for electrochemical carbon dioxide reduction. *Nat. Commun.* **9**, 415 (2018).
150. Costentin, C., Passard, G., Robert, M., Saveant, J. M. Ultraefficient homogeneous catalyst for the CO_2-to-CO electrochemical conversion. *Proc. Natl. Acad. Sci. USA* **111**, 14990–14994 (2014).
151. Zahran, Z. N., Mohamed, E. A., Naruta, Y. Bio-inspired cofacial Fe porphyrin dimers for efficient electrocatalytic CO_2 to CO conversion: overpotential tuning by substituents at the porphyrin rings. *Sci. Rep.* **6**, 24533 (2016).
152. Meshitsuka, S., Ichikawa, M., Tamaru, K. Electrocatalysis by metal phthalocyanines in the reduction of carbon dioxide. *J. Chem. Soc., Chem. Commun.*, 158 (1974).
153. Ogawa, A., Oohora, K., Hayashi, T. Synthesis and characterization of meso-substituted cobalt tetradehydrocorrin and evaluation of its electrocatalytic behavior toward CO_2 reduction and H_2 evolution. *Inorg. Chem.* **57**, 14644–14652 (2018).
154. Zhang, X., Wu, Z., Zhang, X., Li, L., Li, Y., Xu, H., Li, X., Yu, X., Zhang, Z., Liang, Y., Wang, H. Highly selective and active CO_2 reduction electrocatalysts based on cobalt phthalocyanine/carbon nanotube hybrid structures. *Nat. Commun.* **8**, 14675 (2017).
155. Lu, X., Wu, Y., Yuan, X., Huang, L., Wu, Z., Xuan, J., Wang, Y., Wang, H. High-performance electrochemical CO_2 reduction cells based on non-noble metal catalysts. *ACS Energy Lett* **3**, 2527–2532 (2018).
156. Wang, M., Torbensen, K., Salvatore, D., Ren, S., Joulie, D., Dumoulin, F., Mendoza, D., Lassalle-Kaiser, B., Isci, U., Berlinguette, C. P., Robert, M. CO_2 electrochemical catalytic reduction with a highly active cobalt phthalocyanine. *Nat. Commun.* **10**, 3602 (2019).
157. Cheung, P. L., Lee, S. K., Kubiak, C. P. Facile solvent-free synthesis of thin iron porphyrin COFs on carbon cloth electrodes for CO_2 reduction. *Chem. Mater.* **31**, 1908–1919 (2019).
158. Lu, M., Li, Q., Liu, J., Zhang, F.-. M., Zhang, L., Wang, J.-. L., Kang, Z.-. H., Lan, Y.-. Q. Installing earth-abundant metal active centers to covalent organic frameworks for efficient heterogeneous photocatalytic CO_2 reduction. *Appl. Catal., B* **254**, 624–633 (2019).
159. Lin, S., Diercks, C. S., Zhang, Y. B., Kornienko, N., Nichols, E. M., Zhao, Y., Paris, A. R., Kim, D., Yang, P., Yaghi, O. M., Chang, C. J. Covalent organic frameworks comprising cobalt porphyrins for catalytic CO_2 reduction in water. *Science* **349**, 1208–1213 (2015).
Two highly efficient and selective Fe and Co quaterpyridine complexes were employed as catalysts for photocatalytic CO_2 reduction, even using organic dye purpurin as the photosensitizer
160. Shen, J., Kolb, M. J., Goettle, A. J., Koper, M. T. M. DFT study on the mechanism of the electrochemical reduction of CO_2 catalyzed by cobalt porphyrins. *J. Phys. Chem. C* **120**, 15714–15721 (2016).
161. Sonoyama, N., Kirii, M., Sakata, T. Electrochemical reduction of CO_2 at metal-porphyrin supported gas diffusion electrodes under high pressure CO_2. *Electrochem. Commun.* **1**, 213–216 (1999).
162. Shen, J., Kortlever, R., Kas, R., Birdja, Y. Y., Diaz-Morales, O., Kwon, Y., Ledezma-Yanez, I., Schouten, K. J., Mul, G., Koper, M. T. Electrocatalytic reduction of carbon dioxide to carbon monoxide and methane at an immobilized cobalt protoporphyrin. *Nat. Commun.* **6**, 8177 (2015).
163. Atoguchi, T., Aramata, A., Kazusaka, A., Enyo, M. Cobalt(II)–tetraphenylporphyrin–pyridine complex fixed on a glassy carbon electrode and its prominent catalytic activity for reduction of carbon dioxide. *J. Chem. Soc., Chem. Commun.*, 156–157 (1991).
164. Pander, J. E. III, Fogg, A., Bocarsly, A. B. Utilization of electropolymerized films of cobalt porphyrin for the reduction of carbon dioxide in aqueous media. *ChemCatChem* **8**, 3536–3545 (2016).
165. He, L., Sun, X., Zhang, H., Shao, F. G-quadruplex nanowires to direct the efficiency and selectivity of electrocatalytic CO_2 reduction. *Angew. Chem. Int. Ed.* **57**, 12453–12457 (2018).
166. Zhang, J., Pietro, W. J., Lever, A. B. P. Rotating ring-disk electrode analysis of CO_2 reduction electrocatalyzed by a cobalt tetramethylpyridoporphyrazine on the disk and detected as CO on a platinum ring. *J. Electroanal. Chem.* **403**, 93–100 (1996).
167. Magdesieva, T. V., Yamamoto, T., Tryk, D. A., Fujishima, A. Electrochemical reduction of CO_2 with transition metal phthalocyanine and porphyrin complexes supported on activated carbon fibers. *J. Electrochem. Soc.* **149**, D89–D95 (2002).
168. Zhu, M., Cao, C., Chen, J., Sun, Y., Ye, R., Xu, J., Han, Y.-. F. Electronic tuning of cobalt porphyrins immobilized on nitrogen–doped graphene for CO_2 reduction. *ACS Appl. Energy Mater.* **2**, 2435–2440 (2019).
169. Choi, J., Wagner, P., Gambhir, S., Jalili, R., MacFarlane, D. R., Wallace, G. G., Officer, D. L. Steric modification of a cobalt phthalocyanine/graphene catalyst to give enhanced and stable electrochemical CO_2 reduction to CO. *ACS Energy Lett* **4**, 666–672 (2019).
170. Aoi, S., Mase, K., Ohkubo, K., Fukuzumi, S. Selective electrochemical reduction of CO2 to CO with a cobalt chlorin complex adsorbed on multi-walled carbon nanotubes in water. *Chem. Commun. (Cambridge, U. K.)* **51**, 10226–10228 (2015).
171. Yoshida, T., Iida, T., Shirasagi, T., Lin, R.-. J., Kaneko, M. Electrocatalytic reduction of carbon dioxide in aqueous medium by bis(2,2′:6′,2″-terpyridine)cobalt(II) complex incorporated into a coated polymer membrane. *J. Electroanal. Chem.* **344**, 355–362 (1993).
172. Chen, B. T., Morlanés, N., Adogla, E., Takanabe, K., Rodionov, V. O. An efficient and stable hydrophobic molecular cobalt catalyst for water electro-oxidation at neutral pH. *ACS Catal* **6**, 4647–4652 (2016).
173. Ouyang, T., Hou, C., Wang, J. W., Liu, W. J., Zhong, D. C., Ke, Z. F., Lu, T. B A Highly selective and robust Co(II)-based homogeneous catalyst for reduction of CO_2 to CO in CH_3CN/H_2O solution driven by visible light. *Inorg. Chem.* **56**, 7307–7311 (2017).
174. Liu, D.-. C., Huang, H.-. H., Wang, J.-. W., Jiang, L., Zhong, D.-. C., Lu, T.-. B. Highly Efficient and Selective Visible-Light Driven CO_2-to-CO Conversion by a Co(II) Homogeneous Catalyst in H_2O/CH_3CN Solution. *ChemCatChem* **10**, 3435–3440 (2018).
175. Wang, J. W., Huang, H. H., Sun, J. K., Ouyang, T., Zhong, D. C., Lu, T. B. Electrocatalytic and photocatalytic reduction of CO_2

DOI: 10.1016/j.enchem.2020.100034
EnergyChem **2**, 100034 (2020)

to CO by cobalt(II) tripodal complexes: low overpotentials, high efficiency and selectivity. *ChemSusChem* **11**, 1025–1031 (2018).
176. Costentin, C., Robert, M., Saveant, J. M., Tatin, A. Efficient and selective molecular catalyst for the CO_2-to-CO electrochemical conversion in water. *Proc.Natl. Acad. Sci. U. S. A.* **112**, 6882–6886 (2015).
177. Wang, J.-. W., Huang, H.-. H., Sun, J.-. K., Zhong, D.-. C., Lu, T.-. B. Syngas production with a highly-robust nickel(II) homogeneous electrocatalyst in a water-containing system. *ACS Catal* **8**, 7612–7620 (2018).
178. Thoi, V. S., Chang, C. J. Nickel N-heterocyclic carbene-pyridine complexes that exhibit selectivity for electrocatalytic reduction of carbon dioxide over water. *Chem. Commun.* **47**, 6578–6580 (2011).
179. Su, X., McCardle, K. M., Panetier, J. A., Jurss, J. W. Electrocatalytic CO_2 reduction with nickel complexes supported by tunable bipyridyl-N-heterocyclic carbene donors: understanding redox-active macrocycles. *Chem. Commun.* **54**, 3351–3354 (2018).
180. Canales, J., Ramirez, J., Estiu, G., Costamagna, J. Bis-bipyridine hexa-aza-macrocycle complexes of zinc(II) and nickel(II) and the catalytic reduction of carbon dioxide. *Polyhedron* **19**, 2373–2381 (2000).
181. Estiu, G. L., Jubert, A. H., Molina, J., Costamagna, J., Canales, J., Vargas, J. A theoretical investigation of the structure and electronic spectra of porphyrin homolog macrocycles. Hexaazacyclophane and its nickel and copper complexes. *Inorg. Chem.* **34**, 1212–1220 (1995).
182. Cope, J. D., Liyanage, N. P., Kelley, P. J., Denny, J. A., Valente, E. J., Webster, C. E., Delcamp, J. H., Hollis, T. K. Electrocatalytic reduction of CO_2 with CCC-NHC pincer nickel complexes. *Chem. Commun.* **53**, 9442–9445 (2017).
183. Sheng, M., Jiang, N., Gustafson, S., You, B., Ess, D. H., Sun, Y. A nickel complex with a biscarbene pincer-type ligand shows high electrocatalytic reduction of CO_2 over H_2O. *Dalton Trans* **44**, 16247–16250 (2015).
184. Therrien, J. A., Wolf, M. O., Patrick, B. O. Synthesis and comparison of nickel, palladium, and platinum bis(N-heterocyclic carbene) pincer complexes for electrocatalytic CO_2 reduction. *Dalton Trans* **47**, 1827–1840 (2018).
185. Agarwal, J., Shaw, T. W., Stanton„ C. J. III, Majetich, G. F., Bocarsly, A. B., Schaefer, H. F. III NHC-containing manganese(I) electrocatalysts for the two-electron reduction of CO_2. *Angew. Chem. Int. Ed.* **53**, 5152–5155 (2014).
186. Stanton„ C. J. III, Vandezande, J. E., Majetich, G. F., Schaefer, H. F. III, Agarwal, J. Mn-NHC electrocatalysts: increasing π acidity lowers the reduction potential and increases the turnover frequency for CO_2 reduction. *Inorg. Chem.* **55**, 9509–9512 (2016).
187. Franco, F., Pinto, M. F., Royo, B., Lloret-Fillol, J A highly active N-heterocyclic carbene manganese(I) complex for selective electrocatalytic CO_2 reduction to CO. *Angew. Chem. Int. Ed.* **57**, 4603–4606 (2018).
188. Simon-Manso, E., Kubiak, C. P. Dinuclear nickel complexes as catalysts for electrochemical reduction of carbon dioxide. *Organometallics* **24**, 96–102 (2005).
189. DeLaet, D. L., Del Rosario, R., Fanwick, P. E., Kubiak, C. P. Carbon dioxide chemistry and electrochemistry of a binuclear cradle complex of nickel(0), $Ni_2(\mu;$-CNMe$)(CNMe)_2(PPh_2CH_2PPh_2)_2$. *J. Am. Chem. Soc.* **109**, 754–758 (1987).
190. Ratliff, K. S., Lentz, R. E., Kubiak, C. P. Carbon dioxide chemistry of the trinuclear complex $[Ni_3(\mu;_3$-CNMe$)(\mu_3$-I$)(dppm)_3][PF_6]$. Electrocatalytic reduction of carbon dioxide. *Organometallics* **11**, 1986–1988 (1992).
191. Dickie, D. A., Chacon, B. E., Issabekov, A., Lam, K., Kemp, R. A. Nickel(II) and nickel(0) complexes of bis(diisopropylphosphino)amine: synthesis, structure, and electrochemical activity. *Inorg. Chim. Acta* **453**, 42–50 (2016).
192. Miedaner, A., Noll, B. C., DuBois, D. L. Synthesis and characterization of palladium and nickel complexes with positively charged triphosphine ligands and their use as electrochemical CO_2-reduction catalysts. *Organometallics* **16**, 5779–5791 (1997).
193. DuBois, D. L., Miedaner, A. Mediated electrochemical reduction of CO_2. Preparation and comparison of an isoelectronic series of complexes. *J. Am. Chem. Soc.* **109**, 113–117 (1987).
194. Dubrawski, Z., Heidebrecht, J., Puerta Lombardi, B. M., Hyla, A. S., Willkomm, J., Radford, C. L., Lin, J.-. B., Welch, G. C., Ponnurangam, S., Roesler, R., Prokopchuk, D. E., Piers, W. E. Ligand–centered electrochemical processes enable CO_2 reduction with a nickel bis(triazapentadienyl) complex. *Sustainable Energy Fuels* **3**, 1172–1181 (2019).
195. Rao, G. K., Pell, W., Korobkov, I., Richeson, D. Electrocatalytic reduction of CO_2 using Mn complexes with unconventional coordination environments. *Chem. Commun.* **52**, 8010–8013 (2016).
196. Mukhopadhyay, T. K., MacLean, N. L., Gan, L., Ashley, D. C., Groy, T. L., Baik, M.-. H., Jones, A. K., Trovitch, R. J. Carbon dioxide promoted H^+ reduction using a bis(imino)pyridine manganese electrocatalyst. *Inorg. Chem.* **54**, 4475–4482 (2015).
197. Haines, R. J., Wittrig, R. E., Kubiak, C. P. Electrocatalytic Reduction of Carbon Dioxide by the Binuclear Copper Complex $[Cu_2(6$-(diphenylphosphino-2,2′-bipyridyl$)_2(MeCN)_2][PF_6]_2$. *Inorg. Chem.* **33**, 4723–4728 (1994).
198. Appel, A. M., Newell, R., DuBois, D. L., DuBois, M. R. Concentration of carbon dioxide by electrochemically modulated complexation with a binuclear copper complex. *Inorg. Chem.* **44**, 3046–3056 (2005).
199. Kang, S.-. J., Dale, A., Sarkar, S., Yoo, J., Lee, H. Electrocatalytic reduction of CO_2 by copper (ii) cyclam derivatives. *J. Electrochem. Sci. Technol.* **6**, 106–110 (2015).
200. Roy, S., Sharma, B., Pecaut, J., Simon, P., Fontecave, M., Tran, P. D., Derat, E., Artero, V. Molecular cobalt complexes with pendant amines for selective electrocatalytic reduction of carbon dioxide to formic acid. *J. Am. Chem. Soc.* **139**, 3685–3696 (2017).
201. Mostafa Hossain, A. G. M., Nagaoka, T., Ogura, K. Palladium and cobalt complexes of substituted quinoline, bipyridine and phenanthroline as catalysts for electrochemical reduction of carbon dioxide. *Electrochim. Acta* **42**, 2577–2585 (1997).
202. Jeletic, M. S., Mock, M. T., Appel, A. M., Linehan, J. C. A cobalt-based catalyst for the hydrogenation of CO_2 under ambient conditions. *J. Am. Chem. Soc.* **135**, 11533–11536 (2013).
203. Iffland, L., Khedkar, A., Petuker, A., Lieb, M., Wittkamp, F., van Gastel, M., Roemelt, M., Apfel, U.-. P. Solvent-controlled CO_2 reduction by a triphos-iron hydride complex. *Organometallics* **38**, 289–299 (2019).
204. Hameed, Y., Gabidullin, B., Richeson, D. Photocatalytic CO_2 reduction with manganese complexes bearing a $\kappa;^2$-PN ligand: breaking the α-diimine hold on group 7 catalysts and switching selectivity. *Inorg. Chem.* **57**, 13092–13096 (2018).
205. Fogeron, T., Todorova, T. K., Porcher, J.-. P., Gomez-Mingot, M., Chamoreau, L.-. M., Mellot-Draznieks, C., Li, Y., Fontecave, M A bioinspired nickel(bis-dithiolene) complex as a homogeneous catalyst for carbon dioxide electroreduction. *ACS Catal* **8**, 2030–2038 (2018).
206. Dey, S., Ahmed, M. E., Dey, A. Activation of Co(I) state in a cobalt-dithiolato catalyst for selective and efficient CO_2 reduction to CO. *Inorg. Chem.* **57**, 5939–5947 (2018).
207. Chiou, T.-. W., Tseng, Y.-. M., Lu, T.-. T., Weng, T.-. C., Sokaras, D., Ho, W.-. C., Kuo, T.-. S., Jang, L.-. Y., Lee, J.-. F., Liaw, W.-. F. $[Ni^{III}(OMe)]$-mediated reductive activation of CO_2 affording a Ni(κ^1-OCO) complex. *Chem. Sci.* **7**, 3640–3644 (2016).
208. Cheng, M., Yu, Y., Zhou, X., Luo, Y., Wang, M. Chemical versatility of [FeFe]-hydrogenase models: distinctive activity of $[\mu;$-C_6H_4-1,2-($\kappa;^2$-S)2$][Fe_2(CO)_6]$ for Electrocatalytic CO_2 Reduction. *ACS Catal* **9**, 768–774 (2019).

DOI: 10.1016/j.enchem.2020.100034
EnergyChem **2**, 100034 (2020)

209. Gerschel, P., Warm, K., Farquhar, E. R., Englert, U., Reback, M. L., Siegmund, D., Ray, K., Apfel, U. P. Sulfur substitution in a Ni(cyclam) derivative results in lower overpotential for CO_2 reduction and enhanced proton reduction. *Dalton Trans* **48**, 5923–5932 (2019).
210. Pokharel, U. R., Fronczek, F. R., Maverick, A. W. Reduction of carbon dioxide to oxalate by a binuclear copper complex. *Nat. Commun.* **5**, 5883 (2014).
211. Lan, J., Liao, T., Zhang, T., Chung, L. W. Reaction mechanism of Cu(I)-mediated reductive CO_2 coupling for the selective formation of oxalate: cooperative CO_2 reduction to give mixed–valence $Cu_2(CO_2^{\bullet-})$ and nucleophilic-like attack. *Inorg Chem* **56**, 6809–6819 (2017).
212. Cook, B. J., Di Francesco, G. N., Abboud, K. A., Murray, L. J. Countercations and solvent influence CO_2 reduction to oxalate by chalcogen-bridged tricopper cyclophanates. *J. Am. Chem. Soc.* **140**, 5696–5700 (2018).
213. Aranzaes, J. R., Daniel, M.-. C., Astruc, D. Metallocenes as references for the determination of redox potentials by cyclic voltammetry-Permethylated iron and cobalt sandwich complexes, inhibition by polyamine dendrimers, and the role of hydroxy-containing ferrocenes. *Can. J. Chem.* **84**, 288–299 (2006).
214. Zoski, C. G.. Handbook of Electrochemistry (2007). Oxford: Elsevier.
215. Matsuoka, S., Yamamoto, K., Ogata, T., Kusaba, M., Nakashima, N., Fujita, E., Yanagida, S. Efficient and selective electron mediation of cobalt complexes with cyclam and related macrocycles in the *p*-terphenyl-catalyzed photoreduction of carbon dioxide. *J. Am. Chem. Soc.* **115**, 601–609 (1993).
216. Ogata, T., Yanagida, S., Brunschwig, B. S., Fujita, E. Mechanistic and kinetic studies of cobalt macrocycles in a photochemical CO_2 reduction system: evidence of Co-CO_2 adducts as intermediates. *J. Am. Chem. Soc.* **117**, 6708–6716 (1995).
217. Zhang, M., El-Roz, M., Frei, H., Mendoza-Cortes, J. L., Head--Gordon, M., Lacy, D. C., Peters, J. C. Visible light sensitized CO_2 activation by the tetraaza $[Co^{II}N_4H(MeCN)]^{2+}$ complex investigated by FT-IR spectroscopy and DFT calculations. *J. Phys. Chem. C* **119**, 4645–4654 (2015).
218. Sheng, H., Frei, H. Direct observation by rapid-ccan FT-IR spectroscopy of two-electron-reduced intermediate of tetraaza catalyst $[Co^{II}N_4H(MeCN)]^{2+}$ converting CO_2 to CO. *J. Am. Chem. Soc.* **138**, 9959–9967 (2016).
219. Matsuoka, S., Yamamoto, K., Pac, C., Yanagida, S. Enhanced *p*-terphenyl-catalyzed photoreduction of CO_2 to CO through the mediation of Co(III)–cyclam complex. *Chem. Lett.* **20**, 2099–2100 (1991).
220. Fujita, E., Creutz, C., Sutin, N., Brunschwig, B. S. Carbon dioxide activation by cobalt macrocycles: evidence of hydrogen bonding between bound CO_2 and the macrocycle in solution. *Inorg. Chem.* **32**, 2657–2662 (1993).
221. Fujita, E., van Eldik, R. Effect of pressure on the reversible binding of acetonitrile to the "Co(I)−CO_2" adduct to form cobalt(III) carboxylate. *Inorg. Chem.* **37**, 360–362 (1998).
222. Creutz, C., Schwarz, H. A., Wishart, J. F., Fujita, E., Sutin, N. Thermodynamics and kinetics of carbon dioxide binding to two stereoisomers of a cobalt(I) macrocycle in aqueous solution. *J. Am. Chem. Soc.* **113**, 3361–3371 (1991).
223. Fujita, E., Furenlid, L. R., Renner, M. W. Direct XANES evidence for charge transfer in Co−CO_2 Complexes. *J. Am. Chem. Soc.* **119**, 4549–4550 (1997).
224. Craig, C. A., Spreer, L. O., Otvos, J. W., Calvin, M. Photochemical reduction of carbon dioxide using nickel tetraazamacrocycles. *J. Phys. Chem.* **94**, 7957–7960 (1990).
225. Grant, J. L., Goswami, K., Spreer, L. O., Otvos, J. W., Calvin, M. Photochemical reduction of carbon dioxide to carbon monoxide in water using a nickel(II) tetra-azamacrocycle complex as catalyst. *J. Chem. Soc. Dalton Trans.*, 2105–2109 (1987).
226. Katsura Mochizuki, S. M., Ikuyo, Takeda, Takeshi, Kondo Synthesis and structure of [6,6′-bi(5,7-dimethyl-1,4,8,11-tetraazacyclotetradecane)]dinickel(II) triflate and its catalytic activity for photochemical CO_2 reduction. *Inorg. Chem.* **35**, 5132–5136 (1996).
227. Kuehnel, M. F., Sahm, C. D., Neri, G., Lee, J. R., Orchard, K. L., Cowan, A. J., Reisner, E. ZnSe quantum dots modified with a Ni(cyclam) catalyst for efficient visible-light driven CO_2 reduction in water. *Chem. Sci.* **9**, 2501–2509 (2018).
228. Jin, T., Liu, C., Li, G. Photocatalytic CO_2 reduction using a molecular cobalt complex deposited on TiO_2 nanoparticles. *Chem. Commun.* **50**, 6221–6224 (2014).
229. Takeda, H., Koizumi, H., Okamoto, K., Ishitani, O. Photocatalytic CO_2 reduction using a Mn complex as a catalyst. *Chem. Commun.* **50**, 1491–1493 (2014).
230. Gholamkhass, B., Mametsuka, H., Koike, K., Tanabe, T., Furue, M., Ishitani, O. Architecture of supramolecular metal complexes for photocatalytic CO_2 reduction: ruthenium-rhenium bi- and tetranuclear complexes. *Inorg. Chem.* **44**, 2326–2336 (2005).
231. Cheung, P. L., Machan, C. W., Malkhasian, A. Y., Agarwal, J., Kubiak, C. P. Photocatalytic reduction of carbon dioxide to CO and HCO_2H using fac-$Mn(CN)(bpy)(CO)_3$. *Inorg. Chem.* **55**, 3192–3198 (2016).
232. Agarwal, J., Iii, Stanton, J. , C., Shaw, T. W., Vandezande, J. E., Majetich, G. F., Bocarsly, A. B., Schaefer, H. F. III Exploring the effect of axial ligand substitution (X = Br, NCS, CN) on the photodecomposition and electrochemical activity of $[MnX(N-C)(CO)_3]$ complexes. *Dalton Trans* **44**, 2122–2131 (2015).
233. Zhang, J.-. X., Hu, C.-. Y., Wang, W., Wang, H., Bian, Z.-. Y. Visible light driven reduction of CO_2 catalyzed by an abundant manganese catalyst with zinc porphyrin photosensitizer. *Appl. Catal., A* **522**, 145–151 (2016).
234. Guo, Z., Chen, G., Cometto, C., Ma, B., Zhao, H., Groizard, T., Chen, L., Fan, H., Man, W.-. L., Yiu, S.-. M., Lau, K.-. C., Lau, T.-. C., Robert, M. Selectivity control of CO versus $HCOO^-$ production in the visible-light-driven catalytic reduction of CO_2 with two cooperative metal sites. *Nat. Catal.* **2**, 801–808 (2019).
235. Shimoda, T., Morishima, T., Kodama, K., Hirose, T., Polyansky, D. E., Manbeck, G. F., Muckerman, J. T., Fujita, E. Photocatalytic CO_2 reduction by trigonal-bipyramidal cobalt(II) polypyridyl complexes: the nature of cobalt(I) and cobalt(0) complexes upon their reactions with CO_2, CO, or proton. *Inorg. Chem.* **57**, 5486–5498 (2018).
236. Hirose, T., Shigaki, S., Hirose, M., Fushimi, A. Synthesis of new CO_2-soluble ruthenium(II) and cobalt(II) polypyridine complexes bearing fluorinated alkyl chains and their application to photoreduction of liq. CO_2. *J. Fluorine Chem.* **131**, 915–921 (2010).
237. Trickett, C. A., Helal, A., Al-Maythalony, B. A., Yamani, Z. H., Cordova, K. E., Yaghi, O. M. The chemistry of metal–organic frameworks for CO_2 capture, regeneration and conversion. *Nat. Rev. Mater.* **2**, 17045 (2017).
238. Li, R., Zhang, W., Zhou, K. Metal-organic-framework-based catalysts for photoreduction of CO_2. *Adv. Mater.* **30**, 1705512 (2018).
239. Jiao, L., Wang, Y., Jiang, H. L., Xu, Q. Metal-organic frameworks as platforms for catalytic applications. *Adv. Mater.* **30**, 1703663 (2018).
240. Dhakshinamoorthy, A., Asiri, A. M., Garcia, H. Metal-organic framework (MOF) compounds: photocatalysts for redox reactions and solar fuel production. *Angew. Chem. Int. Ed.* **55**, 5414–5445 (2016).
241. Fang, Y., Ma, Y., Zheng, M., Yang, P., Asiri, A. M., Wang, X. Metal-organic frameworks for solar energy conversion by photoredox catalysis. *Coord. Chem. Rev.* **373**, 83–115 (2018).
242. Tu, W., Zhou, Y., Zou, Z. Photocatalytic conversion of CO_2 into renewable hydrocarbon fuels: state-of-the-art accomplishment, challenges, and prospects. *Adv. Mater.* **26**, 4607–4626 (2014).

DOI: 10.1016/j.enchem.2020.100034
EnergyChem **2**, 100034 (2020)

243. Wang, Y., Huang, N. Y., Shen, J. Q., Liao, P. Q., Chen, X. M., Zhang, J. P. Hydroxide ligands cooperate with catalytic centers in metal-organic frameworks for efficient photocatalytic CO_2 reduction. *J. Am. Chem. Soc.* **140**, 38–41 (2018).
244. Guo, Z., Yu, F., Yang, Y., Leung, C. F., Ng, S. M., Ko, C. C., Cometto, C., Lau, T. C., Robert, M. Photocatalytic conversion of CO_2 to CO by a copper(II) quaterpyridine complex. *ChemSusChem* **10**, 4009–4013 (2017).
245. Liu, W. J., Huang, H. H., Ouyang, T., Jiang, L., Zhong, D. C., Zhang, W., Lu, T. B A Copper(II) molecular catalyst for efficient and selective photochemical reduction of CO_2 to CO in a water-containing system. *Chem. Eur. J.* **24**, 4503–4508 (2018).
246. Takeda, H., Ohashi, K., Sekine, A., Ishitani, O. Photocatalytic CO reduction using Cu(I) photosensitizers with a Fe(II) catalyst. *J. Am. Chem. Soc.* **138**, 4354–4357 (2016).
247. Alsabeh, P. G., Rosas-Hernández, A., Barsch, E., Junge, H., Ludwig, R., Beller, M. Iron-catalyzed photoreduction of carbon dioxide to synthesis gas. *Catal. Sci. Technol.* **6**, 3623–3630 (2016).
248. König, E., Ritter, G., Madeja, K. Metal complexes of 2,9-dimethyl-1,10-phenanthroline and derivatives Iron(II) complexes. *J. Inorg. Nucl. Chem.* **43**, 2273–2280 (1981).
249. Rosas-Hernández, A., Steinlechner, C., Junge, H., Beller, M. Earth-abundant photocatalytic systems for the visible-light-driven reduction of CO_2 to CO. *Green Chem* **19**, 2356–2360 (2017).
250. Sakaguchi, Y., Call, A., Cibian, M., Yamauchi, K., Sakai, K. An earth-abundant system for light-driven CO_2 reduction to CO using a pyridinophane iron catalyst. *Chem. Commun.* **55**, 8552–8555 (2019).
251. Cometto, C., Kuriki, R., Chen, L., Maeda, K., Lau, T.-. C., Ishitani, O., Robert, M. A carbon nitride/Fe quaterpyridine catalytic system for photostimulated CO_2-to-CO conversion with visible light. *J. Am. Chem. Soc.* **140**, 7437–7440 (2018).
252. Lin, J., Qin, B., Fang, Z. Nickel bipyridine ($Ni(bpy)_3C_{l2}$) complex used as molecular catalyst for photocatalytic CO_2 reduction. *Catal. Lett.* **149**, 25–33 (2018).
253. Hirose, T., Maeno, Y., Himeda, Y. Photocatalytic carbon dioxide photoreduction by $Co(bpy)_3^{2+}$ sensitized by $Ru(bpy)_3^{2+}$ fixed to cation exchange polymer. *J. Mol. Catal. A: Chem.* **193**, 27–32 (2003).
254. Grodkowski, J., Behar, D., Neta, P., Hambright, P. Iron porphyrin-catalyzed reduction of CO_2. photochemical and radiation chemical studies. *J. Phys. Chem. A* **101**, 248–254 (1997).
255. T. Dhanasekaran, J. G., P. Neta, P. Hambright, Etsuko Fujita *p*-terphenyl-sensitized photoreduction of CO_2 with cobalt and iron porphyrins. Interaction between CO and reduced metalloporphyrins. *J. Phys. Chem. A* **103**, 7742–7748 (1999).
256. Grodkowski, J., Neta, P. Ferrous ions as catalysts for photochemical reduction of CO_2 in homogeneous solutions. *J. Phys. Chem. A* **104**, 4475–4479 (2000).
257. Bonin, J., Chaussemier, M., Robert, M., Routier, M. Homogeneous photocatalytic reduction of CO_2 to CO using Iron(0) porphyrin catalysts: mechanism and intrinsic limitations. *ChemCatChem* **6**, 3200–3207 (2014).
258. Bhugun, I., Lexa, D., Savéant, J.-. M. Homogeneous catalysis of electrochemical hydrogen evolution by iron(0) porphyrins. *J. Am. Chem. Soc.* **118**, 3982–3983 (1996).
259. Bonin, J., Robert, M., Routier, M. Selective and efficient photocatalytic CO_2 reduction to CO using visible light and an iron-based homogeneous catalyst. *J. Am. Chem. Soc.* **136**, 16768–16771 (2014).
260. Rao, H., Bonin, J., Robert, M. Visible-light homogeneous photocatalytic conversion of CO_2 into CO in aqueous solutions with an iron catalyst. *ChemSusChem* **10**, 4447–4450 (2017).
261. Rao, H., Bonin, J., Robert, M. Toward visible-light photochemical CO_2-to-CH_4 conversion in aqueous solutions using sensitized molecular catalysis. *J. Phys. Chem. C* **122**, 13834–13839 (2018).
262. Grodkowski, J., Dhanasekaran, T., Neta, P., Hambright, P., Brunschwig, B. S., Shinozaki, K., Fujita, E. Reduction of cobalt and iron phthalocyanines and the role of the reduced species in catalyzed photoreduction of CO_2. *J. Phys. Chem. A* **104**, 11332–11339 (2000).
263. Grodkowski, J., Neta, P., Fujita, E., Mahammed, A., Simkhovich, L., Gross, Z. Reduction of cobalt and iron corroles and catalyzed reduction of CO_2. *J. Phys. Chem. A* **106**, 4772–4778 (2002).
264. Sinha, W., Mahammed, A., Fridman, N., Diskin-Posner, Y., Shimon, L. J. W., Gross, Z. Superstructured metallocorroles for electrochemical CO_2 reduction. *Chem. Commun.* **55**, 11912–11915 (2019).
265. Behar, D., D. , T., Neta, P., Hosten, C. M., Ejeh, D., Hambright, P. Etsuko Fujita Cobalt porphyrin catalyzed reduction of CO_2. Radiation chemical, photochemical, and electrochemical studies. *J. Phys. Chem. A* **102**, 2870–2877 (1998).
266. Grodkowski, J., Neta, P. Cobalt corrin catalyzed photoreduction of CO_2. *J. Phys. Chem. A* **104**, 1848–1853 (2000).
267. Morris, W., Volosskiy, B., Demir, S., Gandara, F., McGrier, P. L., Furukawa, H., Cascio, D., Stoddart, J. F., Yaghi, O. M. Synthesis, structure, and metalation of two new highly porous zirconium metal-organic frameworks. *Inorg. Chem.* **51**, 6443–6445 (2012).
268. Zhang, H., Wei, J., Dong, J., Liu, G., Shi, L., An, P., Zhao, G., Kong, J., Wang, X., Meng, X., Zhang, J., Ye, J. Efficient visible–light-driven carbon dioxide reduction by a single-atom implanted metal-organic framework. *Angew. Chem. Int. Ed.* **55**, 14310–14314 (2016).
269. Lin, L., Hou, C., Zhang, X., Wang, Y., Chen, Y., He, T. Highly efficient visible-light driven photocatalytic reduction of CO_2 over g-C_3N_4 nanosheets/tetra(4-carboxyphenyl)porphyrin iron(III) chloride heterogeneous catalysts. *Appl. Catal., B* **221**, 312–319 (2018).
270. Zhao, G., Pang, H., Liu, G., Li, P., Liu, H., Zhang, H., Shi, L., Ye, J. Co-porphyrin/carbon nitride hybrids for improved photocatalytic CO_2 reduction under visible light. *Appl. Catal. B: Environ.* **200**, 141–149 (2017).
271. Wu, T., Zou, L., Han, D., Li, F., Zhang, Q., Niu, L A carbon-based photocatalyst efficiently converts CO_2 to CH_4 and C_2H_2 under visible light. *Green Chem* **16**, 2142–2146 (2014).
272. Chan, S. L., Lam, T. L., Yang, C., Yan, S. C., Cheng, N. M. A robust and efficient cobalt molecular catalyst for CO_2 reduction. *Chem. Commun.* **51**, 7799–7801 (2015).
273. Chan, S. L.-F., Lam, T. L., Yang, C., Lai, J., Cao, B., Zhou, Z., Zhu, Q. Cobalt(II) tris(2-pyridylmethyl)amine complexes $[Co(TPA)X]^+$ bearing coordinating anion ($X = Cl^-$, Br^-, I^- and NCS^-): synthesis and application for carbon dioxide reduction. *Polyhedron* **125**, 156–163 (2017).
274. Yang, C., Mehmood, F., Lam, T. L., Chan, S. L., Wu, Y., Yeung, C. S., Guan, X., Li, K., Chung, C. Y., Zhou, C. Y., Zou, T., Che, C. M. Stable luminescent iridium(III) complexes with bis(N-heterocyclic carbene) ligands: photo-stability, excited state properties, visible-light-driven radical cyclization and CO_2 reduction, and cellular imaging. *Chem. Sci.* **7**, 3123–3136 (2016).
275. Zhu, C.-. Y., Zhang, Y.-. Q., Liao, R.-. Z., Xia, W., Hu, J.-. C., Wu, J., Liu, H., Wang, F. Photocatalytic reduction of CO_2 to CO and formate by a novel Co(II) catalyst containing a cis-oxygen atom: photocatalysis and DFT calculations. *Dalton Trans* **47**, 13142–13150 (2018).
276. Wang, F., Cao, B., To, W. P., Tse, C. W., Li, K., Chang, X. Y., Zang, C., Chan, S. L. F., Che, C. M. The effects of chelating N_4 ligand coordination on Co(II)-catalysed photochemical conversion of CO_2 to CO: reaction mechanism and DFT calculations. *Catal. Sci. Technol.* **6**, 7408–7420 (2016).
277. Zhu, C.-. Y., Huang, Y.-. C., Hu, J.-. C., Li, Q.-. K., Tan, H., Gui, M.-. X., Deng, S.-. F., Wang, F. Cis-$[Co^{II}(MPCA)X_2]$ ($X = Cl$ or Br) complexes as catalyst exhibiting different activity for visible light induced photocatalytic CO_2-to-CO conversion. *J. Photochem. Photobiol. A* **355**, 175–179 (2018).
278. Lin, J., Qin, B., Zhao, G. Effect of solvents on photocatalytic reduction of CO_2 mediated by cobalt complex. *J. Photochem. Photobiol. A* **354**, 181–186 (2018).

DOI: 10.1016/j.enchem.2020.100034
EnergyChem **2**, 100034 (2020)

279. Hossain, M. A., Liljegren, J. A., Powell, D., Bowman-James, K. Anion binding with a tripodal amine. *Inorg. Chem.* **43**, 3751–3755 (2004).
280. Liu, D.-. C., Wang, H.-. J., Ouyang, T., Wang, J.-. W., Jiang, L., Zhong, D.-. C., Lu, T.-. B. Conjugation effect contributes to the CO_2-to-CO conversion driven by visible-light. *ACS Appl. Energy Mater.* **1**, 2452–2459 (2018).
281. Liu, D. C., Wang, H. J., Wang, J. W., Zhong, D. C., Jiang, L., Lu, T. B. Highly efficient and selective visible-light driven CO_2-to-CO conversion by a Co-based cryptate in H_2O/CH_3CN solution. *Chem. Commun.* **54**, 11308–11311 (2018).
282. Xiang, D., Magana, D., Dyer, R. B. CO_2 reduction catalyzed by mercaptopteridine on glassy carbon. *J. Am. Chem. Soc.* **136**, 14007–14010 (2014).
283. Burks, D. B., Davis, S., Lamb, R. W., Liu, X., Rodrigues, R. R., Liyanage, N. P., Sun, Y., Webster, C. E., Delcamp, J. H., Papish, E. T. Nickel(II) pincer complexes demonstrate that the remote substituent controls catalytic carbon dioxide reduction. *Chem. Commun.* **54**, 3819–3822 (2018).
284. Zimmermann, P., Hoof, S., Braun-Cula, B., Herwig, C., Limberg, C. A biomimetic nickel complex with a reduced CO_2 ligand generated by formate deprotonation and its behaviour towards CO_2. *Angew. Chem., Int. Ed.* **57**, 7230–7233 (2018).
285. Hong, D., Tsukakoshi, Y., Kotani, H., Ishizuka, T., Kojima, T. Visible-light-driven photocatalytic CO_2 reduction by a Ni(II) complex bearing a bioinspired tetradentate ligand for selective CO production. *J. Am. Chem. Soc.* **139**, 6538–6541 (2017).
286. Matlachowski, C., Schwalbe, M. Photochemical CO_2-reduction catalyzed by mono- and dinuclear phenanthroline-extended tetramesityl porphyrin complexes. *Dalton Trans* **44**, 6480–6489 (2015).
287. Ahsan, H. M., Breedlove, B. K., Piangrawee, S., Mian, M. R., Fetoh, A., Cosquer, G., Yamashita, M. Enhancement of electrocatalytic abilities for reducing carbon dioxide: functionalization with a redox-active ligand-coordinated metal complex. *Dalton Trans* **47**, 11313–11316 (2018).
288. Kimura, E., Wada, S., Shionoya, M., Okazaki, Y. New series of multifunctionalized nickel(II)-cyclam (Cyclam = 1,4,8,11-tetraazacyclotetradecane) complexes. Application to the photoreduction of carbon dioxide. *Inorg. Chem.* **33**, 770–778 (1994).
289. Herrero, C., Quaranta, A., El Ghachtouli, S., Vauzeilles, B., Leibl, W., Aukauloo, A. Carbon dioxide reduction via light activation of a ruthenium-Ni(cyclam) complex. *Phys. Chem. Chem. Phys.* **16**, 12067–12072 (2014).
290. Komatsuzaki, N., Himeda, Y., Hirose, T., Sugihara, H., Kasuga, K. Synthesis and photochemical properties of ruthenium–cobalt and ruthenium-nickel dinuclear complexes. *Bull. Chem. Soc. Jpn.* **72**, 725–731 (1999).
291. Wang, X., Goudy, V., Genesio, G., Maynadie, J., Meyer, D., Fontecave, M. Ruthenium-cobalt dinuclear complexes as photocatalysts for CO_2 reduction. *Chem. Commun.* **53**, 5040–5043 (2017).
292. Fabry, D. C., Koizumi, H., Ghosh, D., Yamazaki, Y., Takeda, H., Tamaki, Y., Ishitani, O A Ru(II)-Mn(I) supramolecular photocatalyst for CO_2 reduction. *Organometallics* **39**, 1511–1518 (2020).

AUTHOR BIOGRAPHIES

Dong-Cheng Liu obtained his B.S. from Hengyang Normal University in 2008, his M.S. from Guangxi Normal University under the supervision of Prof. P. F. Liang in 2011, and Ph.D. from the Sun Yat-Sen University under the supervision of Prof. T. B. Lu in 2016. He currently works at School of Chemistry and Pharmaceutical Sciences, Guangxi Normal University. His research work is focused on the design and synthesis of homogeneous/heterogeneous catalysts for photochemical and electrochemical CO_2 reduction.

Di-Chang Zhong obtained his B.S. in 2003 from Gannan Normal University and his M.S. in 2006 from Guangxi Normal University and Ph.D. in 2011 from the Sun Yat-Sen University. Then, he worked as a JSPS postdoctoral fellow at AIST, Japan. He joined the faculty at Gannan Normal University in 2013 and promoted to professor in 2017. In 2020, he moved to Tianjin University of Technology. His interests focus on the design and synthesis of molecular catalytic materials for energy storage and conversion.

Tong-Bu Lu obtained his B.S. in 1988 and Ph.D. in 1993 from Lanzhou University. After two years postdoctoral fellowship at Sun Yat-Sen University, he joined the faculty at the same university, and became a professor in 2000. He worked as a postdoctor in F. Albert Cotton's group at Texas A&M University in 1998 and 2002, respectively. In 2016, he moved to Tianjin University of Technology. His current research interests focus on the study of artificial photosynthesis, including the design of homogeneous and heterogeneous catalysts for water splitting and CO_2 reduction. He obtained the National Natural Science Foundation for Distinguished Youth Scholar in 2006. He has published over 280 scientific publications with H-index of 48. Now, he is a fellow of Royal Society of Chemistry (FRSC), the Editorial Advisory Board of *CrystEngComm, Current Green Chemistry* and *Current Pharmaceutical Design*, as well as co-editor of *Acta Crystallographica Section C*.

DOI: 10.1016/j.enchem.2020.100034
EnergyChem **2**, 100034 (2020)